THE ANALYSIS OF CD8$^+$ T CELL ANTI-TUMOR RESPONSES

by

Catherine Ami Bessell

A dissertation submitted to Johns Hopkins University in conformity with the requirements for the degree of Doctor of Philosophy

Baltimore, Maryland
July 2020

1 Abstract

Immunotherapy treatments have been a growing trend for treatment cancer since 2012 with the first clinical trial for check point blockade therapy to treat melanoma patients. As researchers have studied the mechanism of action for immune directed killing of patients' tumors, it is becoming clear how much we need to understand the biology of anti-tumor T cell responses to find the characteristics of a robust anti-tumor response. By studying the T cell receptor (TCR) repertoire of the endogenous tumor response in mice and patients, we have created a tool called ImmunoMap to measure and compare a T cell response by its TCR repertoire overtime and even between entirely different T cell targets, while previously only individual clonotypes or clones could be tracked. Along with ability to analyze T cell response both in research and clinical responses, our work have revealed that neo-antigen T cell response comparatively has benefits over self-tumor responses which explains the benefit of targeting patient's cancers based on neo-antigen responses. But not all neo-antigen response show immunogenic response to tumors, which lead us to study a model of immunogenic neo-antigen response by antigen mimicry between commensal bacteria and a non-self tumor antigen. We are excited to show a proof-of-concept in murine melanoma of antigen mimicry in the gut led to a boosting of the tumor T cell response and colonization change and prime the T cell response to create a therapeutic T cell population. I am pleased with the work I have contributed in the Schneck lab, to study what effects the quality of an anti-tumor T cell responses and further understand ways to increase positive patient outcomes with immunotherapy treatments against cancer.

Primary Reader and Advisor: Jonathan P Schneck

Secondary Reader: Jonathan P Powell

2 Thesis Committee

Jonathan P. Schneck, M.D. Ph.D. (primary adviser, *reader)*

Professor, Department of Pathology

Johns Hopkins University School of Medicine

Jonathan D. Powell, Ph.D. *(reader)*

Professor, Department of Oncology

Johns Hopkins University School of Medicine

Abdu Hamad, Ph.D.

Professor, Department of Pathology

Johns Hopkins University School of Medicine

Benjamin Larman, Ph.D.

Assistant Professor, Department of Pathology

Johns Hopkins University School of Medicine

3 Acknowledgements

Although it seems overwhelming to thank all the people who have supported me throughout training, I would like to try.

First I would like to thank Jonathan Schneck for being my mentor and thesis advisor over the last 6 years. When I first joined the lab, he's approach to building projects and approaching science has made me a better scientist and researcher. From our meetings to discuss data to long discussions over projects, I have learned to ask the interesting question and see the forest and not just the trees. I am forever grateful for his patience and desire to see me succeed in science, working on projects that seemed to never work and supporting my own research goals. I think teaching others HOW to think about science is the most critical skill in graduate school and forever grateful the I get to be part of the Schneck lab. You have made it possible for me to thrive as a scientist and mother, and to make a contribution to science with my work in the lab. Thank you, Jonathan.

And the lab would not be the fun, loud, exciting place that is without the Schneck lab members. First, it is essential to thank Joanie Bieler, for her guidance both in science and life. I am so grateful for our late night conversations, your support toward being a wife, mother and scientist and to always get excited for the next piece of data (just like me!). You are a pillar of the lab and you have help support me all these years. Thank you Joanie.

There have been so many other previous lab members who I've worked with and I thank them for the fun times/the frustrating science times/ and working together to create great science and a wonderful work environment. Thanks you Yen, Karlo, Christian, Juan, Kristy, Mattias, John Hickey, and Alyssa, it has been wonderful to work with you.

For labmates that I have seen grow and develop in lab, it has been exciting to first guide you around lab, explain immunology as the resident “immunologist” and see you grow to become an expert. Ariel, you always are overflowing with new ideas and things to try, I know you will do great things in science and I’m grateful that I got to work with you in the Schneck lab. Natalie, working with you is a pleasure and I can’t wait to see what you create. Panam, I am so grateful for your support on our projects together, our discussions about science, and your level of patience and work ethic (seriously, you are amazing).

I’d like to thank the immunology graduate program. When you first accepted me to the program, I thought it was a mistake because I was grateful for the chance to work with such amazing people. All the PI’s were encouraging and worked to create an environment to not just work for amazing scientists, but become confident researchers as well. Thank you Mark and Joel for leading a great program. Thank you to our administration staff, for supporting me and helping me make life/family/research all happen and succeed, thank you Angela and Lori.

Science is not always easy, and I forever grateful for all my friends and family for encouraging me, and reminding me that I can do it. My friends and chosen family through NextLevel has been instrumental for inspiring me, and encouraging me to go after my passions in science and to use my strengths to contribute something to the world.

To my extended family. Thank you for always listening to my work and letting me explain science and the things I’m passionate about. For all the trips, reunions, supportive texts and check-ins to remind me how much I love doing what I do.

To my family: Mom and Dad, you have always been supportive of my passion in science and it’s no surprise I am completing my PhD when I have parents like you. You have ALWAYS encourage me to excel in school and science, never assumed science was an odd choice for your

daughter, and to for listening to all the newest things I was doing in lab (from blueberry and Drosophila research up till now!). Thank you for supporting me as a mother and scientist, for loving your grand-daughter and making it possible for me to go after my passion in science by being there for me. Thank you for Sunday night dinners, weekly check-in calls, and for being such a beautiful support in my life. Thank you David, Jon, and Sarah for being there for me, for the fun trips and hangs out.

To my husband, daughter and new son: Thank you, thank you, thank you. Sung Hwa, you have always supported my decision to go into research, even when that's not your interest at all. Thank you for the late nights in lab, for always being a shoulder to cry on, reminding me I can keep going, and for being a 100% supportive husband. And when we became parents, you were always there to make sure it can work. I love you more than I can say. To Elizabeth and Robert, I am so grateful for the joy I have every day with you. I love you more than life and I want to show you how to go after your passion and talents, whatever they might be.

The last person I would like to thank in me. Thank you Ami for not giving up, for trusting yourself, and for believing in yourself.

4 Dedication

I dedicate this work to my supportive parents Richard and Mary Oben, my loving husband Sung Hwa Bessell and to our beautiful children, Elizabeth and Robert. Thank you for your love, encouragement and support. Sung Hwa thank you for our messy, wonderful life.

5 Table of Contents

6 Table of Figures

7 Summary and Organization of the Dissertation

The organization of the dissertation is as follows:

Chapter 2 provides an overview of the importance of T cells in the adaptive immune response with a description of T cell development, and T cell antigen stimulation. Furthermore, it focuses T cell driven anti-tumor responses, the effect of tumor antigens on T cell populations, and the role of T cells in cancer immunotherapies. Finally, it explains the connection between the microbiome and the immune system, the impact of the microbiome on immunotherapies, and the role of antigens in the microbiome-immune response.

Chapter 3 is the manuscript: Sidhom, John-William, Bessell, Catherine A. et al. "ImmunoMap: A Bioinformatics Tool for T-Cell Repertoire Analysis." Cancer Immunology Research 2 (2018): 151-162. The data and story creates a new analysis tool for TCR repertoires of antigen specific T cell populations. More specifically, TCR clones with similar CDR3 regions are organized into TCR motifs and by comparing the entire TCR repertoire it is possible to observe different anti-tumor responses based on different antigen responses and different patients' responses to immunotherapy.

Chapter 4 is the manscript: Bessell, Catherine A. et al. "Commensal bacteria stimulate anti-tumor responses via T cell cross-reactivity." Unpublished. The data and story center around a homologous sequence between the murine tumor neo-antigen KbSIY and commensal bacteria sequence "SVY". Here we confirm the cross-reactivity between the KbSIY and KbSVY response. Furthermore, we show the colonization of the commensal bacteria boosts the KbSVY T cell response. This proof of concept approach shows when cross-reactivity occurs between commensal bacteria and a T cell response, the microbiome can enhance the anti-tumor response via antigen specific effector T cell induction.

Chapter 5 is a summary of my contribution to other projects that have not been put into a published manuscript. Here I summarize the major findings and outline further work that can be completed to answer outstanding questions.

8 Introduction

8.1 $CD8^+$ T Cells Function in the Immune System

Introduction to T cells: The immune system is a complex system organized into an innate arm that is composed of fast acting cells and soluble factors that broadly target pathogens, and an adaptive immune arm that after initial exposure can create a targeted response toward specific pathogens and even cancer cells. The adaptive immune system can create a specific memory response to a particular pathogen, which can respond faster and more robustly with secondary infection. The innate immune system will have the same speed and response to infections no matter the number of exposures to the same pathogen. Within the adaptive compartment, $CD8^+$ T cells have both the ability to detect and directly attack infected cells, and as the memory $CD8^+$ T cells survey the body they can protect the host over an entire lifetime.

During initial activation of T cells, a specificity receptor (signal 1) and co-stimulatory receptor (signal 2) engagement are necessary to create a robust, and effective T cells response. The signal 1 ensures individual T cells that are specific to a particular antigen are activated. An antigen is a short peptide sequence, 8-10 amino acid long sequence, which results from cutting up larger proteins expressed by pathogens in antigen presenting cells. The T cell receptor (TCR), is activated by binding to the combination of antigen that is folded and presented by a MHC protein molecule. Along with this signal 1, the signal 2 on an antigen presenting cells bind with the receptor on T cells to initiate a signaling cascade to differentiate the cell into an effector T cell and proliferate to create daughter cells. The two signals together are essential for optimal binding and activation of T cells and without the signaling pathways from each, the threshold of activation will not be reached inadvertently. Once a $CD8^+$ T cell is activated, they can traffic throughout the host body and when detecting the correct peptide-MHC complex can release lytic

molecules to lyse target cells and soluble cytokines that help with an inflammatory response against the infection. As T cells protect against a particular antigen, each T cell clone has a unique TCR to detect the antigen with specificity. Because each T cell has a unique, a polyclonal T cell population made up of multiple clones can recognize the same antigen with their own TCRs and within a given infection multiple antigens may be recognized by $CD8^+$ T cells, which creates a diverse T cell population even for a single infection.

T cell Development: T cell development occurs in the thymus, where pre-lymphocytes develop into $CD4^+$ and $CD8^+$ T cells, each with a unique TCR. To create the TCR during development, T cells will rearrange the DNA at the CDR3 region of the alpha and beta chains of the TCR. As the TCR goes through VDJ recombination to create a functioning TCR, $CD8^+$ T cell create a range of affinities toward their antigen target. During positive selection, the TCR is educated to bind to the host MHC alleles which are the proteins responsible for presenting peptide antigens to T cells. During negative selection, if the TCR binds a self-antigen it can be deleted or develop into a $CD4^+$ T regulatory T cell. This process of selecting TCRs based on self-reactivity for limiting the self-reactive T cell response and stop high affinity autoreactive T cells from attacking healthy tissue in the body[1]. Since foreign antigens do not have the same selection in the thymus, there is a potential for higher TCR affinities to non-self antigens or mutated antigens that no longer respond like self antigens[2].

The negative selection that removes the auto-reactive T cells is referred to as central tolerance. After T cell leave the thymus and begin circulating around the body as naïve T cells, peripheral tolerance can further inhibit the auto-reactive $CD8^+$ T cells. This is thought to occur by presenting the antigen without the presence of co-stimulatory signal and produces a tolerized

T cell response or anergic T cell. Anergic T cells have lower T cell activity upon activation and future T cell responses from inhibit clones do not response as robustly to their antigen[3].

Creating T cell Antigens and presenting them: The cells responsible for activating T cells are termed antigen presenting cells (APCs), cells such as dendritic cells (DCs), B cells and macrophages; although all cells (except platelets) express MHC class I for T cells to recognize healthy tissue. APCs express the MHC proteins loaded with different short peptide sequences that bind to T cells TCRs along with co-stimulatory molecules for activation. Normally, MHC class I molecules load ER proteins or irregular formed endogenous proteins that are transported into the ER and load into the MHC groove as the protein is expressed. When cells are infected with an intracellular pathogen, the viral peptides can be loaded into the MHC class I molecule and presented on the surface for activating anti-viral T cells to target infected cells. As healthy tissue is infected viral antigens are loaded into MHC class I and the infected cells can be targeted by the activated T cell population. In non-infected cells, the peptides from self proteins are loaded into the MHC class I molecule and unless presented with co-stimulatory signals does not signal an auto-reactive response. Extracellular antigens can be taken up by APCs by "cross-presentation," a cellular pathway that transports proteins inside the cells and into the ER to be loaded and presented on the APC cell surface for T cell stimulation.

The Schneck lab has been a seminal group in the production of artificial APCs, aAPCs, which are constructed of a particle platform what has both a signal 1 and signal 2 conjugated to the surface and along with supplemental cytokines that can stimulate T cells *in vitro* for antigen specific populations. The aAPC has gone through multiple cycles design, and in the current system a paramagnetic nanoparticle can be used to enrich and expand rare, antigen specific T cells from the endogenous T cell population in both murine and human system (Figure 8.1)[4].

Using a Ig molecule with MHC class I molecules a dimer is created that can be actively loaded with peptide antigens and along with anti-CD28 or other co-stimulatory molecules to expand antigen specific $CD8^+$ T cells for analysis and even for therapeutic settings in murine ACT models (Figure 8.2)[4].

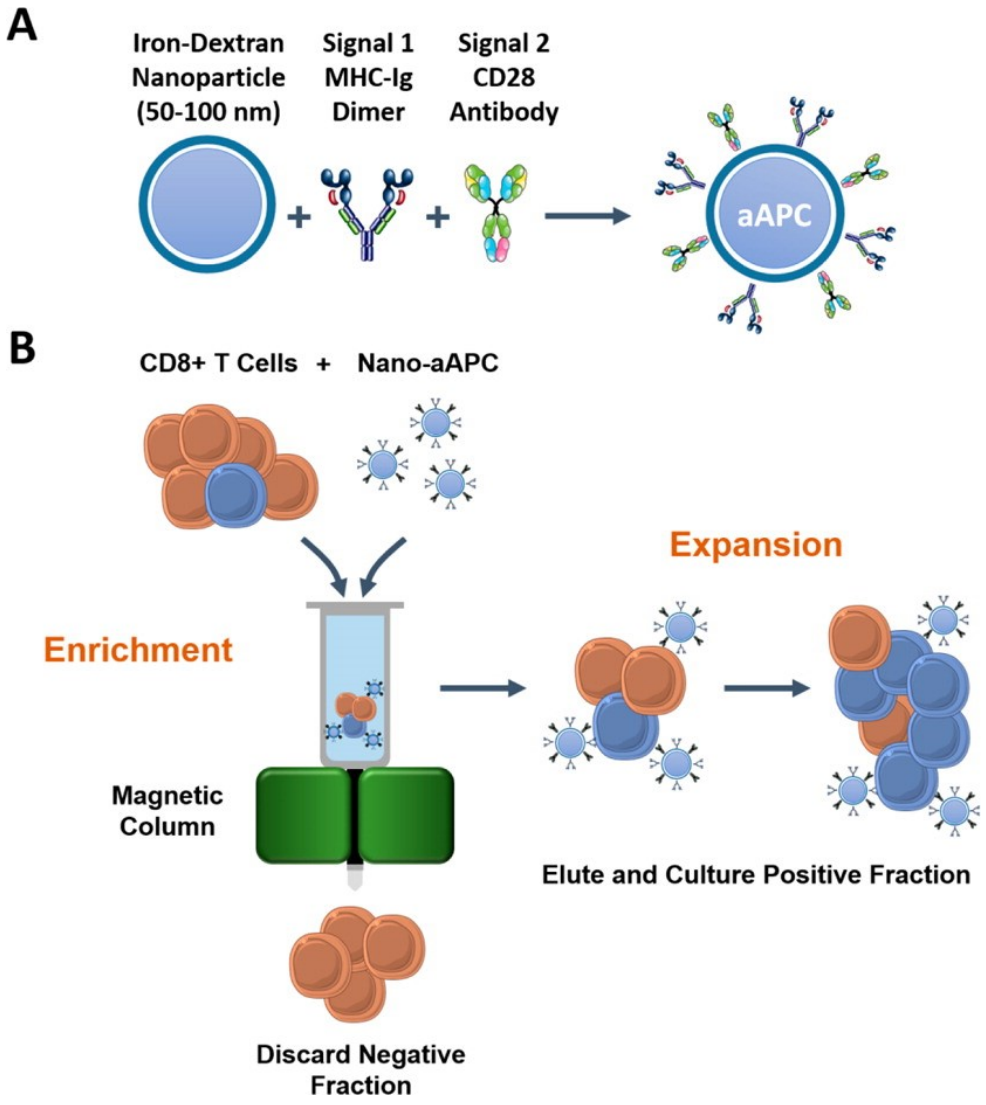

Figure 8.1 aAPCs enrich and expand for antigen specific CD8+ T cells.

A) aAPCs have a signal 1 peptide-MHC Ig complex and signal 2 anti-CD28 directly conjugated to a 100nm iron dextran particle. B) CD8+ T cells are enriched and expanded with aAPCs by removing non-specific T cells and directly stimulating the T cell response with a signal 2 along with the enrichment strategy. (Figure taken from[5])

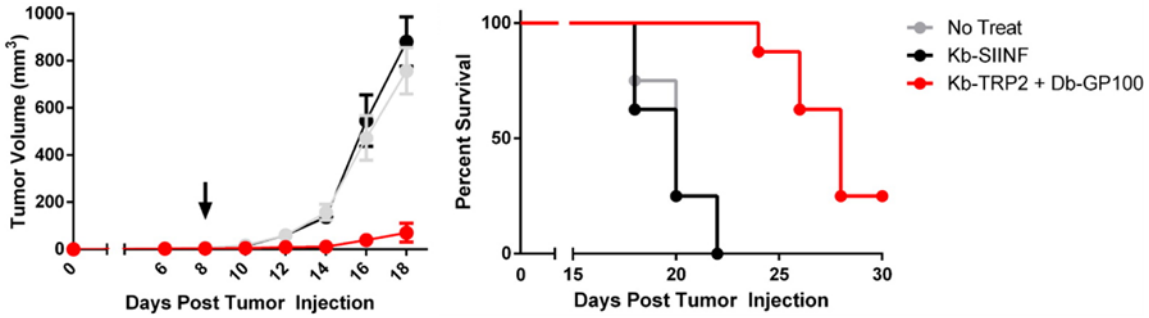

Figure 8.2 Adoptive transfer of E&E T cells mediates tumor rejection.

(Left) Kb-TRP2 and Db-GP100 Enriched + Expanded lymphocytes cultured for 7 days prior to adoptive transfer inhibited melanoma growth ($p < 0.01$ by two-way ANOVA, 8 mice/group, red). Mice were injected with subcutaneous melanoma 8 days prior and irradiated with 500 cGy gamma irradiation 1 day prior. Noncognate E+E lymphocytes (SIINF; black) did not inhibit tumor growth (compared to untreated, gray), whereas cognate E+E (TRP2+GP100, red) did. (Right) Survival of animals from C. 2/8 mice showed complete rejection of tumors in the Kb-TRP2 and Db-GP100 treated group, which had significantly longer survival compared to noncognate and untreated groups ($p < 0.01$ by Mantel-Cox). (Figure Taken from[5])

8.2 T cell Driven Anti-Tumor Immunity

As tumors develop the immune system has a substantial role to clear premalignant and malignant cells. As pre-cancerous cells develop mutations and begin to replicate some of the malignant cells grow faster and or turn on pathways to inhibit the immune system to clear the tumors[6]. This immunoediting of the tumor on the immune system shows the interplay between

what the immune system can detect and methods to shut off or silence the anti-tumor immune response[7].

Tumor Antigens: The T cell population can detect the cancer cells through several different antigen types: self antigens (also called tumor associated antigens), cancer/testis antigens, and mutated antigens also called neo-antigens[8]. While each type of antigen can be presented if the cancer cells have a functioning processing and presentation machinery, each T cell antigen type can have a different ability to detect and respond to their appropriate antigen. Self antigens are normal antigens expressed by healthy tissue as well as the cancerous cells. MART-1 is a common melanoma $CD8^+$ antigen that is expressed by healthy melanocytes but is highly expressed on melanoma tumor cells and MART-1 specific T cells can detect their target antigens on tumor cells and lead to clearance in some patients receiving adoptive cellular therapy[9]. As described earlier, self antigens have the pressure of both central and peripheral tolerance which can limit both the high affinity clones from entering the circulating T cell population and also inhibit the available T cell clones (Figure 8.3). Cancer/testis antigens are epitopes that are processed from proteins expressed during limited times in tissue development and are not expressed by healthy tissue. The T cell clones that can detect cancer/testis antigens can have pressure through central tolerance if those epitopes are expressed in the thymus, but unless the tumor cells start expressing this new target, those T cells will not be able to detect the tumor. Finally, neo-antigens result from mutations expressed by tumor cells. The majority of neo-antigens develop from random point mutations as the cancer grows and accumulates mutations, called passenger mutations[10]. If the DNA mutation leads to a new peptide sequence and section of DNA is expressed, the processed and presented neo-antigen can be detected by the antigen specific $CD8^+$ T cell. If the wildtype sequence does not create a T cell response, the

mutated neo-antigen response has the potential for higher affinity clones and has not been limited as self-antigen T cell responses (Figure 8.3).

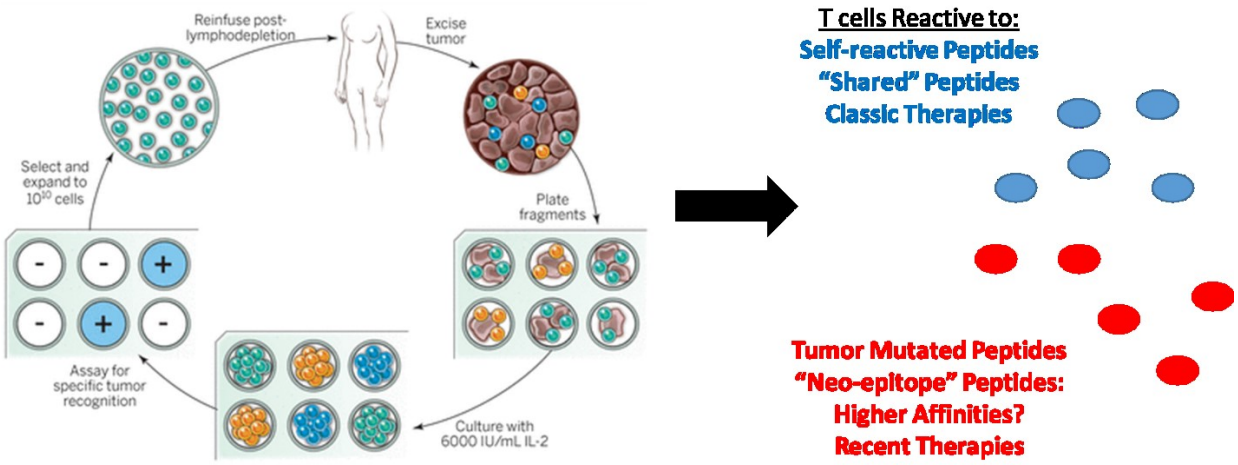

Figure 8.3 Tumor specific T cell populations comparison based on antigen type.

Excising both self reactive antigen T cells present in the tumor or neo-antigen reactive T cells may select for personalized therapy instead of established tumor antigen response, yet may be higher affinity and function. (Figure adapted from[11])

Comparison of self and neo-antigen tumor responses: By defining both self and neo-antigen by their ability to detect and activate against tumor cells researchers and clinicians can ask: what is the benefit of targeting different tumor antigen types? Asked another way: what are the benefits and risks of targeting cancers by the two antigen types? Self antigen $CD8^+$ T cell responses although can target healthy tissue, can be activated against the tumor and all the tumor cells can potentially express the self antigen. Neo-antigens develop as mutations accumulate in the dividing tumor cells, and if a neo-antigen target occurs in one cell of the tumor, the parental expansions do not carry the neo-antigen target. This polyclonal expression of neo-antigens in the

tumor carries the risk that a neo-antigen response, even if highly productive, will only be able to target a portion of the tumor cells. As previously stated, the neo-antigen T cell responses may have less central and peripheral tolerance which does not limit the higher affinity or functional activity compared to self antigen T cell responses. Yet, the largest road block to robust neo-antigen targeted T cell responses is the rate of production of immunogenic, neo-antigen targets in tumor cells. To identify neo-antigens, tumor cells must be DNA sequenced and compared to healthy tissue DNA sequences to identify changes in the amino acid sequence of proteins. The tumor must also be RNA sequenced to determine which possible mutations are expressed in the tumor cells. From the potential neo-antigen targets, an algorithm that ranks immunogenic epitope sequences by predicted ability to bind a suggested HLA allele for presentation to T cells. Depending on the restrictive criteria used for binding prediction, the efficiency of prediction can increase but some neo-antigens may not be identified if the binding prediction is only selecting for the "high binding neo-antigens". The predicted neo-antigens are tested for immunogenic response, by immunizing mice in murine systems and testing for T cell effector responses[12,13], and testing for T cell effector responses, using mass spectrometry to identify neo-antigens on DCs[14,15], or creating a mini-gene approach to express neo-antigen sequencing on patient's endogenous DCs for T cell stimulations[11]. Although, all methods have revealed $CD8^+$ neo-antigen responses, groups that have created immunogenic enriched criteria for neo-antigens neo-antigen T cell responses who have also looked within the $CD4^+$ T cell response have found more immunogenic $CD4^+$ T cell responses compared to $CD8^+$ neo-antigen responses[13]. Even in clinical settings, trying to identify potential neo-antigens, the majority of detected neo-antigen response are due to $CD4^+$ T cell responses while treating melanoma patients with a cancer vaccines and

checkpoint blockade[16]. Looking at the responses to overall response rate to immunotherapy, the neo-antigen targeted response hold promise for patients undergoing immunotherapies.

Immunotherapies: The expansion of immunotherapies into multiple cancer types shows the power of activating the immune system against tumor cells. T cell driven responses against cancer has shown long-term beneficial responses, and even after the malignant cells can no longer be detected the tumor specific T cells can still be found in patients[17]. There a few different approaches to immunotherapy, I will categorize the approaches as: checkpoint blockade therapies, cellular based therapies, and cancer vaccines. Each has their own efficacy and each engages the T cell response yet the method of immune activation toward the tumor cells vary. Checkpoint blockade therapy (CPB therapy) takes advantage of inhibitory molecules expressed by the tumor cells, such as CTLA-4 and PD-L1. Both are ligands expressed on the cell surface and engage CD28 and PD-1, respectively, which shuts off T cell activation and effectively silences T cell response against their target cell. With administration of α-CTLA4 or α-PD-L1/α-PD-1 there is an influx of lymphocytes to tumor tissues, and decrease in tumor burden[18]. It has been shown that CPB has increased benefit when PD-L1 is expressed on the tumors, and lymphocytes are present in the tumor prior to treatment[19]. This suggests CPB can re-activate previously inhibited T cell populations. Work to identify the tumor antigens responsible for T cell response show both self antigen responses and neo-antigen populations are activated by CPB[20], although cancers that have a higher rate of mutation and potentially more neo-antigens have an increased response to αPD-1 therapy[21]. Since CPB is a pan T cell activator throughout the body, T cells can become activated in healthy tissues and lead to toxicities, so even though multiple T cell responses can be activated simultaneously without having to identify the antigen

targets, there is a risk of developing massive T cell activation in the gut, skin, pituitary and even cardiac tissues[22].

Cellular based therapies directly treat patients with anti-tumor T cells. Classically endogenous T cells are collected from the tumors of patient during surgery and the T cells are expanded into large numbers and intravenously transferred back into the patient to kill any residual tumor cells. This adoptive cellular therapy approach has been used to expand known self-tumor antigens such as MART1 reactive $CD8^+$ T cells in melanoma patients but requires tumors to have T cells previously trafficked and reside in the tumor before tumor resection[23]. More recent approaches for ACT is to expand potential neo-antigen T cells for cellular transfer[24]. Alternatively, effector T cells can be collected from blood and genetically engineered to express a chimeric antigen receptor (CAR), and CAR can recognized a ligand expressed by the tumor and the CAR signaling induces T cell activation and killing of the targeted tumor cells. Using either endogenous, specific cells or CAR T cells for adoptive transfer requires the antigen to be defined on the tumor and the adoptively transferred cells will only target the portion of the tumor that expresses the antigen of interest.

Finally, cancer vaccines have seen an increase in beneficial response in approaches that target multiple neo-antigens simultaneously[15,16] and has recently showed positive results in classically non-immunogenic cancers such as breast cancer[25]. As with neo-antigen focused cellular therapies, neo-antigen tumor vaccines are a personalized therapy for each patient, and before beginning therapy the antigen targets must be defined. The vaccines developed usually house both CD4+ and CD8+ T cell neo-antigen targets, and responding patients have shown both $CD4^+$ and $CD8^+$ response post therapy in melanoma patients[16]. Further work on the benefit of

targeting both $CD4^+$ and $CD8^+$ antigens simultaneously may be beneficial in other immunogenic cancers.

8.3 The Microbiome and the Immune System

The Immune System and the Gut: The symbiotic relationship between the microbiome and the immune system supports the maintenance of immune cells around the gut, and the bacteria in microbiome that promote the immune system itself[26]. In germ-free animals, with no gut microbiome, the immune cells in the gut lymphoid tissues are severely depleted[27–29]. Alternatively, in genetic knockout mice for IL-22, a key cytokine produced by immune cells during gut homeostasis, there is a change in the major classes of bacteria that can colonize the gut[30]. The microbiome supports the immune system by supplying the immune system with metabolites for gut barrier maintenance and immune cell population and their function at the gut[31–33].

Multiple immune cell subsets are involved in normal gut regulation: innate-lymphoid cells activate the epithelial cells to support a proper barrier wall between the lumen and inner walls of the gut[30,34]. α/β and γ/δ T cells surround the gut to defend against bacterial infection[35–37]. DCs are continuously taking up antigens from the epithelial layer secreting bacterial products, as well as taking up bacteria directly[38]. DCs help maintain $CD4^+$ Tregs in around the gut to regulate inflammation[39,40]. Effector $CD4^+$ T cells defending against infection can create pro-flammatory conditions that can cause gut and microbiome dybiosis and lead to irritable bowel diseases[39]. $CD4^+$ T cells can also differentiate at the gut can produce IL-17 and IL-22 directly as well as activate the epithelial layer to secrete the key cytokines[41]. $CD8^+$ effector T cells can develop

around the based on the bacterial strains that are present, and the bacteria seem to be a source of both adjuvant and antigen[42]. B cells in Peyer's patches around the gut produce IgA, the antibody isotype that can transfer across the gut barrier, to bind to bacterial antigens[43]. Taken together, the different immune cell populations are all present at the gut and form the largest peripheral accumulation of immune cells.

Gut microbiome creates a safe barrier; the gut is responsible for inhibition of the immune system and at the same time continuous surveillance of the gut by immune system ensure bacterial colonization remains only in the gut lumen. Multiple immune cell types, both pro and anti-inflammatory cells differentiate and with dysbiosis of gut, bacteria can break through the gut barrier and the immune system can have autoimmunity toward the gut, all of which creates a delicate balance between the gut and immune system that surrounds it.

The Microbiome and immunotherapy: In terms of response to immunotherapy, particularly checkpoint blockade therapy (CPB), the composition of the gut microbiome seems to correlate with patient outcomes. Multiple groups have shown a distinction in the microbiome of responder and non-responder patients[44–49], yet there is no one clear mechanism of action between increased CPB response and how the bacteria in the gut alter the immune response. In the previous section, we've discussed the development of the immune response corresponds to the development of the microbiome. In some patients, having "healthy gut bacteria" is associated with decreased irritable bowel diseases associated with CPB therapy, and the presence of the healthy bacteria result in overall better response to CPB[46,50]. One suggested mechanism of action is the bacteria activate DCs by microbial stimulation or metabolites, and DCs then have increased trafficking to Peyer's patches, mesenteric lymph nodes and active T cells to trigger antigen responses at other sites[51]. By looking at the T cell driven responses from the gut,

combinations of bacteria alter T cell activation via DCs activation not only in overall stimulation but different unfolding patterns in the DC based protein processing machinery, creating effector T cell responses that could be responsible for increased benefit by CPB[42,52,53]. To summarize, the metabolites produced, the adjuvant source or even antigens presented at the gut microbiome activate epithelial cells and DCs to produce effector T cell responses that associate with benefit to CPB therapy, but the antigens the T cells are responding to have not identified.

Antigen mimicry and immunogenicity: In the field of autoimmunity antigen mimicry has been defined as self-antigen and foreign antigen have enough similarity to activate an autoreactive T or B cell by the foreign antigen[54]. In terms of potential neo-epitope responses in anti-tumor targeted therapies we have previously discussed the differences in the overall T cell response of neo-eptiopes. Within the neo-antigen T cell response, the immunogenicity of the neo-antigen can further define productive neo-antigen target. From a study in pancreatic cancer patients, it was observed that the patients surviving diagnosis from 5 years or more did not have more neo-antigen response but more potential immunogenic neo-antigens, even without immunotherapy interventions[55]. The group defining immunogenic neo-antigen responses defined 3 criteria for immunogenic neo-antigens: 1) the mutation increases the ability of the peptide sequence to load in the MHC allele, 2) the expression frequency of the mutation in the tumor clones, 3) the homology of the mutation sequence with a pathogen[56]. The first criteria corresponds to the stable processing and presentation ability of the neo-antigen because if the neo-antigen cannot be presented by tumor cells, the T cells cannot be activated or detect the target neo-antigen. The second criteria refers to the fact that mutations develop in the tumor overtime, and activated T cells can only detect and lyse the cancer cells that have the particular neo-antigen mutation in their DNA. The third criteria refers to homology between a foreign

sequence and the neo-antigen peptide sequence that can be stimulated through antigen mimicry and the cross-reactive T cells from antigens could target the cancer cells. A few groups have been able to show commensal gut bacteria promoting $CD8^+$ T cell responses with potential cross-reactivity between the bacterial and tumor response[45,49,57,58] but showing the presence of the bacteria inducing an antigen specific and cross-reactive response will be able to show how the mutational landscape of tumors with microbiome antigen mimicry can lead to increased anti-tumor T cell responses.

9 ImmunoMap: A Bioinformatics Tool for T-Cell Repertoire Analysis[1]

9.1 Introduction

The advent of high-throughput immune sequencing has allowed scientists and clinicians to understand antigen-specific interactions of the immune response with various pathologies from a systems-like perspective. TCR sequencing creates a detailed analysis of a polyclonal T cell population and study both individual clonal dominance as well as the overall diversity of a T cell response. Its initial applications showed the depth and breadth of the T-cell receptor (TCR) and B-cell receptor (BCR) repertoire[59–62]. Further applications of immune deep-sequencing have contributed to vaccine development and to tracking disease progression in malignancies[63–65]. Sequencing efforts have improved our understanding of immune responses to cancer, characterizing the TCR repertoire of circulating as well as tumor-infiltrating lymphocytes (TILs)[15,66] and responses to immunotherapies[15,67]. With the abundance of new "big data" sets, a need has arisen to develop biologically meaningful techniques for analysis of TCR repertoire sequences. Current analysis methods fall short of providing an intuitive understanding of the immune system repertoire for two reasons. First, as purely mathematical constructs, they focus on diversity defined as a function of the number of different sequences and their respective frequencies, Shannon entropy, and ignore sequence relatedness[68]. Second, methods that compare different repertoires apply stringent criteria by only comparing exact TCR clonotypes (whether at the nucleotide or amino acid level) to assess similarity[66,69,70].

[1] This chater is reprinted (adapted) with permission from "Sidhom, John W., Bessell, Catherine A., Havel, Jonathan J., Kosmides, Alyssa, Chan, Timothy A., and Schneck, Jonathan P. ImmunoMap: A Bioinformatics Tool for T-Cell Repertoire Analysis." Cancer Immunology Research (2017)."

However, biological sequence similarity, not identity, is the relevant parameter. Ignoring sequence relatedness is a significant omission, becauseTCRs with similar, homologous sequences likely recognize related MHC/peptide targets[71]. Several groups have sought to understand the structural aspects of the underlying TCR repertoire through a variety of techniques that cluster homologous CDR3 sequences, showing that, indeed, TCRs that recognize the same antigen have highly homologous sequences[71–73]. Although this work highlights the relevance and rationale behind analyzing TCR sequence repertoire data via clustering methods, we sought to create structural diversity metrics for whole TCR repertoires and not just a single motif. To address this, we developed ImmunoMap, which visualizes and quantifies immune repertoire diversity in a holistic fashion. ImmunoMap not only enables assessment of similarity between TCR sequences, but compares the scope of diversity among different repertoires. Our approach combines information about the frequency and relatedness of TCR sequences by using a sequence analysis inspired by phylogenetics to determine relatedness among CDR3 sequences of an antigen-specific T-cell response, as well as the similarities of a particular TCR repertoire to other repertoires for the same antigen specific response.

We initially trained ImmunoMap on the TCRs used by T cells responding to K^b-TRP2, a shared self-peptide tumor antigen, and K^b-SIY, a model neo-antigen, in a model of murine melanoma. ImmunoMap analysis showed that in naïve animals, the response to K^b-SIY was highly conserved, with many TCR sequences having high sequence homology, a biological observation that we missed when using Shannon entropy calculations. In contrast, the bulk of the self-antigen response was comprised of fewer and more distantly related sequences, suggestive of central tolerance eliminating dominant T cell clones. The presence of tumor had a differential effect on the shaping of the repertoire in the model neo-antigen and self-antigen responses,

greatly altering the TCR repertoire of the self-antigen response, with a smaller effect on the response to the neo-antigen antigen. The two different TCR repertoire changes suggests that self responses are either so diverse because of central tolerance, or that self responses are more impacted by pheriphal tolerance and the conservation of the repertoire in naïve settings cannot be stimulated at the tumor and alternative clones are present and expandable at the tumor. To understand the clinical utility of ImmunoMap, we compared ImmunoMap to Shannon entropy analysis of TILs from melanoma patients on anti–PD-1 therapy. Whereas Shannon entropy calculations did not find any clinically relevant correlates, ImmunoMap TCR diversity score found clinically relevant, predicative TCR signatures in patients who responded to anti–PD-1 therapy after just 4 weeks on therapy. Thus ImmunoMap proved more effective in finding a clinically useful parameter that another repertoire analysis technique could not. Overall, observing the pressure of tumor antigen type of T cell repertoires was highlighted by analyzing and measuring TCR homology of the CDR3 region as well as looking beyond individual antigen specific responses for changes to the entire T cell immune response.

9.2 Results

9.2.1 Overview of ImmunoMap Algorithms

Weighted Repertoire Dendrograms: In order to visualize the immune response, we created weighted dendrograms (See Figure 9.1~~Figure 9.1~~); combining information about sequence relatedness with information about sequence frequency. We initially applied this analysis to data (from the Adaptive Biotechnologies Data Portal[74]) on the response of tetramer-sorted human $CD8^+$ T cells to cytomegalovirus (CMV) (Figure 9.1~~Figure 9.1~~). The distance from the end of the

dendrogram branches denotes distance in terms of sequence homology; the size of the circles at the ends of the branches denotes frequency of the sequence, and color denotes Vβ usage. Sequence distance is determined as a function of global alignment scores (Needleman-Wunsch[75], PAM10 scoring matrix[76], Gap Penalty = 30) between all unique combination of sequences as follows:

$$Score12 = Sequence\ Alignment\ Score\ (Sequence\ 1, Sequence\ 2)$$

$$Score11 = Sequence\ Alignment\ Score\ (Sequence\ 1, Sequence\ 1)$$

$$Score22 = Sequence\ Alignment\ Score\ (Sequence\ 2, Sequence\ 2)$$

$$Sequence\ Distance = (1 - \frac{Score12}{Score11})(1 - \frac{Score12}{Score22})$$

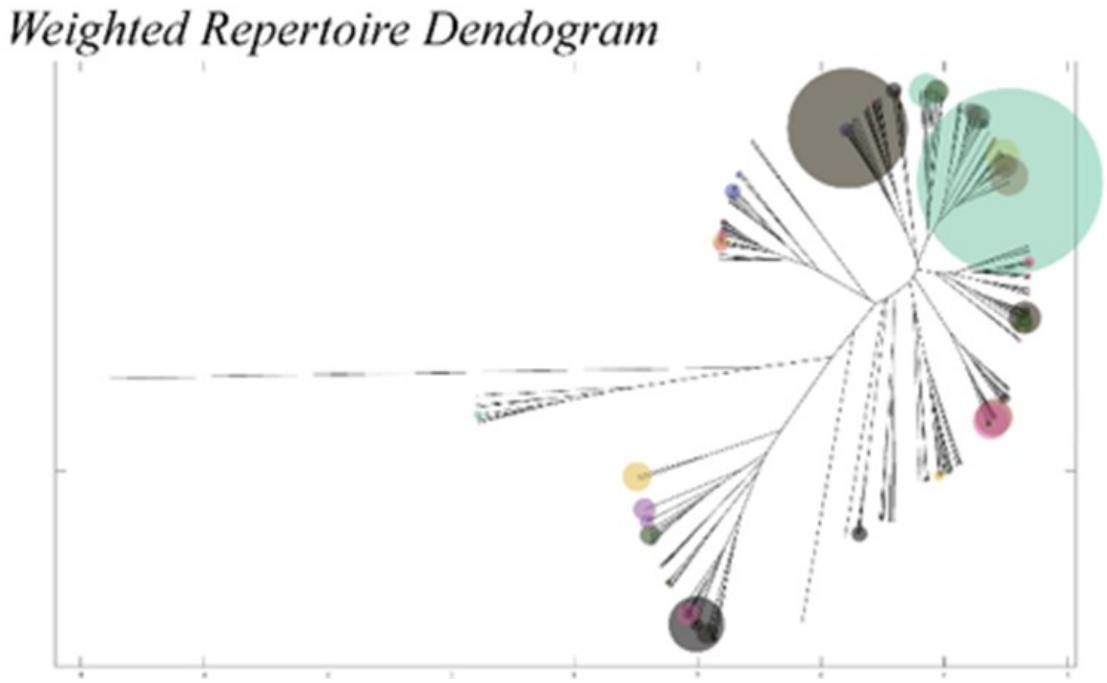

Figure 9.1 TCR homology of CMV specific T cell population.

Weighted Repertoire Dendogram visualize relatedness of sequences within repertoire along with relative frequency of CDR3 amino acid sequences.

Dominant Motif Analysis: In order to parse the many sequences that are detected in antigen-specific CTL expansion, we sought to perform hierarchical clustering to determine structural motifs that dominated the response. Thresholds for sequence homology and frequency were set by analyzing the sequences of the naïve B6 $CD8^+$ repertoire, taken from the Adaptive Biotechnologies Data Portal. We used these thresholds to define homology clusters based on sequence distance and then examined clusters that met a predefined frequency threshold and termed them “dominant motifs”(Figure 9.2).

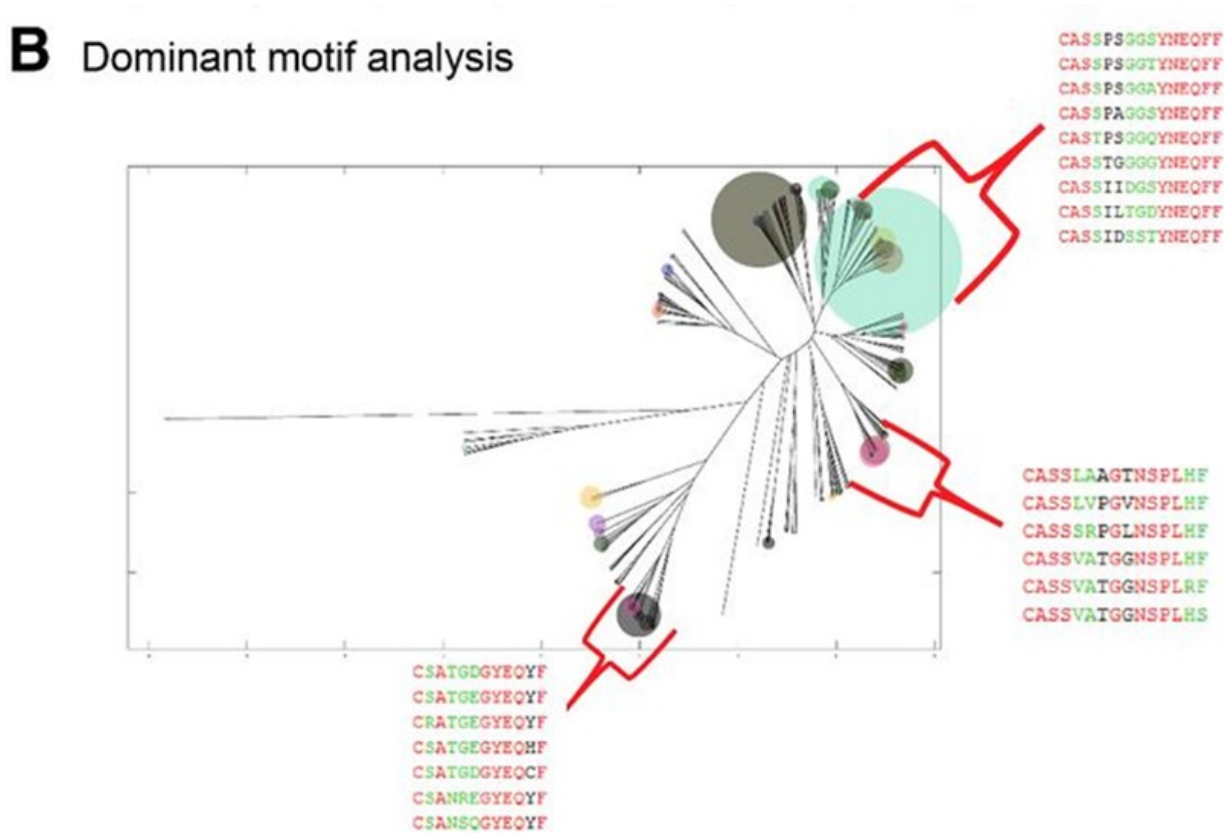

Figure 9.2 TCR Repertoire Dominant Motif Creation

Figure 2 from immunoMap.

Singular and Novel Structural Clones Analysis: We also defined a "singular structural clone" as one that has expanded 10x more than the summation of all other homologous clones in a sample, representing a singular solution in "sequence space.". When comparing two separate CMV-specific sequencing samples, from different individuals, we defined a "novel structural clone" as one that has expanded 10x more than the summation of all homologous clones to it in another sequencing sample, representing a newly expanded structural clone.

TCR Diversity Score: To quantify the diversity of the entire TCR repertoire, we created a metric to quantify the relatedness of an entire sample; defined as the average mapped sequence distance of all unique combinations of sequences in a sample, weighted by number of reads per sequence.

$$Mapped\ Sequence\ Distance = 1 - \frac{1}{1 + [Sequence\ Distance]}$$

The TCR Diversity score is bounded between 0 and 1, in which a score of 0 would correspond to all TCRs in a response being identical and 1 would correspond to all TCRs being infinitely different.

9.2.2 Tumor Exerts Differential Expansion Pressure on Antigen-Specific Repertoire

To understand the clonal diversity of antigen specific responses, $CD8^+$ T cells from naïve B6 mice were pooled and expanded against a model neo-eptiope antigen K^b-SIY, or against a self-tumor antigen, K^b-TRP2 (180-188), as described in literature[4]. Briefly, $CD8^+$ T cells were enriched and stimulated with nanoparticle artificial antigen-presenting cells (aAPCs) containing peptide-MHC-Ig molecules and cultured *in vitro* for 7 days. The resultant $CD8^+$ T-cell cultures were antigen-specific by both peptide-MHC-Ig staining and cytokine analysis, confirming their functional specificity. Initial precursor frequency was also measured in the endogenous repertoire and, even though T cells that recognize either antigen could be expanded from naïve animals, K^b-SIY antigen–specific T cells had a higher naïve precursor frequency. Antigen-specific populations were sorted and the CDR3 region of the TCR Vβ chain was sequenced. ImmunoMap analysis of K^b-SIY-specific and K^b-TRP2-specific TCRs visualized unique aspects of the polyclonal response for both antigens (Figure 9.3). K^b-SIY $CD8^+$ T cells consisted of

clones with homologous TCR sequences; however, the naïve response to K^b-TRP2 was more clonal in nature (more high frequency clones) and used more unrelated sequences, each creating a distinct clonal variant for antigen recognition.

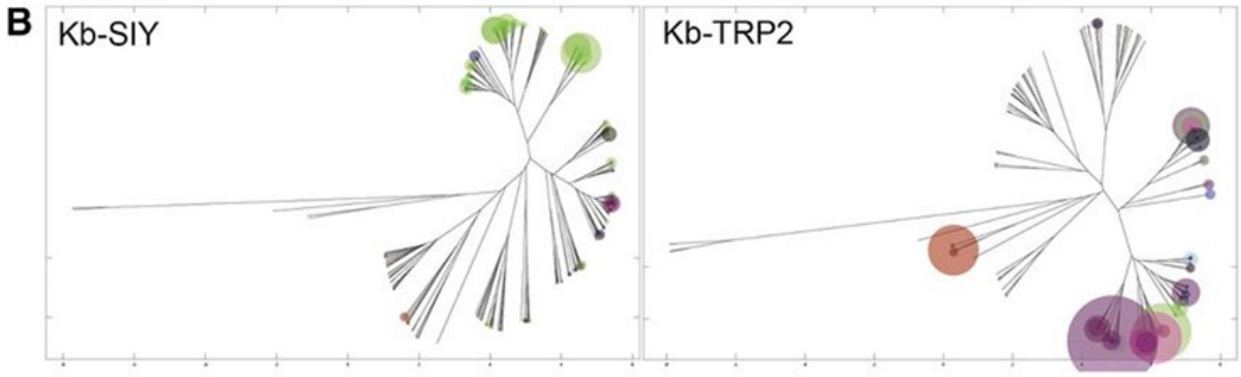

Figure 9.3 Naïve Repertoire to Kb-SIY vs Kb-TRP2 antigens.

Weighted Repertoire Dendograms where distance of ends of branches denotes sequence distance, size of circles denotes frequency of sequence, and color of circle denotes specific V beta segment usage.

Dominant motif analysis showed that anti-K^b-SIY TCR had fewer, yet richer (more sequences per motif), dominant motifs than K^b-TRP2 (Figure 9.4). K^b-TRP2 specific T cells had a higher percentage of clones representing singular structural T-cell expansions and they took up a larger portion of the overall TRP-2 antigen-specific response (Figure 9.4, bottom). Comparing the TCR diversity scores, K^b-SIY stimulated a more homologous response, whereas K^b-TRP2 had a more diverse response. The response to K^b-SIY had a more conserved Vβ usage,

predominantly using Vβ13, whereas the response to K^b-TRP2 exhibited a more diverse use of Vβ segments (Figure 9.5).

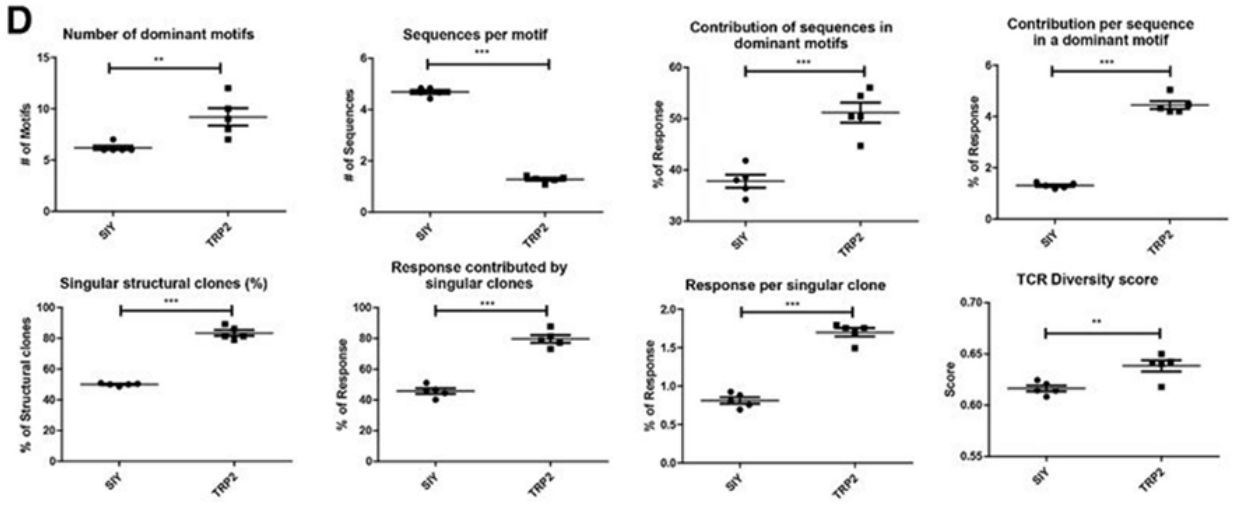

Figure 9.4 KbSIY naïve TCR repertoire has a more conserved dominant motif, while KbTRP2 has a more divergent motifs and creates a larger baseline diversity.

Top Row – Quantification of Dominant Motif Analysis comparing the number of dominant motifs, the number of sequences per motif, the contribution of the sequences in the dominant motifs to the response, and the contribution to the response per sequence in a dominant motif. *Bottom Row* – Singular Structural Clone and TCR Diversity analysis metrics. N = 5 mice pooled.

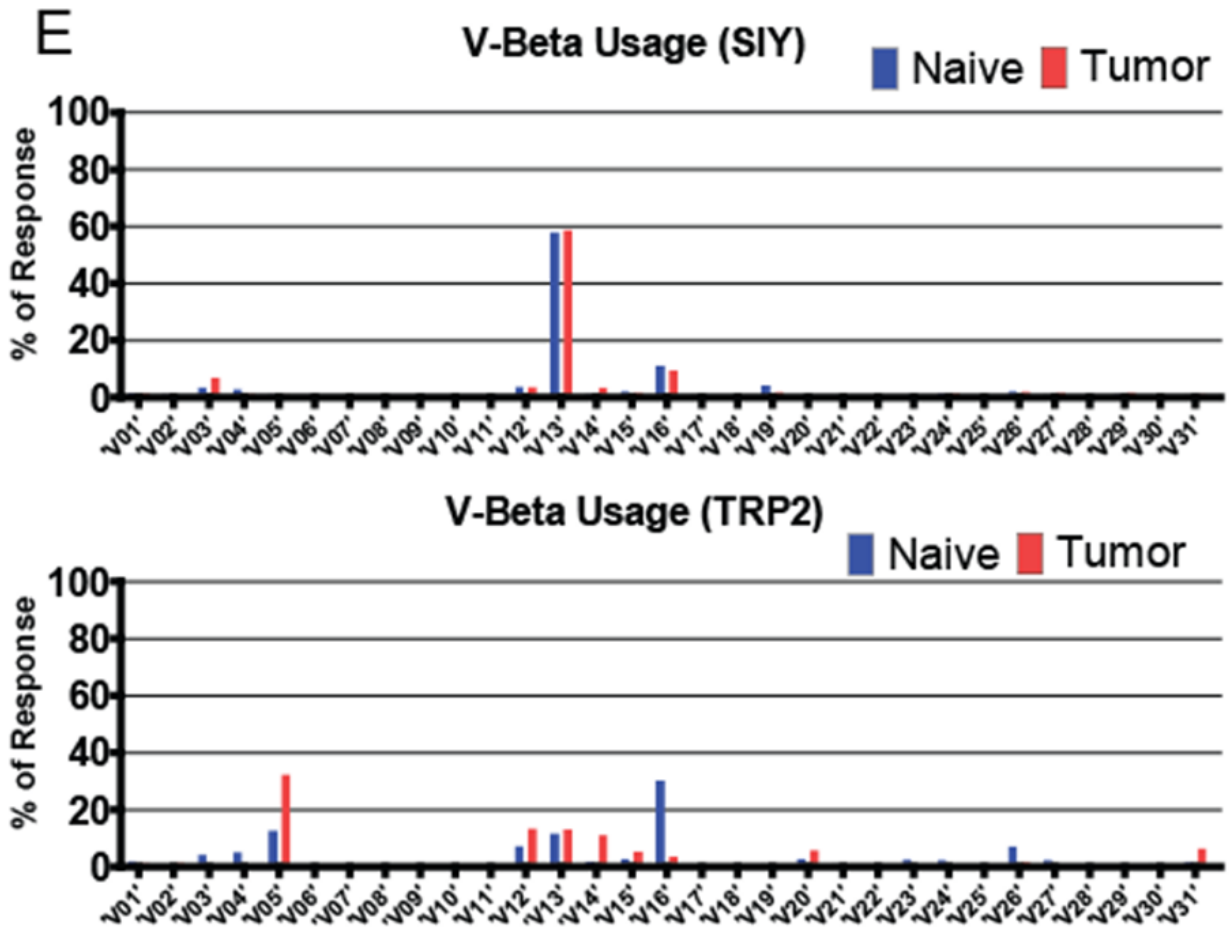

Figure 9.5 The SIY response uses the same V beta genes, while the self response is more varied and is shifted in tumor bearing animals.

V Beta usage of Kb-SIY and Kb-TRP between Naïve and Tumor-Bearing Repertoire. 3 mice pooled.

To demonstrate the advantages of the ImmunoMap analysis over traditional analytic methods, we calculated Shannon entropies for K^b-SIY vs K^b-TRP2 responses. Shannon entropies revealed the diversity of the K^b-SIY response to be higher than that of the K^b-TRP2 response. However, because the Shannon entropy is largely determined by the number of sequences that

are present in the K^b-SIY response and not their relatedness, it missed the fact that although more sequences responded to K^b-SIY, they were more homologous than the fewer sequences that responded to K^b-TRP2. Thus, the ImmunoMap TCR diversity score and dominant motif analyses reflected novel relatedness-information that could not be seen by conventional Shannon entropy calculations.

9.2.3 Tumor Exerts Differential Expansion Pressure on Antigen-Specific Repertoire

Although we know that tumors exert pressure on the immune response, it is not clear how this alters the repertoire of responding T cells. The ImmunoMap approach can provide insight into the biological impact of tumors on polyclonal T-cell responses and TCR usage by studying TCR repertoire changes in the presence of a murine melanoma tumor model (B16SIY) that contains the self/tumor KbTRP2 epitope as well as a model neo-epitope KbSIY[77]. Visualization of the TCR repertoire by ImmunoMap analysis showed differential effects of tumors on the repertoire of pooled splenic T cells specific for K^b-SIY or K^b-TRP2. The K^b-SIY $CD8^+$ T cell repertoire was largely unaltered in response to tumors (Figure 9.6). In contrast, as seen by ImmunoMap, the K^b-TRP2 response was not only more clonal, but also used TCR sequences that had minimal sequence homology to the TCRs seen in the naïve C57BL/6 response.

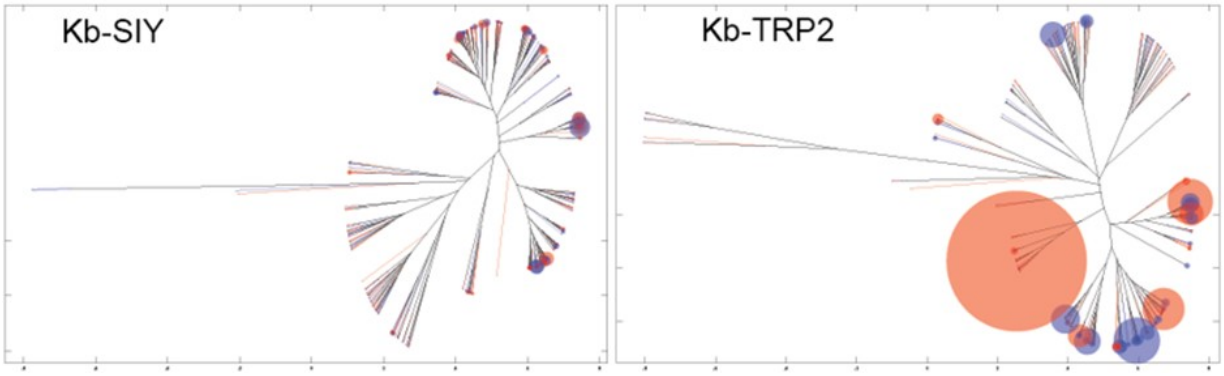

Figure 9.6 The tumor alters the self/tumor antigen response, but leaves the neo-epitope response unchanged.

The presence of tumor does not change the splenic neo-epitope response, but expands for certain to cell clones of the self/tumor response. Overlapped weighted repertoire dendograms of tumor-bearing vs naïve antigen-specific splenic CD8 responses. Mice spleens were pooled from tumor bearing or naïve mice, expanded for antigen and sorted for CD8 specificity on day 7. (Red = Tumor-bearing repertoire. Blue = Naïve repertoire).

Dominant motif analysis showed that the presence of tumors increased the number of dominant motifs in the K^b-SIY response. In contrast, the presence of tumors decreased the number of dominant motifs in the K^b-TRP2 response, suggesting directed immune pressure on the self vs foreign antigens in the context of tumor (Figure 9.7). Four dominant K^b-SIY motifs were conserved between naïve and tumor bearing animals. In contrast, no common dominant motifs were shared in the K^b-TRP2 response in tumor-bearing animals compared to the naïve response. When examining novel structural clones, the K^b-TRP2 response in tumor-bearing mice had more structurally novel sequences that, combined, were a larger portion of the response as compared to the naïve response. Selective pressure by tumors on the immune response was also

seen in analyzing the Vβ usage between naïve and tumor-bearing animals (Figure 9.5). We saw the elimination of the use of Vβ16 in the K^b-TRP2 response, and an increased use of Vβ5. In contrast, Vβ usage was conserved in the K^b-SIY response between naïve and tumor-bearing animals. Additionally, when examining the effect of tumors on Shannon entropy, we see that although maintenance of entropy in the K^b-SIY response and its decrease in the K^b-TRP2 response generally complement the ImmunoMap dominant motif analysis, Shannon entropies are uninformative about the conservation, or lack thereof, of TCR sequence structure in response to the tumor.

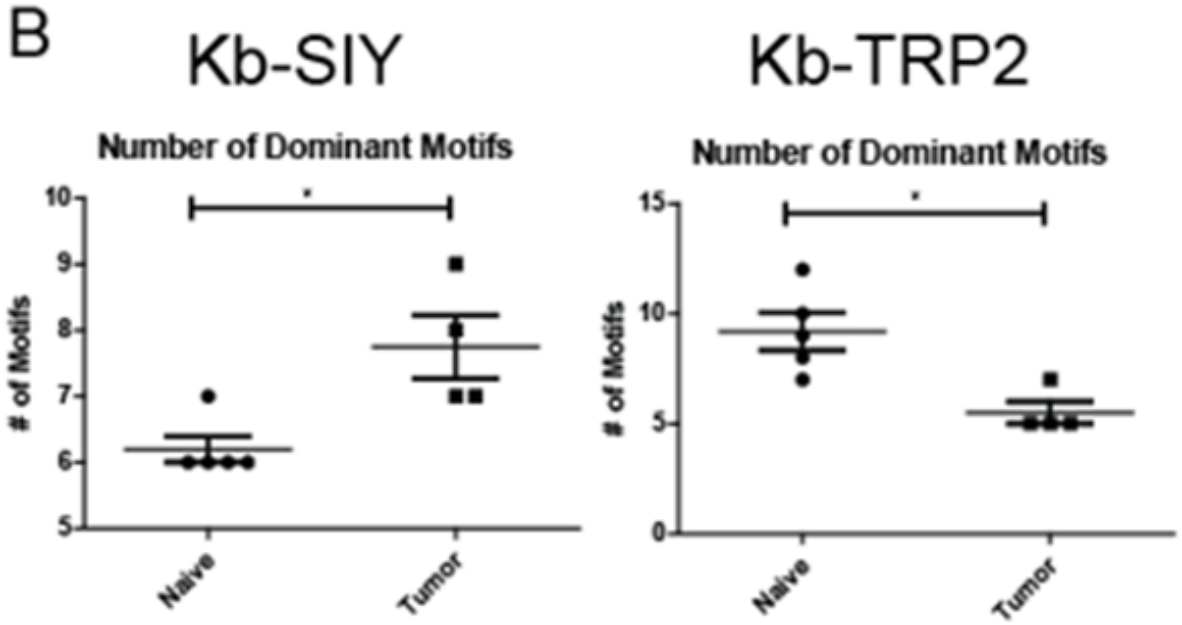

Figure 9.7 Tumor exposure expands the dominant motifs in the neo-epitope response and constricts the self/tumor response.

Dominant Motif analysis for Kb-SIY and Kb-TRP2 responses before and after exposure to tumor.

9.2.4 Lymphoid Organ-Dependent Differences in TCR Repertoires in Tumor-Bearing Mice

We hypothesized that the influence of tumors on the repertoire may also vary depending upon the relationship of the lymphoid organ to the tumor site. This was studied by analyzing antigen-specific TCR repertoires in the spleen versus draining lymph node (dLN), and tumor infiltrating lymphocytes (TILs) in pooled tumor-bearing mice lymph nodes and tumors. ImmunoMap analysis revealed that the K^b-SIY repertoire selects for a selected structural motifs by comparing T cell compartments closer to the tumor site. This is seen as the richness of

dominant motifs decreases, the response contributed by singular clones increases, and the TCR diversity score drops as one moves from the spleen towards the tumor. Additionally, the structural clones expanded in the spleen, dLN, and TILs are generally conserved, as can be visualized by the dendrograms and by tracking dominant motifs in the 3 lymphoid compartments (Figure 9.8)**.** In contrast, the opposite trend was seen in the K^b-TRP2 response. Dominant motifs between the spleen and draining lymph node were not conserved; we were unable to expand any K^b-TRP2 specific cells from the TILs in multiple experiments.

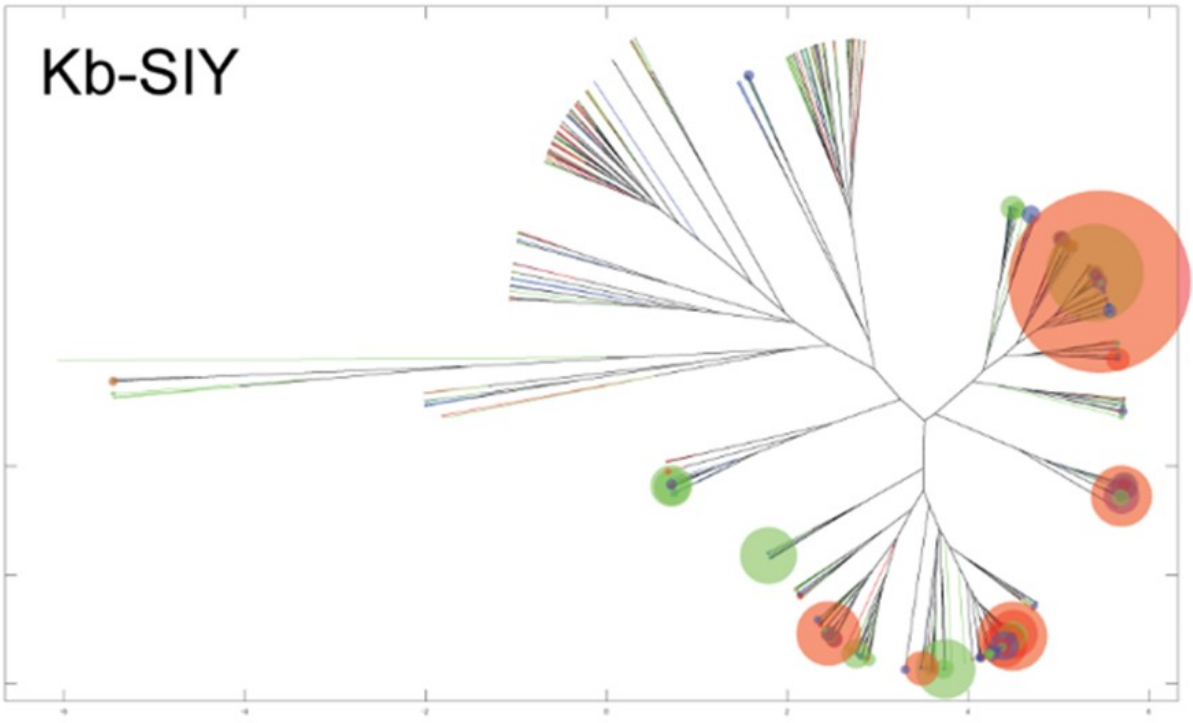

Figure 9.8 Tumor focuses the KbSIY TCR Repertoire but maintains dominant motif overlap.

Overlapped weighted repertoire dendograms of KbSIY expanded T cells from the spleen, draining lymphoid and tumor, (blue = spleen, green = draining lymph node, red = TILs).

9.2.5 Analysis of anti–PD-1 Clinical Trial Data Reveals Indicators of Response

Recent studies have implicated changes in T-cell responses as important in clinical outcomes to checkpoint blockade. We therefore applied ImmunoMap analysis to clinical trial data (BMS-038) from patients with metastatic melanoma undergoing anti–PD-1 therapy (nivolumab). For this analysis, formalin-fixed, paraffin embedded scrapings were taken from 34 patients, the percentage of TILs estimated as per suggested protocol (Materials and Methods) and

CDR3 regions of Vβ-chains sequenced before and while on therapy. The number of TCRs sequenced in all samples analyzed was not significantly different.

ImmunoMap was used to compare the TCR repertoire before and after 4 weeks of anti–PD-1 therapy. Weighted repertoire dendrograms revealed distinct differences between responders and nonresponders. Dominant motif analysis showed that patients who had more dominant motifs prior to initiation of therapy had more favorable responses to therapy (Figure 9.9)**.** Additionally, those patients who had a decrease in their TCR diversity score on therapy had more favorable outcomes to therapy. In contrast, no clinically relevant signature could be found by Shannon entropy calculations. Thus ImmunoMap analysis was superior in its ability to reveal repertoire characteristics that could predict response to therapy after only four weeks of treatment.

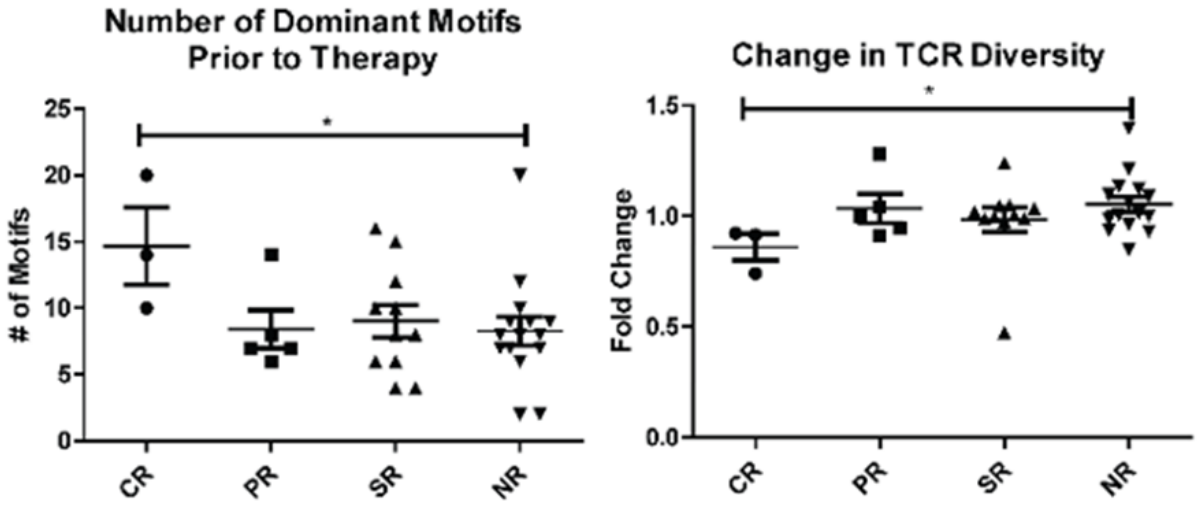

Figure 9.9 TCR Repertoire Analysis of Patients Undergoing α-PD1 (Nivolumab) Therapy shows differences in repertoire between responders and non-responders.

Dominant Motif and TCR Diversity analysis from lymphoctyes collected pre and post 4 weeks of therapy in TILs.

9.3 Discussion

Here we introduce ImmunoMap, a bioinformatics approach to analyze TCR repertoire sequence data based on beta chain CDR3 sequence overlap, and used it to characterize repertoire changes in responses to model murine tumors and in patients undergoing immunotherapy for melanoma. By combining information about sequence relatedness and frequency, ImmunoMap allows an intuitive appreciation of TCR repertoire characteristics that reconciles the structure and function of the repertoire.

ImmunoMap analysis comparing model neo-antigen (K^b-SIY) and self antigen (K^b-TRP2) showed distinct differences in the naïve repertoire to these two different antigens. Although

interesting, the conclusions of this analysis cannot be expanded to all foreign vs self-antigens. The presence of multiple dominant motifs in the K^b-TRP2 response in combination with greater clonality of motifs suggests that central and peripheral tolerance mechanisms limited the clonal responses. Shown by distinct and more frequent clones occupying a larger portion of the expanded TRP2-specific repertoire. High affinity self-reactive clones that would produce a dominant motif during T cell expansion, with TRP2-specific TCRs would either be removed during central thymic development or tolerized in the periphery, explaining the inability to find more numerous TCR sequences per dominant motif[78–80]. Because our analysis was conducted on expanded antigen-specific populations, our results demonstrate the "expansion potential" of the antigen-specific T-cell repertoire for a model neo-antigen and shared tumor antigen in the setting of both naïve and tumor-bearing animals. It is possible that the limited TCR relatedness of TRP2 responses could be due to the lower precursor frequency in naïve animals, and the T cells that have the ability to expand do not cluster in the same dominant motif due to lower initial cell frequency. The impact of pooling animals prior to expansion and sequencing must also be considered. In this scenario, one could be selecting for "public" clones and possibly enriching for these parts of the repertoire over "private" clones, unique to each animal and observing a diverse motif of expanded KbTRP2 TCRs suggests the T cell population has been tolerized. Although individual mice are genetically identical, VDJ recombination occurs as an independent process in each animal and the primary TCR repertoire capable of responding to a given antigen could vary between individual animals yet by looking for clones with expansion ability we are selecting for the dominant, public clones. Therefore, the effects on shaping of the repertoire for self and neo-antigen antigens may be most relevant to "public" or conserved sequences. Finally, the higher TCR diversity score of K^b-TRP2 alongside with the higher number of dominant motifs

suggests that the immune system has created multiple CDR3 sequences to bind to cognate antigen/MHC complex. With the high-affinity CDR3 sequences are removed from the repertoire, the alternative antigen specific CDR3 sequences have lower affinity but may not share structural similarities.

Although prior work on TCR clustering has focused on understanding the structural aspects that confer antigen-specificity[71,72], the effects of perturbations to the immune system on antigen-specific responses has not been studied. With ImmunoMap, we studied the changes in repertoire in response to tumor. We observed that the effects of tumor on the anti-self-K^b-TRP 2 peptide repertoire indicate that tumors exert greater pressure on the self- than on the foreign-antigen. Not only did the presence of the tumors correlate with an increase the clonality of the response to self, via decreases in the number of dominant motifs and increases in their contribution to the net response, but tumor-bearing mice could shift their response to different motifs. Additionally, the differences in repertoire characteristics among various lymphoid organs for the two different model antigens indicates that tumors effectively eliminated the expansion of certain clones from its microenvironment. The consequences of these findings are relevant to both antigen-discovery and targeting for immune therapies related to treating cancer. Due to limitations of personalized antigen-specific therapy, targeting shared antigens like MART1, a self-antigen specific for melanocytes, has been a mainstay of antigen-specific cancer immunotherapy[81–83]. This approach has typically relied on TCR transgenic models in which a single TCR clone is chosen as the source for the antigen-specific receptor[84–86]. Given our analysis, several problems with this approach become apparent: (1) antigen-specific expansion not only generates a diversity of TCR sequences but one that spans the entire sequence distance of the naïve repertoire, (2) self-antigen expansion represents a limited repertoire and arsenal

against a given epitope due to effects of tolerance, and (3) the tumor can exert pressure on the self-antigen–specific immune response in a more profound way than in the case of a foreign antigen. Our findings call into question the approach of using self or over-expressed antigens as targets for immune therapy and highlight the importance of exploring responses to neoantigens, novel MHC-specific epitopes that arise from mutations in a patient's individual malignancy[21,87–89].

We also have used ImmunoMap algorithms to understand mechanisms of successful immune responses to cancer against 4T1, a murine breast cancer model[89]. In that model, when analyzing TILs from animals treated with anti–CTLA-4, radiation, or the combination of these therapies, we found that the TCR structural repertoire before therapy from TILs was highly conserved, seemingly targeting a single antigen, whereas after combination therapy, the structural response broadened within the TILs and each individual animal developed its own uniquely expanded repertoire.

Finally, we used ImmunoMap to study TILs from clinical trial specimens to determine if structural diversity is an important parameter in determining successful immune responses to cancer immunotherapy. Our analysis revealed that patients who had more dominant motifs prior to therapy responded more favorably to therapy. Additionally, the change in TCR diversity suggest that patients who respond to therapy converge on a solution of successful TCR sequences and thus their repertoire is actually less diverse after therapy. In contrast to previous work by Madi *et. al* that demonstrated a structural broadening of the peripheral repertoire to anti–CTLA-4 therapy in melanoma patients, but did not correlate this finding with response, we focused our analysis on studying changes in the repertoire within the TILs and could determine structural signatures of response[73]. Although our findings are significant, we note the scope of

the clinical trial was limited, which impacted the distribution of clinical responses. Nevertheless, taken together, ImmunoMap analysis revealed that patients with a broader repertoire prior to therapy have a higher probability of expanding effective TCR sequences and converging on selected TCR clones on therapy.

ImmunoMap not only has potential for the clinical monitoring of patients on therapy, through predictions of their likelihood to respond, but enables the acquisition of biological insights about antigen-specific immune responses that could alter current immune therapies.

9.4 Conclusion

In conclusion, we have created a new method to analyze the polyclonal TCR repertoire of antigen specific T cell responses. Instead of monitoring individual clonotypes of a T cell response, the entire polyclonal response and the frequency of multiple clones gives a more detailed description of the overall T cell response. By using the ImmunoMap algorithm to categorize similar TCRs, TCR motifs structures can be identified for groups of T cell clones and create quantitative comparisons between entire T cell repertoires. Using this approach, we have shown different tumor antigens change their TCR motifs structure suggesting immunoediting of the tumor upon anti-tumor T cell responses on self tumor antigens but the foreign antigen remains unchanged. Also, ImmunoMap analysis tool to create T cell diversity as a biomarker for immunotherapy response and hopefully identify a predictive marker of response based on initial TCR repertoire characteristics.

9.5 Experimental Methods

Mice: C57BL/6j mice were purchased from Jackson Laboratories (Bar Harbor, ME). All mice were maintained according to Johns Hopkins School of Medicine IACUC 4-5 mice (gender and age matched) were used and pooled for each stimulation condition, based on previous T-cell expansion experiments, and each stimulation and sequencing run was performed once. Mice were randomly selected for naïve or tumor-bearing treatments and principal investigator was blinded to which mice received tumors. Murine experiments for naïve and tumor-bearing spleens were duplicated in separate pools of animals to demonstrate reproducibility of antigen-specific repertoire characteristics (Supplementary Fig. S7).

Preparation of MHC-Ig dimers and nano-aAPC: Soluble MHC-Ig dimers, K^b-Ig, was prepared and loaded with peptides as described[90]. Nano-aAPC were manufactured by direct conjugation of MHC-Ig dimer and anti-CD28 antibody (37.51; Biolegend) to MACS Microbeads (Miltenyi Biotec) as described previously[91].

Lymphocyte isolation: Mouse lymphocytes were obtained from homogenized mouse spleens after hypotonic lysis of RBC. Cytotoxic lymphocytes were isolated using a CD8 magnetic enrichment column from Miltenyi Biotec (Cologne, Germany) following the manufacturer's instructions. Lymphocytes from lymph nodes were obtained from homogenized inguinal lymph nodes and enriched with nano-aAPCs and plated for 7 days. For tumor-bearing animals, murine melanoma cell line B16-SIY, obtained with the consent of Tom Gajewski (The University of Chicago, IL, USA) through Charles Drake in 2011, and re-authenticated in the past year by flow cytometry, was injected subcutaneously after 5 days of culture, measured by calipers and harvested when tumors reach over $50mm^2$. The B16-SIY cell line is a tumor model modified to express SIY, a completely foreign epitope to the murine B6 background. In naïve mice setting

experiments, it was used as a model foreign antigen such as would be a viral epitope and in tumor-bearing animals serves as a tumor antigen. Tumor-infiltrating lymphocytes were obtained from tumors by manual digestion and washing, a density gradient centrifugation (Lympholyte Cell Separation Media, Mouse, Cedar Lane), and then tumor cells plated for 3 hours at 37°C and lymphocytes washed off and plated with nano-aAPCs ($1.25x10^9$ particles/mL). All cell lines underwent testing for mycoplasma contamination.

Enrichment and expansion: Nano-aAPC were stored at a concentration of 8.3 nM (5×10^{12} particles/mL), and all volumes refer to particles at this concentration. Ten million $CD8^+$-enriched lymphocytes at ~10^8 cells/mL were incubated with 10 μL of nano-aAPC for 1 hr at 4 °C, for an approximate bead:cell concentration of 5000:1. Cell-particle mixtures were subsequently passed through a magnetic enrichment column, the negative fraction was collected and the positive fraction eluted. Positive fractions were mixed and cultured in 96-well round-bottom plates for 7 days in complete RPMI-1640 medium supplemented L-glutamine, non-essential amino acids, vitamin solution, sodium pyruvate, β-mercaptoethanol, 10% FBS, ciproflaxin, and 1% T-cell growth factor, a cytokine cocktail derived from stimulated PBMC as described in[92], in a humidified 5% $C0_2$, 37 °C incubator for 1 week. Specificity of CTLs was monitored on day 7, by FACS analysis following LIVE/DEAD cell stain (Thermo Fisher), anti-CD8 (BD Pharmingen, Cat# 553035, 53-6.7), and dimeric MHC-Ig staining. The number of antigen-specific cells was calculated by multiplying the number of total T cells by the fraction of $CD8^+$ and antigen-specific T cells; the fraction of antigen-specific cells was calculated after subtracting the non-cognate MHC staining from cognate MHC staining.

Sorting and sequencing of antigen-specific $CD8^+$ T cells: Following LIVE/DEAD cell stain (Thermo Fisher), anti-CD8 (BD Bioscience), and dimeric MHC-Ig staining, cells were sorted by

gating on cells with cognate Dimeric MHC-Ig staining over non-cognate staining. Antigen-specific $CD8^+$ T cells were sent directly for CDR3 β-chain sequencing by Adaptive Biotechnologies.

In vitro *nano-aAPC functionality assay*: 7 days following enrichment and expansion antigen specificity is confirmed by intercellular cytokine staining. Briefly, RMA-S, given by Michael Edidin (Johns Hopkins University, MD, USA) in 1996 (reauthenticated in the past year by peptide stabilization assays and cultured for 7 days prior to use) are peptide pulsed (10 μM) overnight at room temperature with relevant or no peptide and mixed 1:2 RMAS:T-cell ratio with expanded T cells. Unpulsed RMAS cells were used as background stimulation. After 6 hours, cells were washed twice with FACS wash buffer and then stained with viability dye and anti-CD8 for 20 minutes. Cells were then fixed and permeabilized with the Cytofix/Cytoperm kit (BD Biosciences) following the manufacturer's protocol. Anti-TNFα (Biolegend, Cat# 506324, MR6-XT22) was added to the cells and stained for an hour.

Precursor frequency assessment: On day 0 following $CD8^+$ T-cell isolation from splenic cells, $CD8^+$ T cells were stained with LIVE/DEAD cell stain (Thermo Fisher), anti-CD8 (BD Bioscience), and dimeric MHC-Ig staining viability stain with either unloaded or peptide-loaded MHC-Ig. Cells gated on Live cells and anti-$CD8a^+$ staining.

Collection of TILs from patients undergoing α-PD1 therapy: Eighty-five patients, providing written consent, were accrued to a multi-arm, multi-institutional, institutional-review-board-approved, prospective study (BMS-038) to investigate the pharmacodynamic activity of nivolumab. All patients received nivolumab (3 mg/kg Q2W) until progression for a maximum of 2 years. Tumor samples were collected prior to and four weeks after initiation of nivolumab therapy. The samples were stored in RNA*later*®(Ambion). 34 patients permitted TCR

sequencing, and DNA was extracted and submitted to Adaptive Biotechnologies for survey level TCR β-chain sequencing[93,94]. Clinical response was assessed via CT scan after 24 weeks of therapy.

Deconvolution methods: Due to the fact that animals were pooled together on day 0 prior to expansion of antigen-specific cells, there was only one sequencing run. In order to determine the variance of calculated indicators of the repertoire, the reads from the sequencing file were randomly distributed into the number of bins corresponding to the number of animals that went into the experiment. This method of random deconvolution assured that the variance of the indicator by random chance was not greater than the difference observed between conditions.

Weighted repertoire dendrograms: For the antigen-specific sequencing, productive sequences with a frequency > 0.01% were taken for analysis. For anti–PD-1 clinical trial analysis, Adaptive Biotechnologies' files were first filtered to only include sequences with reads greater than or equal to 5 and then top 40% of response was taken for analysis. Sequence distances were calculated based on sequence alignments scores using a PAM10 scoring matrix and gap penalty of 30. Distance matrix was used to create a dendrogram using the Bioinformatics toolbox in MATLAB. Circles were overlaid at the end of the branches corresponding to the CDR3 sequences with diameters proportional to the frequency of the sequence. When using the terminology "weighted repertoire dendrogram," this does not infer that the distance matrix used to create the dendrogram is weighted; rather, the dendrogram is visually 'weighted' by frequency.

Dominant motif analysis: Using the cluster function in MATLAB toolbox, dendrogram was divided into homologous clusters using a homology threshold obtained from analyzing an unexpanded adult $CD8^+$ T cell population from a C57BL/6 animal (Supplementary Fig. S1).

Clusters whose average sequence distance within cluster <= threshold and met a certain frequency cutoff (3% - Supplementary Fig. S1 were denoted as "Dominant Motifs." Cluster frequency was lowered to 1% for α-PD1 clinical trial analysis but held consistent across all patients due to the fact that this was not a single antigen-specific population of cells.

Singular and novel clone analysis: In order to define singular clones, a matrix was setup to calculate the mapped sequence distance of every unique combination of sequences in the repertoire. Using standard matrix operations within MATLAB, a singular clone was defined as a clone whose frequency was 10x the sum of all other homologous clones. Homologous clones were those who had a sequence distance determined from the dominant motif analysis. In order to define novel clones, the same approach was used, but the matrix was setup in that it calculated the mapped sequence distance of every unique combination of sequences between the two repertoires being compared. A novel clone was defined as a clone whose frequency was 10x the sum of all homologous clones in the other sample.

TCR diversity score: This measurement of diversity was calculated in a similar method as the singular & novel clone analysis. An initial matrix is created where the mapped sequence distance is calculated for every unique combination of sequences in the repertoire. Then the average of the unique combination calculations is taken, weighted by reads, and reported as the TCR diversity score. Additional details of the algorithm behind this calculation are shown in Supplementary Fig. S6.

Shannonntropy calculations: Calculation of Shannon entropy was completed by the following formula where p_i represents the frequency of each amino acid sequence and n represents the total number of sequences present in the response:

$$Shannon's\ Entropy = \sum_{i=1}^{n} p_i \ln(p_i)$$

Statistical methods: No specific statistical method was used to determine sample size for the stimulation cohorts. Two-tailed *t*-tests were used as provided by GraphPad Prism 5 software for all comparative statistics given we expect normal distributions across all experiments.

Code availability: In order to use the ImmunoMap algorithms, we have developed a MATLAB-based Graphical User Interface (GUI) that can be found along with the source code at https://github.com/sidhomj/ImmunoMap. Supplementary Fig. S8 demonstrates the use of the GUI.

Data Availability: TCR β-chain sequencing raw data for the murine experiments is found in supplementary materials.

10 Commensal bacteria stimulate anti-tumor responses via T cell cross-reactivity

10.1 Introduction

The basis for differential patient responses to cancer immunotherapy involves many biological processes including: genetic variability amongst different patients, differences in tumor mutational load, and differential microbiome composition. Higher tumor mutational load is correlated with beneficial responses to checkpoint blockade outcomes in melanoma and non-small cell lung carcinoma[17]. Mechanistically mutations in the tumor can result in novel peptides, called neoantigens, which can be targeted by T cells. These neoantigen specific responses are critical for tumor clearance after checkpoint blockade immunotherapy (CPI)[14,95]. In addition to the quantity of potential neoantigens, several studies have also considered their "quality" to help identify which patients will be responsive to CPI[55,56].

Another important parameter for patient outcome is the gut microbiota. Responders to checkpoint blockade have a different gut bacterial composition than non-responders[49,96], however the potential mechanisms underlying antitumor effects are unclear. Evidence has emerged that the gut microbiota modulates the efficacy of various tumor therapies possibly by engaging the innate and/or adaptive immune systems[97,98,10]. Retrospective analysis of pancreatic cancer long-term survivors revealed that some high quality neoepitope responses bear sequence homology with pathogenic or commensal bacteria[56]. However, the effect of homologous epitopes between the tumor and microbiota on T cell populations is unknown. Therefore, identifying antigens expressed by microbiota and their potential cross-reactivity with T cells recognizing tumor-specific neoantigens will provide insight into tumor-reactive T cell populations that can be activated by cancer immunotherapy. However, mechanistic studies must address how cross-

reactive T cell populations react to tumor cells and the effect of bacterial colonization on the cross-reactive T cell populations. These studies will provide insight into how antigen mimicry between the commensal bacteria and tumor antigens can lead to beneficial anti-tumor responses.

Here, we identify an epitope, SVYRYYGL (SVY), found in the *B. breve* genome with homology to the tumor model neoepitope antigen SIYRYYGL (SIY) expressed in B16.SIY tumors. Molecular dynamics simulations show that SVY peptide loaded on the murine H2-Kb MHC binds to a model TCR specific for the KbSIY complex, the 2C transgenic TCR but with an altered configuration. Heterogeneous $CD8^+$ T cell populations, expanded from wild type C57BL/6 animals specific for either SIY or SVY, cross-react with both the bacterial and tumor antigens. Indeed, Bifidobacteria colonization, as seen by differences in C57BL/6 mice obtained from different suppliers, Jackson versus Taconic, boosts expansion of SVY specific T cell populations *in vitro* and differences in commensal bacteria influence the SVY population in vivo. In addition, immunization of Taconic mice with the SVY antigen led to activation of SVY-specific T cells that cross-react and kill SIY-pulsed target cells in vivo. Furthermore, C57BL/6 mice, obtained from different commercial sources, have differences in their anti-tumor response to B16.SIY tumors which grew more slowly in Jackson than Taconic mice. C57BL/6 mice also have an altered TCR repertoire dependent on their source. Finally, in an adoptive cellular therapy (ACT) treatment model, SVY expanded T cells target SIY-expressing tumor cells in vivo, inhibit tumor growth, and extend survival. These studies, for the first time, mechanistically identify that commensal bacteria can augment anti-tumor immunity by amplifying T cells that cross-react with model tumor neoantigens.

10.2 Results

Results.

10.2.1 B. breve Contains a Peptide Epitope (SVY) that is Homologous to the SIY Epitope

To identify commensal bacteria epitopes that may influence the B16.SIY anti-tumor response, we conducted a search of microbial genomes with the Basic Local Alignment Search Tool (BLAST) using the SIY peptide sequence as the query. Genetic alignment (Figure 10.1, a) identified a single peptide sequence, SVYRYYGL that varies by only one amino acid from the murine H2-Kb MHC restricted model neoepitope "SIYRYYGL" (SIY), [valine (Val) versus isoleucine (Ile) at position two]. The SVY epitope sequence, derived from the *B. breve* exopolysaccharide biosynthesis protein, has a 126-fold stronger predicted binding constant for H2-Kb compared to the next highest predicted epitope sequence from the EBP protein (Figure 10.1, a). Processing of the *B. breve in vitro* was studied by incubating heat-killed *B. breve* with splenocytes and the resultant antigen-specific T cell expansions were analyzed (Figure 10.1. b). By day eleven, approximately 3.5% of $CD8^+$ T cells were cross-reactive with the H2-Kb SIY complex (KbSIY) (Figure 10.1, b). In contrast, a control commensal bacterium, *Lactobacillus rhamnosus*, did not stimulate a KbSIY cross-reactive response. Thus, *B. breve* expresses an antigen that can be processed and presented and stimulate KbSIY cross-reactive $CD8^+$ T cells.

Processing of the *B. breve* bacterium *in vitro* was studied by incubating heat-killed *B. breve* with splenocytes and the resultant antigen-specific T cell expansions were analyzed (Figure 10.1, b). By day eleven, approximately 10% of CD8+ T cells were cross-reactive with the H2-Kb SIY complex (KbSIY). In contrast, a control commensal bacterium, *Lactobacillus*

rhamnosus, did not stimulate a KbSIY cross-reactive response. Thus, *B. breve* expresses an antigen that can be processed and presented, which stimulate KbSIY cross-reactive CD8 T cells.

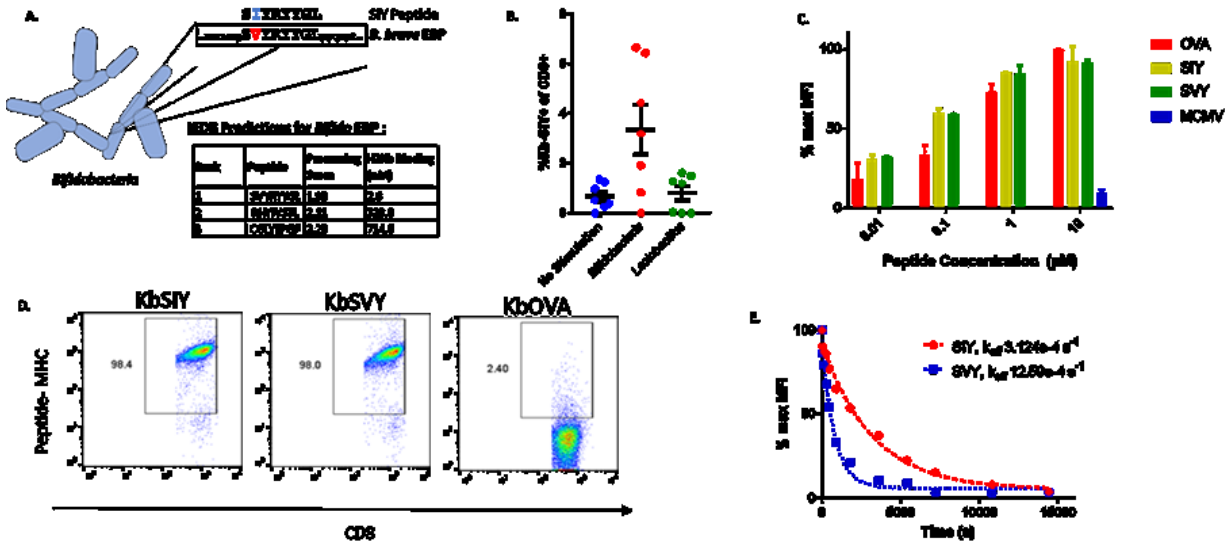

Figure 10.1 Commensal bacteria *Bifidobacterium breve* harbors the CD8$^+$ T cell epitope SVY.

A) Genetic map of *B. breve*, highlighting the homology of a peptide derived from *B. breve* exopolysaccharide biosynthesis protein (EBP) to the model epitope KbSIY. Listed in the table are the top three predicted H2-Kb restricted epitopes from the EBP protein using the Immune Epitope Database (IEDB) prediction algorithm. (B) Jackson C57BL/6 mice splenocytes and mesenteric lymph node cells were cultured with or without heat-killed bacteria and tested for SIY-specific T cell expansion by staining with SIY peptide loaded-Kb-Ig dimer on day 11. Live, CD8$^+$ lymphocytes were analyzed by flow cytometry for KbSIY binding, frequency determined by subtracting unloaded Kb-Ig staining frequency. Error bars indicate SEM. p-value = 0.011 by One-way ANOVA and Dunnett's post-hoc test for multiple comparisons. N=7. (C) MHC stabilization assay; RMA-S cells were incubated overnight with peptide as indicated. Cell surface expression of H2-Kb was determined by flow cytometry. Reported values are relative to the H2-Kb median fluorescence intensity (MFI) observed with 10 uM OVA peptide. mCMV, a non-

Kb-restricted peptide, was used as a negative control. N=3, error bars indicate SEM. (D) $CD8^+$ T cells were isolated from the spleens of 2C TCR (SIY-reactive) transgenic mice and stained with 1 ug of cognate KbSIY-Ig, cross-reactive KbSVY-Ig, or irrelevant KbOVA-Ig. (E) Competitive off-rate binding assay of 2C $CD8^+$ T cells with KbSIY or KbSVY peptide MHC dimer over time by the addition of 1B2 TCR binding antibody. Cells were gated on $CD8^+$. Cells were stained with KbOVA as negative control or experimental pMHC to gate on antigen specific cells over time. This competitive binding assay was performed twice, with similar K_{off} rates determined each time.

To characterize the biophysical interaction of the antigens, we compared their ability to stabilize the MHC Kb complex. Both SVY and SIY peptides stabilized the H2-Kb MHC molecule to a similar extent, with half-maximal stabilization seen at approximately 100 nM (Figure 10.1, c) indicating that SIY and SVY bind H-2 Kb MHC with equal affinity. Using T cells from the 2C transgenic mouse, which recognize the KbSIY peptide MHC (pMHC) complex, the cross-reactive SVY antigen and the cognate SIY peptides stimulated 2C cytotoxic lymphocytes (CTLs) to a similar extent as measured by proliferation ability (data not shown). However, differences were seen in the overall binding affinity of the pMHC complexes to 2C CTL. Off-rate assays revealed that the H2-Kb SVY complex (KbSVY) has a 4-fold faster k_{off} rate and overall lower affinity for the 2C T cells than does KbSIY (Figure 10.1, d). This was also seen functionally, as lower frequency of cytokine producing cells were seen over a wide range of peptide concentrations in response to SVY and SIY peptide-based stimulations (Figure 10.1, f). Thus, it appears that, with similar peptide stability in the MHC molecule, the peptide configuration in the MHC complex may be different due to the single amino acid change, thus altering the 2C TCR affinity for the Kb-peptide complex.

10.2.2 Modeling the Interaction Between KbSVY and KbSIY with the 2C TCR

To better understand potential cross-reactivity at the TCR level, we investigated the change in Kb-peptide-TCR binding for the Val to Ile mutation at position 2 in the epitope sequence using molecular dynamics (MD) simulation. Figure 2a shows the constructed three-way binding complex HLA-epitope-TCR, using the published individual X-ray structures of the Kb-epitope and TCR[99,100] (see more details in methods). Although the two epitope sequences differ only in the second position, the root-mean square deviations (RMSD) per residue calculated between the highest populated binding pose of each epitope shows that Tyr3 (4.6 Å), Arg4 (3.6 Å), and Leu8 (4.3 Å) deviate more than the mutated residue (Ile2/Val2) (2.9 Å) (Table 1). The overlapping binding poses of KbSIY and KbSVY show that the side chains of the three residues with larger RMSDs deviate between the two epitopes. While the binding poses of the two epitopes differ from each other, the binding poses from the same epitope are generally consistent among the top five populated clusters, which account for over 98 % of the MD trajectories. Through conducting a contact analysis, we found that the contacts at the interface between the peptide epitope, Kb, and TCR in the three-way complex vary between epitopes due to conformational changes. The frequencies of either Kb or TCR atoms, making close contact (less than 6 Å) with the epitopes in the MD trajectories, are presented on the surfaces of Kb and TCR. The difference in SIY and SVY contact frequency (Figure 10.2, b) shows the contact frequency on both the Kb and TCR surfaces. The contact frequency difference is greater than 80 % at several regions on the TCR-epitope interface, specifically where TCR atoms contact Tyr3, Arg4, and Leu8 of the epitope. These data are consistent with the RMSD analysis, shown in Table S1, indicating that the structures of the two epitopes deviate the most at these residues

(Figure 10.2, c). Meanwhile, the contact profile at the Kb-epitope interface is more similar between epitopes, without the large differences observed at the TCR-epitope interface, indicating the altered peptide configuration is mainly on the TCR side.

We next computed the binding affinity for each of two intermediate steps in the formation of the ternary complex, where each epitope is loaded onto the Kb protein, and then the Kb-epitope binary complex binds to TCR binds, using the free energy perturbation (FEP) method. We found a change in binding affinity (SVY → SIY) of 0.09 ± 0.36 and –1.2 ± 0.2 kcal/mol for the epitope loaded into Kb, and the subsequent binding to the TCR, respectively (Figure 10.2, d). The FEP calculation results indicate that the binding affinity of the SVY binding to H2-Kb MHC is similar to that of the SIY binding, however the binding affinity the KbSVY complex to TCR is somewhat weaker than KbSIY (about 2KT, or equivalent to ~7.6 fold difference in the binding equilibrium constant at room temperature). These results are in excellent agreement with the biophysical and functional data shown in Figure 10.1 c-e, indicating that epitopes indeed have similar binding affinity for Kb, but KbSVY has somewhat weaker interactions with the 2C TCR than KbSIY due to the altered peptide configuration. Thus, the processing and presentation of EBP from *B. breve* leads to a SIY cross-reactive response, and in fact the SVY antigen can load nicely onto the MHC molecule. However, the amino acid substitution alters TCR recognition creating a slightly lower biophysical binding of 2C TCR to p-MHC which may impact T cell population cross-reactivity.

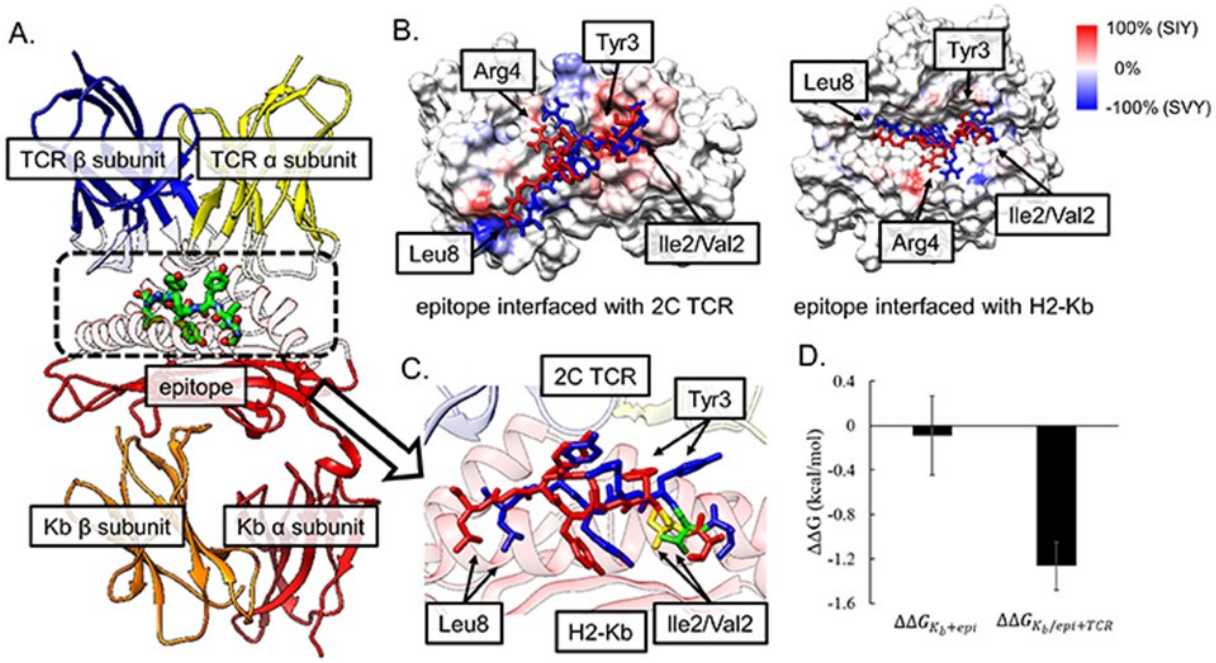

Figure 10.2 Modeling highlights differences in SIY and SVY binding to MHC and TCR

(A) Structure of the H2-Kb/epitope/2C TCR complex. The α and β chains of 2C TCR and H2-Kb are represented by ribbon models in yellow, blue, red, and orange, respectively, and are transparent at the epitope interface. The epitope in the box at the center with a dotted line, is represented by a stick model. (B) The difference in contact frequency between the SIY and the SVY epitopes on the 2C TCR-epitope (left) and the Kb-epitope (right) interfaces. The SIY and the SVY epitopes are colored in red and blue, respectively. The surfaces of TCR and Kb proteins are colored from blue to red, as the difference of the contact frequency is changed from -100 % (SVY) to 100 % (SIY). The red color indicates that protein atoms contact the SIY epitope more often than the SVY epitope, while the blue color does for the opposite. (C) A zoomed-in image of the binding poses of the

SIY (red) and the SVY (blue) epitopes, which are interfaced with H2-Kb and 2C TCR on the top and the bottom sides of the figure. The structure of each epitope is taken from the frame at the center of the most populated cluster in the MD trajectory. Ile2 of the SIY epitope and Val2 of the SVY epitope are colored in yellow and green, respectively. The α and β chains of 2C TCR and the α chain of H2-Kb are represented by ribbon models in yellow, blue, and red, respectively. (D) The relative free energies for the binding of the epitope to Kb ($\Delta\Delta G_{K_b+epi}$), and the binding of TCR to the Kb-epitope complex ($\Delta\Delta G_{K_b/epi+TCR}$), between the SIY and the SVY epitopes. Each free energy value was calculated by the FEP method.

sequence	Ser1	Ile2/Val2	Tyr3	Arg4	Tyr5	Tyr6	Gly7	Leu8
RMSD (Å)	2.45	2.94	4.56	3.63	2.18	1.56	2.24	4.32

Table 1 The RMSD per residue between the SIY and the SVY epitopes.

The protein structures were taken from the frame at the center of the highest populated clusters in the MD trajectories. The alpha carbons of H2-Kb and 2C TCR were aligned between two structures, then the RMSD was calculated for each residue between the SIY and the SVY epitopes.

10.2.3 KbSIY and KbSVY specific T cell populations are cross-reactive

To study cross-reactivity in endogenous, heterogeneous T cells populations, we analyzed SVY- and SIY specific T cells from naïve C57BL/6 mice. $CD8^+$ T cells from C57BL/6 mice were enriched and stimulated with KbSIY or KbSVY based artificial antigen presenting cells (aAPC). The resultant day 7 cultures represent a heterogeneous mix of $CD8^+$ T cells specific for each individual antigen, as previously described [4] (Figure 10.3, a). Expansion with KbSIY aAPCs led to approximately 50.4% KbSIY specific T cells as seen by cognate KbSIY dimer staining (Figure 10.3, b, top row, left-hand panel). These were cross-reactive with KbSVY dimer which had a similar 49.8% staining and an average expansion frequency of 36.4% (Figure 10.3, b, top row, middle panel). MFIs of the antigen reactive populations were 685 for the cognate KbSIY dimer and 549 (i.e.: ~20% lower) for the cross-reactive response to KbSVY pMHC (Figure 10.3, b, top row). Background noncognate staining was less than 1%. Similarly, expansion of T cells with KbSVY aAPCs led to a cognate KbSVY bound T cell population of 58.1% and a cross-reactive KbSIY bound population of 54.4% of $CD8^+$ T cells with similar MFIs and an average expansion frequency on of 31.7% (Figure 10.3, b, lower row).

Antigen-specific T cells were stained with varying concentrations of KbIg molecules to determine the IC50 of the expanded T cells for each peptide-MHC complex and overall T cell avidity (Figure 10.3, c). Similar to the findings from the 2C transgenic T cells, KbSIY expanded T cells had a higher IC_{50} (0.1ug) for KbSVY compared to KbSIY(0.01 ug) (Figure 10.3, c, top panel). Differences in overall TCR affinity were also seen functionally as KbSIY expanded T cells exhibited a lower trend of cytokine production for the cross-reacting KbSVY antigen re-stimulation (15% IL-2) than for the cognate SIY pulsed RMA-S cells (30% IL-2) but was not significantly different (data not shown).

Interestingly, T cells expanded with KbSVY based-aAPCs had equal affinity (0.1 ug) for both KbSVY and KbSIY pMHC-Ig complexes (Figure 10.3, c, lower panel) and KbSVY expanded T cells produced similar amounts of cytokines in response to both SIY and SVY stimulations (data not shown). Cross-reactivity was also tested by analyzing the ability of SVY-expanded cells to recognize naturally processed KbSIY antigen on B16.SIY murine melanoma cells. Recognition of the naturally processed tumor antigen SIY was seen by cytokine release (Figure 10.3, d). Therefore, heterogeneous KbSVY-specific T cells had equal affinity for both SIY and SVY and recognize SIY-expressing tumor cells. These data highlight the differences in T cell populations expanded by SIY or SVY antigens which result in subtle differences in the cross-reactive T cell responses. Together, this demonstrates the overall cross-reactivity of polyclonal, heterogeneous, T cell populations that recognize two distinct but closely related antigens.

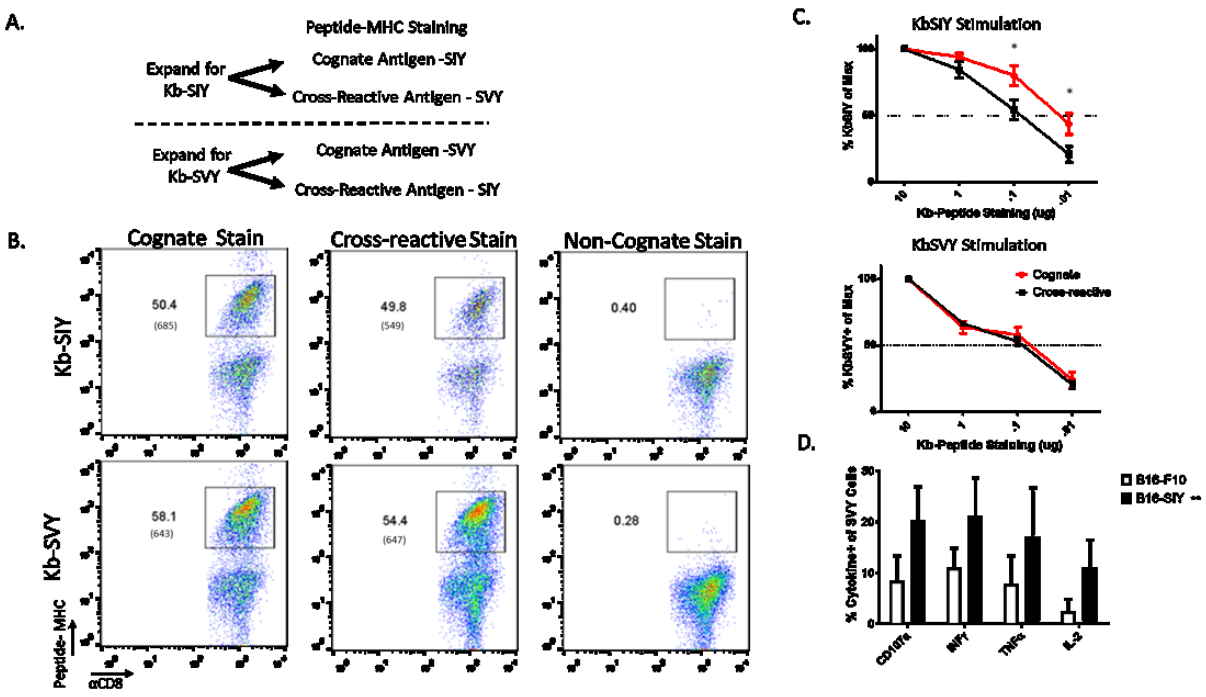

Figure 10.3 KbSVY and KbSIY specific T cells are cross-reactive.

(A) Schematic for isolation, expansion, and staining of antigen specific T cells from mouse splenocytes. Nanoparticles tethered to both peptide-Kb complexes and agonistic anti-CD28 antibodies were used as artificial antigen presenting cells to enrich and expand antigen-specific T cells. Expanded T cells were then stained for SIY or SVY epitope reactivity. (B) Representative flow cytometry results of KbSIY and KbSVY staining of antigen-specific $CD8^+$ T cells enriched from Jackson C57BL/6 mouse splenocytes and expanded for seven days. Cells were gated on live, $CD8^+$ cells. (C) Jackson C57BL/6 mouse splenocytes were isolate and expanded as in in A. KbSIY stimulations top and KbSVY stimulations below. On day seven, $CD8^+$ T cells were harvested and stained with a titration of pMHC-Ig as indicated and analyzed by flow cytometry. Results are reported as percent peptide-MHC positivity relative to that observed at 10 ug pMHC. KbSIY stimulations have a difference in cognate (red) and cross-reactive (black) binding with a p-value = 0.016 by 2 way ANOVA Bonferroni post hoc test for multiple comparisons.

KbSVY stimulations shows no difference. p = 0.016 N=3 for each antigen expansion. Error bars indicate SEM. (D) KbSVY-reactive T cells were isolated from Jackson C57BL/6 mouse splenocytes and expanded for seven days as in A. T cells were then stimulated with B16.SIY or parental B16.F10 tumor cells and measured for cytokine response by intracellular cytokine staining. N=3, p=0.0038 by 2-way ANOVA for B16.SIY and B16.F10 response. Error bars indicate SEM.

10.2.4 Bifidobacterium colonization enhances SVY-specific T cell expansion.

Previously commensal Bifidobacterium was shown to promotes antitumor immunity and the bacterium associated with anti-tumor response was most similar to B. breve, B. longum, and B. adolescentis (99% identity)[10]. Based on the sequence homology with the cross-reactive antigen between B16SIY and B. breve (Figure 10.1, a), we focused our studies on the SVY antigen and examined the presence or absence of Bifidobacterium in mice obtained from Jackson labs or mice obtained from Taconic, lacking all Bifidobacterium species[10] (data not shown). KbSVY induced more antigen-specific T cells with a higher average MFI from Jackson than Taconic mice (Figure 10.4, a). On average we were only able to expand approximately 8% SVY-specific T cells from Taconic mice versus 22% from Jackson mice and overall obtained about 4-fold less SVY-specific T cells from Taconic mice (Figure 10.4, b and c). A lower MFI, 109 versus 262 was also seen in cells stimulated from Taconic mice. Similarly, T cells from germ-free mice showed reduced frequency and total number of SVY-stimulated cells compared to Jackson mice (data not shown).

Overall KbSVY-specific effector T cells from Taconic mice had a lower TCR avidity compared to KbSVY-specific T cell populations from Jackson mice (Figure 10.4, d). However,

KbSVY-specific T cells from both populations produced cytokines upon re-stimulation with SVY peptide loaded RMA-S cells (data not shown). The impact of *Bifidobacterium* colonization was also seen in analysis of SVY-specific precursory frequency. Jackson mice trended to have more KbSVY specific splenocytes compared to Taconic mice (Figure 10.5). Thus *B. breve* exposure increases the expansion capacity of KbSVY-reactive cells leading to higher affinity responses and more robust KbSVY T cell expansion.

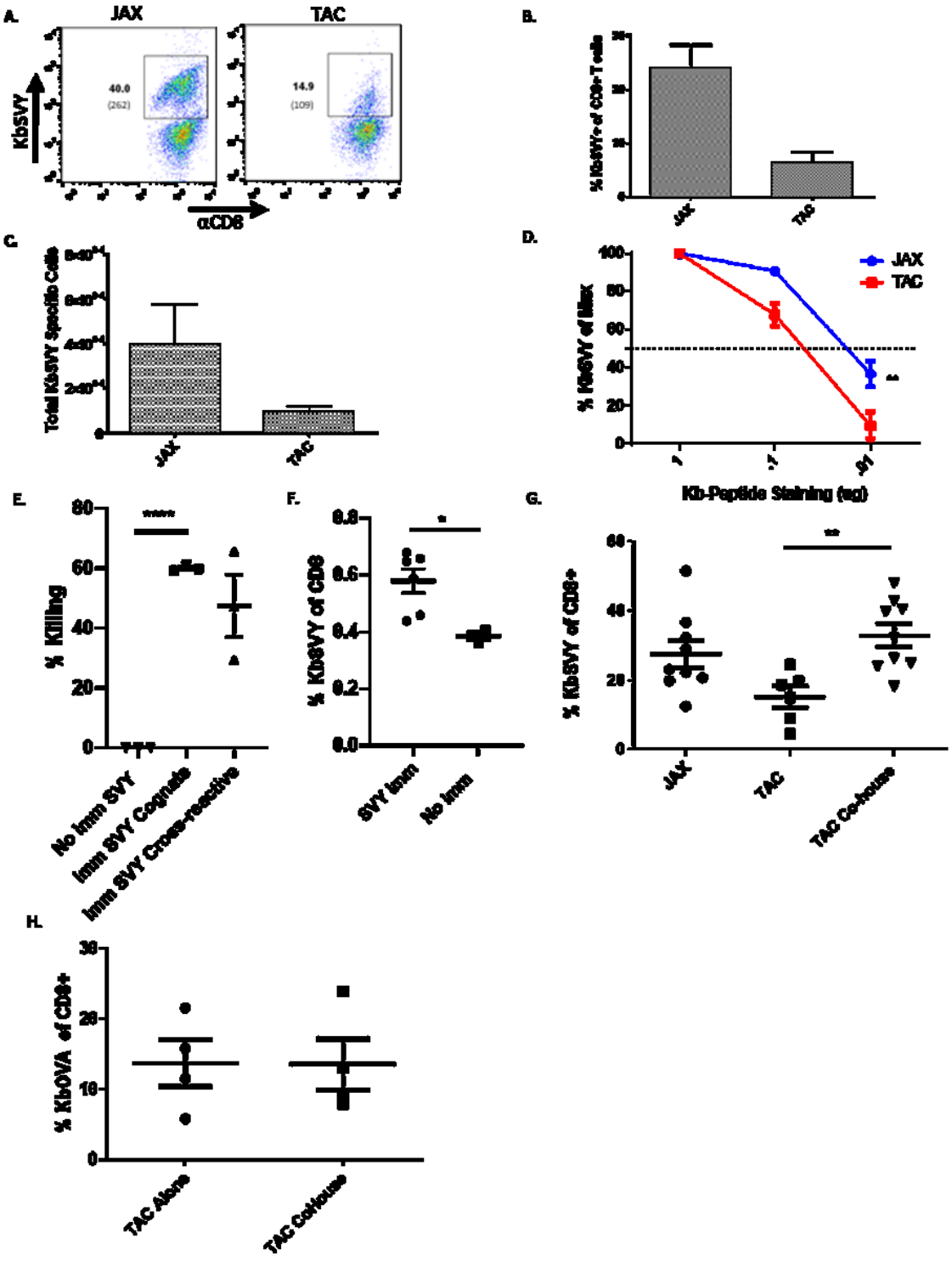

Figure 10.4 SVY antigen in *B. breve* bacteria stimulates an immunogenic T cell response.

(A) $CD8^+$ T cells were isolated and expanded from Jackson and Taconic mouse splenocytes with KbSVY aAPCS as in 3A. Cells were harvested and stained for antigen specificity on day seven. Representative results from one of 5 independent experiments are shown. Gating: live, $CD8^+$ cells. (B) $CD8^+$ T cells were harvested and expanded from Jackson and Taconic mouse splenocytes with KbSVY aAPCs and stained for KbSVY reactivity. The average percent KbSVY-positivity values from five independent experiments are presented. Significance was measured by a one-tailed t test ($p>0.005$). Error bars indicate SEM. (C) Total cells numbers for $CD8^+$ T cells enrichment and expansion with KbSVY aAPCs, graph represents 5 independent experiments. Significance measured by one-tailed t test ($p=0.08$) Error bars indicate SEM. (D) Antigen-specific $CD8^+$ T cells were isolated and expanded from Jackson and Taconic C57BL/6 mouse splenoctyes using KbSVY aAPC particles. On day seven, cells were harvested and stained with a titration of KbSVY as indicated and analyzed by flow cytometry. Gating: live, $CD8^+$ cells. Results are reported as percent peptide-MHC positivity relative to that observed at 10 ug pMHC. Jackson (blue) and Taconic (red) peptide stains were compared at a given concentration via 2-way ANOVA and Bonferroni post hoc test for multiple comparisons. N=3 **$p<0.0071$. (E and F) Taconic mice were immunized by intraperitoneal injection of αCD40 on day -8 and subcutaneous injection of KbSVY on day -7. (E) On day 0, control or immunized mice were injected intravenously with CFSE-low (antigen loaded) and CFSE-high (no peptide) autologous splenocytes mixed at a 1:1 ratio. Spleens were harvested from mice on day 1 and the CFSE-low to CFSE-high ratio was analyzed by flow cytometry to determine *in vivo* antigen-specific killing. N=3 mice per group. $P<0.0001$ by two-tailed unpaired t-test. Error bars indicate SEM. (F) Taconic mice were immunized as described in E. The mice were sacrificed on day 1 and spleens and draining lymph nodes were harvested and

stained for KbSVY specificity. Gating: live, $CD8^+$ cells. p=0.019 by two-tailed upaired t-test. Error bars indicate SEM. (G) Jackson and Taconic C57BL/6 mice were either co-housed for seven days or housed with their respective littermates. $CD8^+$ T cells from splenocytes were isolated and enriched and expanded with KbSVY aAPCS. Cells were harvested and stained for antigen specificity on day seven. Antigen specificity was measured by subtracting the non-cognate (negative control) antigen reactivity. N=5 for Taconic Only, N = 8/group for co-housed animals. P value = 0.0014 by a one tailed t-test. Error bars indicate SEM. (H) Jackson and Taconic C57BL/6 mice were either co-housed for seven days or housed with their respective littermates. $CD8^+$ T cells were isolated and enriched and expanded with KbOVA aAPCS from splenocytes as a control antigen expansion. Cells were harvested and stained for antigen specificity on day seven. Antigen specificity was measured by subtracting the non-cognate (negative control) antigen specificity. N=4 No statistical difference between groups was seen. Error bars indicate SEM.

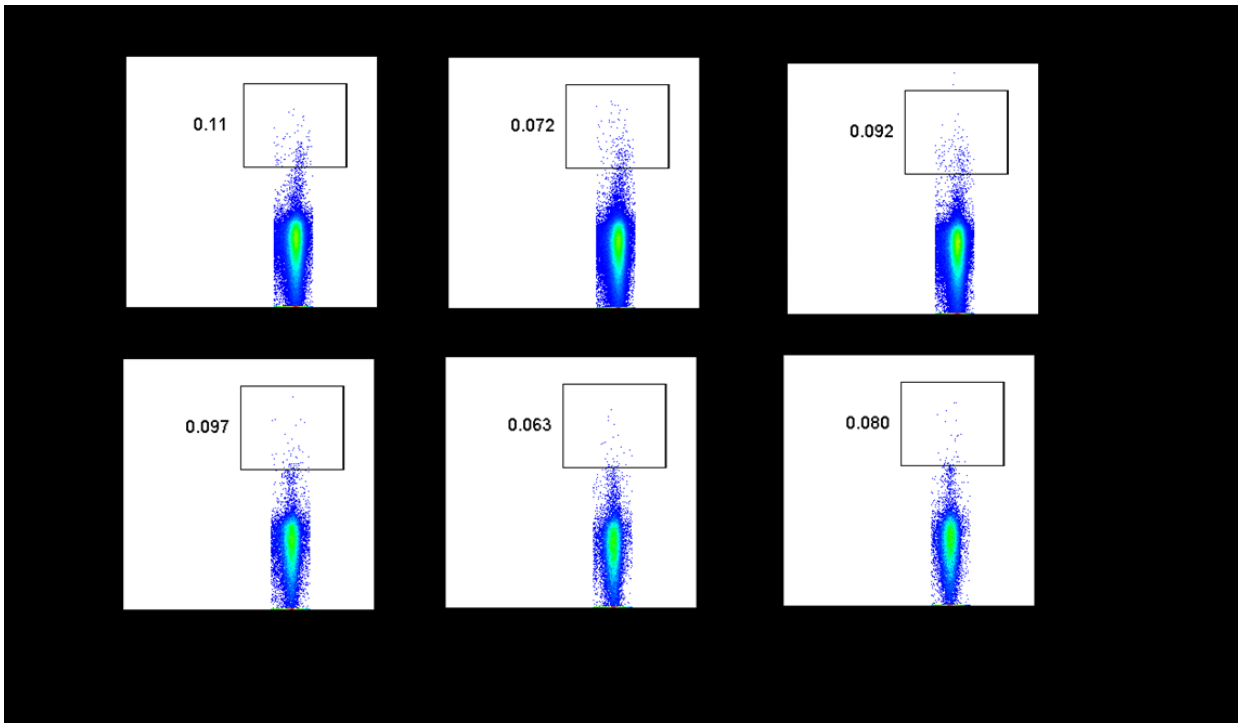

Figure 10.5 Jackson mice have a higher precursor frequency of KbSVY cells compared to Taconic mice.

Jackson and Taconic B6 mice splenocytes were isolated and stained with Live/Dead, CD8+ T cells, and 1ug of Kb-SVY dimer. Shown is the flow cytometry for 3 individual mice, cells gated on Live, CD8+ T cells.

10.2.5 SVY antigen is immunogenic and response is transferable via gut colonization.

If SVY is indeed a cross-reactive antigen, one should be able to immunize mice and test for cross reactive responses *in vivo*. Immunization of *Bifidobacterium* negative Taconic mice with SVY-loaded Kb complexes, as previously described[101], led to approximately 60% killing of SVY target cells *in vivo*, and a cross-reactive killing of approximately 50% of SIY-pulsed

targets *in vivo* (Figure 10.4, e). This was associated with an increased number of KbSVY effector T cells, from 0.4% to 0.6% (Figure 10.4, f). Thus, immunization with SVY elicited an *in vivo* response which was cross-reactive with SIY.

To investigate if the differences seen between Jackson and Taconic mice were due to microbiome, we studied the effect of microbiome transfer on the differences in SVY reactivity. Taconic mice co-housed with Jackson mice for a week had a significant increase in KbSVY expansion compared to Taconic mice that were not co-housed (Figure 10.4, g). This effect was SVY antigen-specific as control KbOVA responses were not influenced by co-housing before T cell expansion (Figure 10.4, h). This antigen specific T cell response based on microbiome colonization confirms $CD8^+$ T cells primed *in vivo* leads to increased expansion capabilities of SVY-specific T cells.

10.2.6 Jackson mice have delayed growth of B16.SIY melanoma tumors.

An implication that differences in the commensal bacteria between Taconic and Jackson mice drive a cross-reactive antigen-specific targeting of B16.SIY tumors is that there should be differences in tumor growth between the two strains of mice. Indeed B16.SIY tumors grew more slowly in Jackson mice than in Taconic mice (Figure 10.6, a) while B16.F10 tumors grew identically in the two strains (Figure 10.7). Of note, initially it appeared that tumors grew slightly more rapidly in Jackson than Taconic mice, (Figure 10.6, a), but by day 10 tumors in Jackson mice were consistently smaller than in Taconic mice. By day 24, Taconic mice had an average tumor size of approximately 146 mm^2, whereas Jackson mice were, on average, only 54 mm^2 and individual spider plots display the slower tumor progression (data not shown). By day 32, all Taconic mice succumbed to disease, while 71% of the Jackson mice survived (Figure 10.6, b).

We hypothesized that if differences between growth of B16.SIY in Jackson versus Taconic mice were driven by antigen-specific recognition of the SIY neoantigen, we should see evidence for pressure on SIY antigen in tumors from Jackson mice. Tumors were collected from individual mice and analyzed for GFP expression which is encoded by the same vector as SIY in the B16.SIY tumors. B16.SIY tumors in Jackson mice had a significant loss of GFP expression, from 50% in Taconic mice tumors to 10% in Jackson mice tumors (Figure 10.6, c).

Tumor infiltrating T cells in B16.SIY tumors show cross-reactivity for KbSIY and KbSVY in Jackson mice tumors. Jackson mice TILs were stained for KbSIY specificity or cross-reactivity for KbSVY and show significant staining over background KbOVA, which is not expected to be present in the B16.SIY tumor (Figure 10.6, d). Notably, when TCR sequencing was performed on TILs derived from B16.SIY tumors, we found that 22% of TIL clones were identical to those detected independently in splenocyte populations sorted and expanded by KbSVY. Overlapping TIL clones consisted of nine of the 198 KbSVY-reactive sequences identified by *in vitro* enrichment and expansion of healthy C57BL/6 mouse splenocytes ($P = 3.42\text{x}10^{-30}$ for enrichment of SVY-reactive clones in the TIL population by the hypergeometric test). Taken together, Jackson mice have a beneficial anti-tumor response that is antigen driven, have higher selective pressure against the tumor antigen, and KbSVY cross-reactive T cells can be detected in the tumor, all highlighting the beneficial cross-reactive T cell population that is present in the Jackson mice.

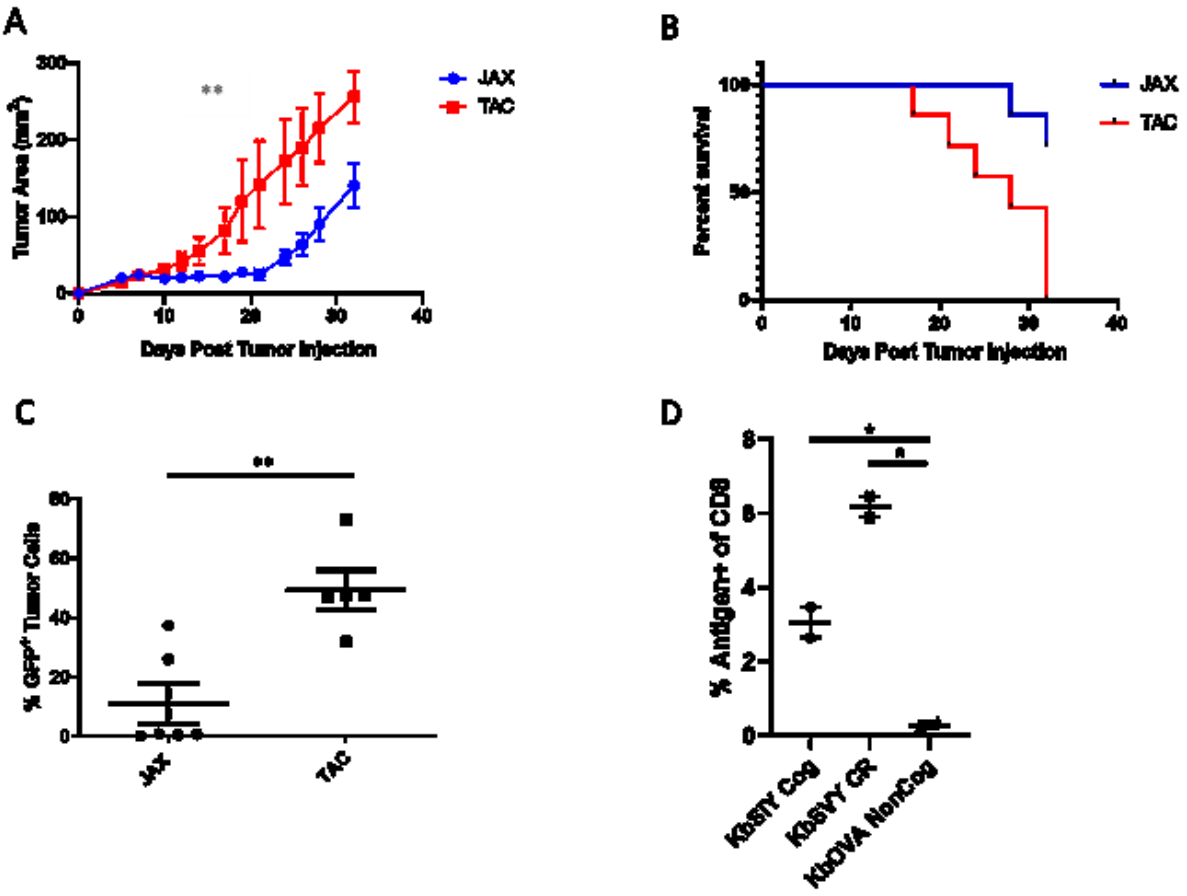

Figure 10.6 Jackson mice have an increased anti-tumor response and antigen selective pressure on the tumor.

Jackson C57BL/6 mice (n= 7) and Taconic C57BL/6 mice (n=7) were injected with $2x10^6$ B16.SIY cells subcutaneously on Day 0. Tumor growth curves show Jackson mice have significantly delayed tumor growth as compared to Taconic mice. Significance was measured by two-way ANOVA with Bonferroni post-hoc test for multiple comparisons (p=0.0455). (B) Additionally, Jackson mice had significantly increased survival compared to the Taconic mice. Significance was measured by the log-rank test (Mantel-Cox tex) ** P=0.0065 n=7 TAC and n=7 JAX (C) Jackson and Taconic C57BL/6 mice were injected with $2x10^6$ B16.SIY cells subcutaneously on Day 0. Tumors were

harvested at an approximate size of 200-250 mm^2 and analyzed by flow cytometry for GFP expression. Jackson have a significantly lower GFP expression by unpaired t-test, two tailed ** P=0.0030 (n=5 TAC and n=6). (D) Jackson and Taconic C57BL/6 mice were injected with $2x10^6$ B16.SIY cells subcutaneously on Day 0. Tumor infiltrating lymphocytes were harvested on Day 24 and analyzed by flow cytometry for $CD8^+$ T cell specificity, gated on live, $CD8^+$ T cells. P-value = 0.011, KbSIY; 0.012, KbSVY by Unpaired, one-tailed t-test. Error bars indicate SEM.

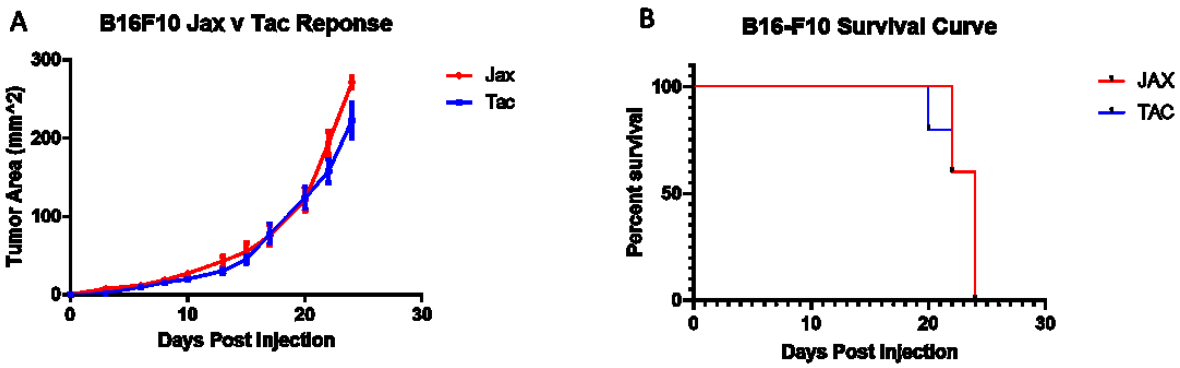

Figure 10.7 Jackson and Taconic mice have a similar tumor growth response to B16-F10. Jackson and Taconic B6 mice were injected subcutaneously with B16.F10 (3x10^5 cells) in the flank and measured for tumor growth with calipers over time and for overall survival. N=5/group for B16.F10 experiment. B16F10 repeated twice with similar results. Error bars for SEM.

10.2.7 Bifidobacterium alters the composition of the SVY-responsive TCR repertoire

The impact of *B. breve* colonization on T cell-specificity was also studied by analyzing TCR repertoires expanded by KbSIY or KbSVY from *B. breve* colonized (Jackson) mice and

those lacking *B. breve* (Taconic). KbSIY and KbSVY-specific T cells from Jackson and Taconic mice were stimulated and sorted based on KbSIY or KbSVY staining (Figure 10.8, a). The eight T cell populations were analyzed by TCR beta chain sequencing to determine how *B. breve* shapes KbSVY TCR repertoires.

All four expanded TCR repertoires showed significant overlap when stained with cognate or cross-reactive Kb-peptide dimer (Figure 10.8, b). Independent of *B. breve* colonization, we found many overlapping clones when comparing the cognate and cross-reactive sorted populations. By heatmap analysis, the overlapping pairs were in distinct groups with little overlap with other repertoires and led to a selection of four distinct TCR populations of SIY and SVY cross-reactive clones (Figure 10.8, b). Within Jackson mice T cell repertoires expanded by KbSIY, the KbSIY sorted and KbSVY sorted populations shared 47 identical clones comprising 79.9% of the response (Figure 10.8, b). These populations also shared the same V and J allele expression based on heat map analysis (data not shown). Within Jackson mice T cell repertoires expanded by KbSVY, the KbSVY sorted and KbSIY sorted populations shared 93 unique clones comprising 95.6% of the response (Figure 10.8, b). In Taconic mice, T cell populations expanded with KbSIY and sorted on KbSIY or KbSVY had 45 overlapping clones that made up 85.9% of the response, while the T cells expanded with KbSVY and sorted on KbSVY or KbSIY had 49 shared clones comprising 77.1% of the response. Thus, identical T cell clones from cognate and cross-reactive staining of expanded cells showed that T cells are cross-reactive for both antigens, regardless of the commensal bacteria colonization.

The relationship between TCR repertoires was also examined using ImmunoMap, a TCR homology program we recently developed[102]. ImmunoMap characterizes the overall homology patterns between different T cell repertoires based on homologous complementarity-determining

region 3 (CDR3) sequences. In this fashion multiple repertoires can be overlaid to compare homology among various TCRs repertoires (Table 2). The effect of *B. breve* on TCR repertoire composition can be seen when comparing the overlap of SIY or SVY stimulation in Jackson and Taconic mice (Figure 10.8, c and d). *B. breve* negative mice (Taconic) cells stimulated with KbSVY reactivity have only 51.1% homology with KbSVY stimulated repertoire from *B. breve* positive (Jackson) mice (Figure 10.8, c, note highlighted boxes and d). In contrast, KbSIY TCR repertoire had a significantly overlapping response between Jackson and Taconic stimulations, with 71% overlap between both repertoires and highlights that *B. breve* colonization has a greater effect on the composition of the KbSVY-stimulated TCR repertoire than on that of the KbSIY-stimulated repertoire (Figure 10.8, d).

Principal component analysis (PCA) was used to compare the TCR clones based on homology of dominant motifs identified from individual repertoires[102]. While individual repertoires all shared similar diversity metrics (Table 2), KbSIY or KbSVY-specific TCR motifs from *B. breve* colonized (Jackson) or non-colonized (Taconic) mice reveal four distinct pairings, each driven by supplier and the epitope used for expansion; however, the separation within and between pairs was qualitatively greater for Taconic mice than for Jackson mice (Fig. 6e). Taken together, TCR repertoire sequencing indicates that the majority of SIY- or SVY-stimulated T cell clones are cross-reactive with both epitopes and that *B. breve* colonization is associated with a significantly greater shift in the clonal composition of the SVY-stimulated repertoire than in that of the SIY-stimulated repertoire.

The effect of Bifidobacteria stimulation on the TCR repertoire was also analyzed on T cells stimulated *in vitro* with heat-killed Bifidobacteria. After bacterial stimulation, TCR repertoire analysis of the expanded T cells identified 255 unique clones that overlap with Jackson

KbSIY or KbSVY stimulated and sorted repertoires by a Hamming distance of 1. The TCR clones similar to SIY- or SVY-peptide-reactive TCR repertoires were at a significantly higher productive frequency compared to clones present in non-Bifidobacteria stimulated controls (Fig. 6f). Thus, similar to our *in vivo* findings, *in vitro* stimulation with Bifidobacteria expanded a KbSIY reactive TCR repertoire that could have anti-tumor activity.

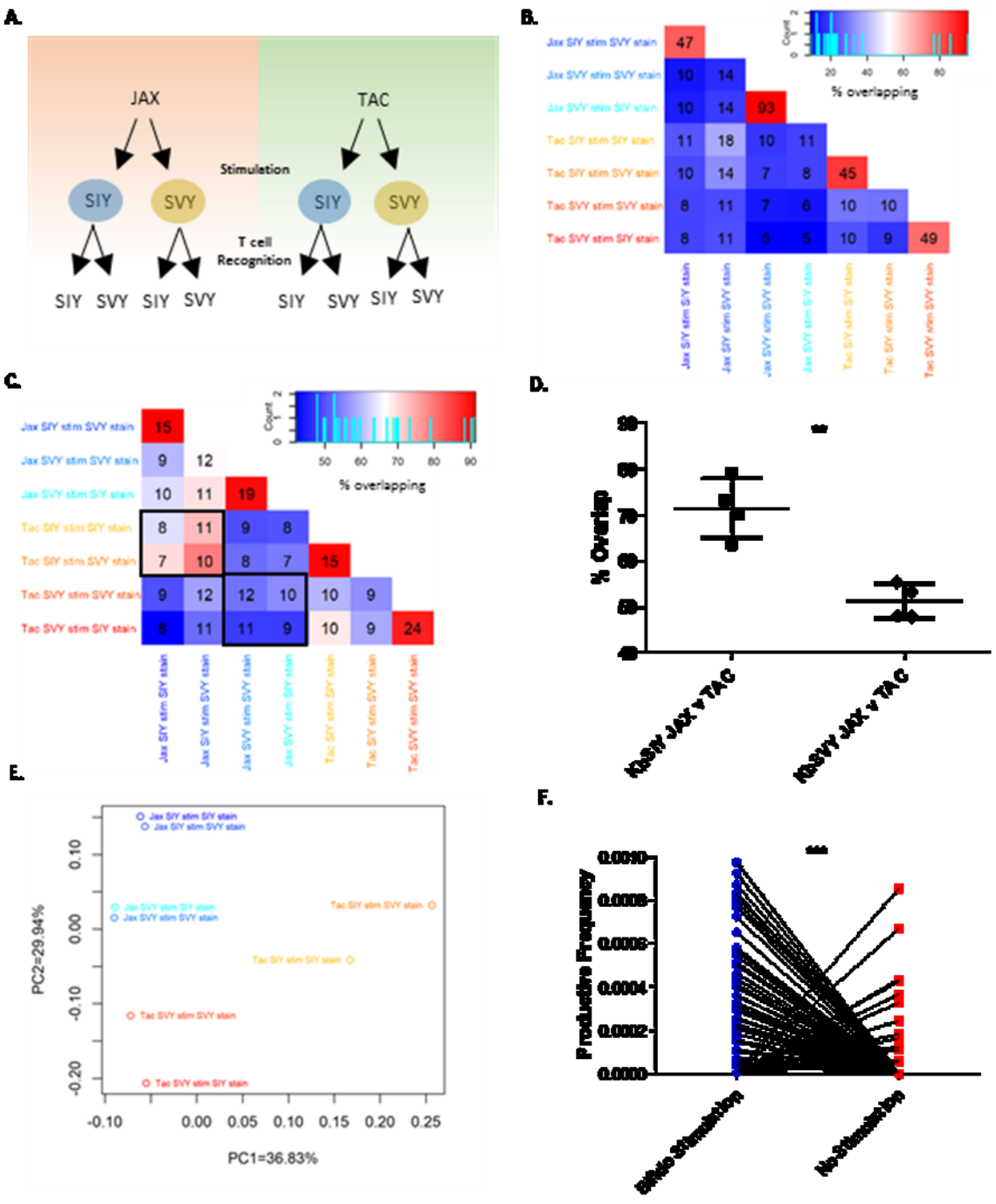

Figure 10.8 *B. breve* colonization shapes the KbSVY TCR repertoire.

(A) Schematic setup of TCR Repertoire Analysis. $CD8^+$ T cells from Jackson and Taconic mice were stimulated with KbSIY or KbSIY aAPCs. On day seven, cells from

each stimulation were stained and sorted by antigen reactivity (KbSIY or KbSVY) and processed for TCR beta chain deep sequencing. (B) Exact TCR clone overlap between all repertoires. Numbers indicate the number of unique overlapping clones between two TCR repertoires and the color scale indicates the percent contribution of the overlapping sequences to the total combined repertoire for each pair. (C) TCR clone overlap between all repertoires based on TCR homology using ImmunoMap algorithm. Numbers indicate the number of homologous clusters shared between two TCR repertoires and the color scale indicates the percent contribution of shared clusters to the total combined repertoire for each pair. (D) Overlap between Jackson and Taconic mice of T cell repertoires stimulated by SIY or SVY based on the frequency of homologous TCR clones and overlap between SIY and SVY stimulations for Jackson or Taconic mice groups. Data included the cognate and cross-reactive sorted populations, as indicated by the black boxes in C. P=0.0016 by two-tailed t-test. Error bars indicate SEM. (E) PCA of homology-based TCR clusters. TCR repertoires were analyzed by CDR3 sequence homology and separated into dominant motifs. (F) TCR beta chain deep sequencing was performed on Jackson mouse splenocytes incubated with or without heat-killed *Bifidobacterium*. TCR clones with a Hamming Distance of 1 were defined as homologous to clones from aAPC expanded KbSIY or KbSVY-specific T cells. Productive frequency of these homologous clones from *Bifidobacterium* stimulated and unstimulated cells are shown (p-value = 0.0001 by two-tailed t-test).

Sample	Unique Clones	Shannon Entropy	Dominant Motifs	Sequences/ Motif	Singular Response	Singular Contribution	TCR Diversity Score	Mean Hamming Distance
Jax SIY stim SIY stain	47.00	3.48	20.00	1.95	61.70	70.78	0.51	5.55
Jax SIY stim SVY stain	121.00	4.12	21.00	3.76	51.24	73.24	0.50	5.53
Jax SVY stim SVY stain	112.00	4.02	28.00	2.89	51.79	74.23	0.54	5.82
Jax SVY stim SIY stain	100.00	3.85	21.00	3.00	53.00	73.56	0.54	5.64
Tac SIY stim SIY stain	70.00	3.65	20.00	2.60	57.14	73.45	0.52	5.24
Tac SIY stim SVY stain	57.00	3.28	16.00	2.50	57.89	78.10	0.51	5.06
Tac SVY stim SVY stain	75.00	3.86	27.00	2.26	61.33	78.23	0.53	5.95
Tac SVY stim SIY stain	61.00	3.57	24.00	2.25	60.66	80.18	0.53	5.31

Table 2 Summary of TCR clustering of cross-reactive populations by homology.

TCR clusters analyzed based on homology ImmunoMAP algorithm. Each repertoire is described by Shannon Entropy and TCR Diversity Score (based on ImmunoMap algorithm), show little difference between the overall diversity of each T cell population.

10.2.8 KbSVY reactive T cells inhibit growth of established SIY-expressing tumors in vivo.

One critical question is whether KbSVY-reactive T cells cross-react with the SIY epitope *in viv*o and mediate an effective anti-tumor response. This was studied using KbSVY effector T cells from *B. breve* positive mice (Jackson) for adoptive cellular therapy (ACT). Effector T cell populations were generated *in vitro* and adoptively transferred into B16.SIY tumor bearing mice. KbSVY expanded T cells inhibited B16.SIY tumor growth and extended survival in tumor bearing mice. By day 22, untreated mice had an average tumor size of approximately 89.87 mm^2, whereas SVY ACT-treated mice were, on average, only 22.37 mm^2 (Fig. 7a, S14a). When we analyzed survival data, 60% of KbSVY ACT treated mice survived past 41 days while no control mice survived that long (Fig. 7a).

ACT-treated mice which eventually developed resistant tumors, were analyzed for antigen loss. Tumors were isolated at approximately 135 mm^2 and measured for GFP intensity as a marker of SIY expression[103]. The resistant tumors had a decrease in GFP expression compared to tumors isolated from a non-treated mouse (Fig. 7b) demonstrating that KbSVY specific cells placed selective pressure on B16.SIY tumors resulting in loss of antigen expression. As expected, KbSIY-expanded T cells also delayed tumor progression in tumor bearing mice and extended survival (Fig. 7c), showing that the repertoire present in KbSIY specific T cells also has anti-tumor activity. Thus polyclonal, cross-reactive T cell populations expanded with KbSVY decreased tumor growth and increased survival, demonstrating the potential benefits of commensal bacteria-responsive T cell cross-reactivity on anti-tumor immunity.

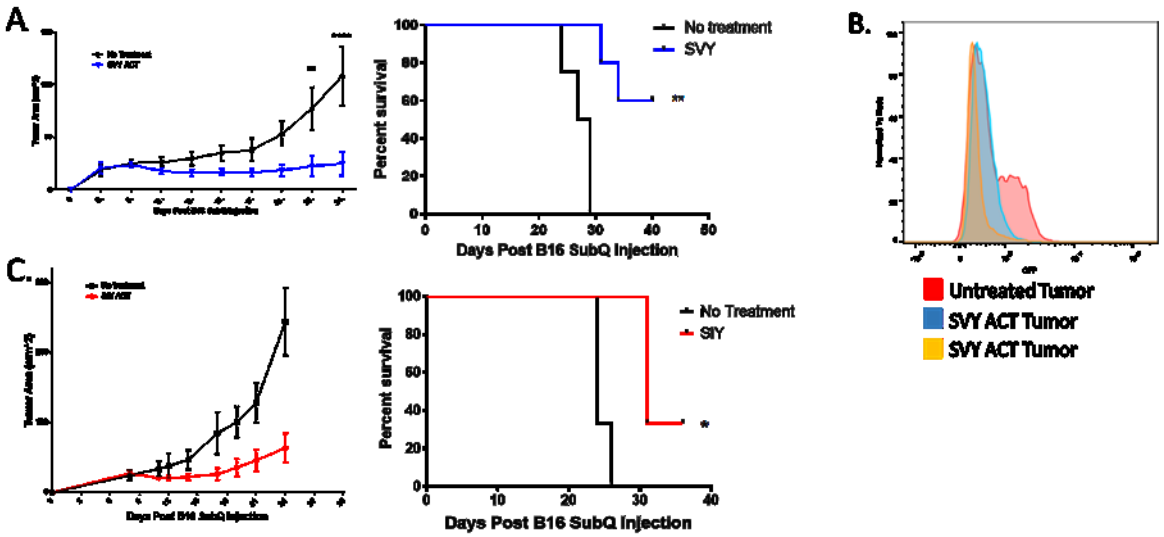

Figure 10.9 Commensal bacteria epitope cross-reactivity mediates an anti-tumor response.

(A) Jackson C57BL/6 mice (n= 5 SVY adoptive cell therapy [ACT], n = 4 No Treatment) were injected with $2x10^6$ B16.SIY cells subcutaneously on Day 0. $CD8^+$ T cells were harvested from spleens of independent Jackson mice and stimulated with KbSVY/anti-CD28 nanoparticles. $1.3x10^5$ of the resultant KbSVY-specific $CD8^+$ T cells were injected intravenously into the tumor-bearing mice on day 8. Tumor growth curves show SVY ACT treatment significantly delayed tumor growth as compared to no treatment. Significance was measured by two-way ANOVA with Bonferroni posthoc test for multiple comparisons ($p<0.05$). Additionally, KbSVY ACT significantly increased survival compared to the no treatment group. Significance was measured by the log-rank test ($p = 0.0015$, n= 4 no treatment and n=5 SVY ACT). (B) Jackson C57BL/6 mice were

injected with $2x10^6$ B16.SIY cells subcutaneously on Day 0 and treated on day 8 with $1.3x10^5$ KbSVY-specific $CD8^+$ T cells via intravenous injection. Tumors were harvested on day 24 and analyzed by flow cytometry for GFP expression. Orange and blue indicate SVY T cell-treated mice and red indicates untreated mice. (C). Jackson C57BL/6 mice (n= 3 SIY ACT, n = 3 No Treatment) were injected with $2x10^6$ B16.SIY cells subcutaneously on Day 0. $CD8^+$ T cells were harvested from spleens of independent Jackson mice and stimulated with KbSIY/anti-CD28 nanoparticles. $1.3x10^5$ of the resultant SIY-reactive T cells were injected intravenously into tumor-bearing mice on day 8. Tumor growth curves show SIY ACT treatment significantly delayed tumor growth as compared to no treatment. Significance was measured by two-way ANOVA with the Bonferroni posthoc test for multiple comparison ($p<0.05$). ACT also significantly extended survival. Significance was measured by the log-rank test (P=0.024, n= 3 per group).

10.3 Discussion

Understanding the role of antigen mimicry leading to T cell-mediated anti-tumor responses is essential in understanding how microbiota can lead to anti-tumor effects. *B. breve* contains a peptide with homology to the SIY epitope, which influences anti-B16.SIY melanoma specific responses. Use of *B. breve* as a source of homologous antigen does not limit the possibility of other sources of antigen, although throughout the paper the *B. breve* antigen sequence shows robust cross-reactivity and ability to induce the anti-tumor T cell response both *in vitro* and *in vivo*. Looking closely, the isoleucine substitution to valine at the second position, did not affect

peptide-MHC binding, however the substitution appears to shift the orientation of more distant amino acids in the binding pocket, leading to altered TCR recognition. While differences in binding with the 2C transgenic TCR illustrated that an individual TCR can display somewhat lower affinity for KbSVY than KbSIY, endogenous murine polyclonal SIY and SVY T cell responses exhibit striking cross-reactivity. On a closer examination, TCR beta sequencing reveals the exact same clones can bind to both the SIY and SVY antigens after a single stimulation. The endogenous KbSIY response is cross-reactive and recognizes both antigens, SIY and SVY, albeit with a lower affinity and less robust functional response to the SVY antigen. In contrast, KbSVY reactive T cells recognize both peptide antigens with similar affinity as well as functional ability, as assessed by their ability to release cytokines in response to tumor cells. This difference in cross-reactivity relative to the initial T cell stimulation suggests that C57Bl/6 mice possess a heterogeneous SIY/SVY T cell population that can be stimulated by *B. breve* and the polyclonal population contains a range of affinities for SIY and SVY based on ability to bind to the slightly altered amino acid orientation in the MHC pocket.

One of the most interesting findings is that the gut microbiota primes an SVY reactive T cell response. While the mechanism of T cell activation and selection by components of the gut microbiota is not understood, analysis of mice with and without *Bifidobacterium* indicates that *in vivo* priming occurs and boosts the ability to expand SVY-reactive T cells. The SVY antigen is immunogenic and can induce an effector T cells that are cross-reactive *in vivo* with the SIY antigen. In addition, the antigen specific T cell response is transferable as demonstrated by co-housing experiments. Comparing the TCR repertoires between colonized and non-colonized animals revealed SVY-reactive T cells that express TCRs with little or no overlap between the *B. breve*-naïve (Taconic), and *B. breve* experienced (Jackson) mouse repertoires. An altered SVY-

expandable TCR repertoire developed in the colonized mice, while the SIY-expandable populations showed significantly greater homology between Taconic and Jackson mice. The SVY-stimulated TCR repertoires from *B. breve*-colonized (Jackson) mice contained homologous TCR clones that are shared with the Jackson KbSIY stimulation. These findings suggest that differences in B16.SIY, B16.F10 tumor growth between Taconic and Jackson mice may be driven in part by a cross-reactive, SVY-primed subset of the TCR repertoire. In addition, stimulating T cells directly with *B. breve* expands T cell clones that are similar to the Jackson KbSIY or KbSVY T cell populations. These data highlight how commensal bacterial antigens may affect the host immune repertoire landscape through antigen mimicry. An important characteristic of the SVY-reactive T cells was their ability to kill SIY expressing tumors *in vivo*. Treatment of B16.SIY tumor bearing animals with adoptively transferred KbSVY-reactive T cells showed cross-reactive anti-tumor activity of an endogenous, polyclonal commensal-bacteria antigen-stimulated T cell population.

Importantly, our study illustrates the potential of antigen-mimicry from gut microbes to influence T cell immunity, and how this can generate a cross-reactive anti-tumor response. Current work identifying beneficial bacteria from responders to immunotherapy as well the benefits of fecal transplant in patients has yet to isolate a clear mechanism of action of beneficial commensal bacteria; antigen mimicry may play a role in patient responses. Our work has confirmed that antigen homology between B. breve SVY and murine melanoma SIY antigen stimulates cross-reactive T cells. Furthermore, the addition of B. breve in the microbiome can boost the KbSVY T cell population and the new KbSVY response can target and slow tumor progression. $CD8^+$ T cell populations driven by commensal bacteria stimulation have shown functional responses[42,45,49,57], but by identifying the antigen presenting cells responsible and their

function will let us further understand the mechanism of effector CD8+ responses produced at the gut-immune interface. To translate commensal bacteria homology to tumor antigens in patient responses further work needs to be completed, yet the overall diversity of the microbiome has been linked to positive respones in patients, potentially with a larger array of antigens available to stimulate the T cell response[49,50,104].With this mechanism in mind, we believe that a rigorous, pan-species genomic analysis of commensal organisms would aid a more precise understanding of the effects of microbiota on anti-tumor immunotherapy. Comparing the potential neo-antigen T cell responses to the homologous sequences found in patients microbiome can provide an effective way to isolate unique T cell populations that can be stimulated by both gut microbes and tumor cells and to generate robust antitumor T cell responses and use those neo-antigen targets for immunotherapy or identify patients whose mutational landscape might better responds to immunotherapy.

10.4Conclusion

In conclusion, we have created a proof of concept approach to further understand the role of antigen mimicry in the microbiome leading to cross-reactive T cell response and colonization can boost the T cell response (Figure 10.10). We have demonstrated the cross-reactivity that can occur between the KbSIY and KbSVY antigens. In a system of distinct housing facilities, Taconic mice had a lower KbSVY T cell responses, suggesting an *in vivo* T cell stimulation occurring at the gut/immune system interface. Though we have studied this model of gut microbiome cross-reactivity with microbiome changes, our model can be studied in detail with

B. breve direct feeding and look closer at the ability to induce a $CD8^+$ T cell response from commensal bacteria colonization.

I hope to continue my work with Panam by comparing the phenotype of $CD8^+$ T cells immunize in the classic fashion or via gut colonization with commensal bacteria housing a tumor cross-reactive antigen. By creating a model of *B. breve* SVY+/-, we will confirm the ability of *B. breve* to rescue the KbSVY expansion defect in Taconic housed B6 mice or in germ-free animals. With confirmed colonization we can compare the quality of the KbSVY T cell response compared to a peripheral immunization model to detect effector function and TCR repertoire changes. Also of interest, is to identify the method of cross-presentation of the SVY antigen during gut colonization: to identify the responsible antigen presenting cells and elucidate the mechanism of CD8+ effector T cells from the commensal microbiome without gut dysbiosis. Our work has only just started to understand the mechanism of antigen mimicry from the gut to effect the anti-tumor immune response. To understand the clinical application for this mechanism, identifying mutations from patients' tumors and comparing them to commensal bacteria will start the process to see if those patients had positive outcomes to CPB immunotherapy.

In terms of translating the work we have completed toward understanding patient responses in the context of the microbiome and immunotherapy, the work we have conducted is critical in showing the direct effect the microbiome can have on developing an functional T cell response. Multiples groups are studying the composition of the microbiome in responders and non-responder patients and although certain bacteria diverge for patients in a given study; there is limited consistency between studies, which does not suggest a common general activator of immune response. Some have argued it is not a particular bacteria but the overall diversity of the

microbiome that is the key biomarker to distinguish responder patients[105]. In terms of the mechanism, the microbiome is suggested to boost the maturation and activation potential of dendritic cells, although how the activation antigen presenting cells traffic directly to the tumor micro-environment is not well supported. To translate this work to patients, by comparing the neo-antigen responses and ranking based on homology compared to clinical outcome to vaccine or checkpoint blockade may better explain the frequency of antigen mimicry on T cell responses. Alternatively, using a *Bifidobacterium* based gut platform with expressed tumor antigens expressed in the genome, a tumor antigen T cell response may be induced via gut T cell activation. Either as a predictor of patient response or use as a potential therapy directly, the hypothesis of mutational landscape responses shaped by the microbiome-immune response is an exciting field for future study.

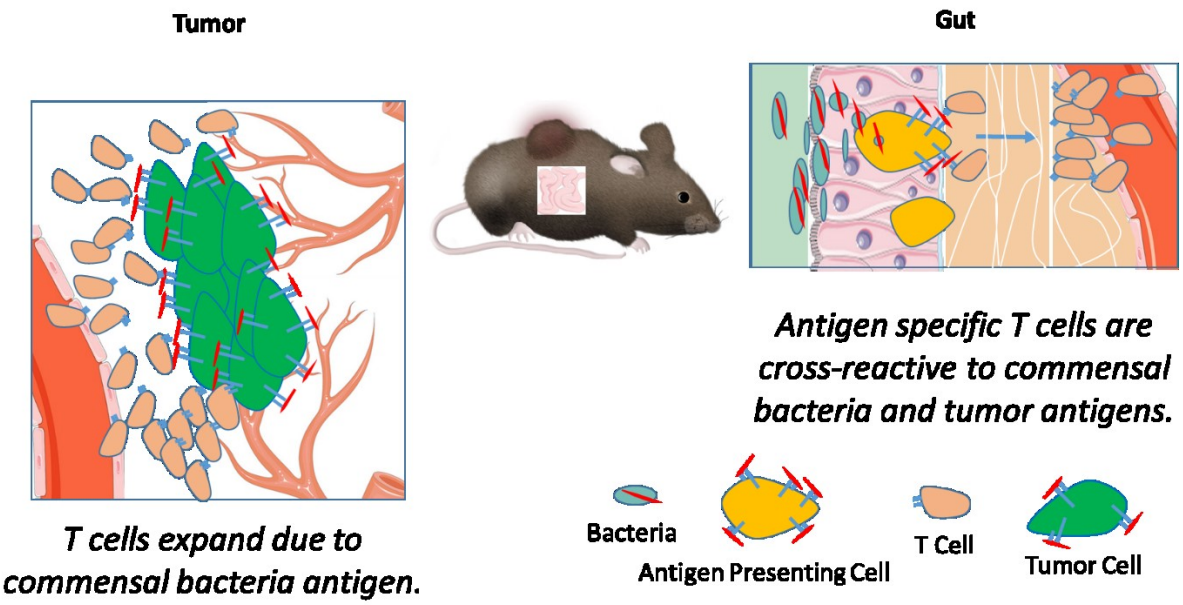

Figure 10.10 Antigen mimicry on commensal bacteria leads to tumor clearance.

A schematic representation of the cross-reactive T cell population resulting from antigen mimicry between commensal bacteria and tumor antigen. Commensal bacteria antigen is taken up at the gut by antigen presenting cells to stimulate T cells which traffic to the tumor microenvironment and can detect and lyse tumor cells.

10.5 Experimental Methods

Mice: C57BL/6 were purchased from Jackson Laboratories (Bar Harbor, ME, USA) and Taconic Farms. 2C TCR transgenic mice were kept as heterozygotes by breeding on a C57/BL6 background. All mice used were 8-12 weeks of age and were maintained according to Johns Hopkins University's Institutional Review Board.

Peptide Stabilization Assay: RMA-S cells were left at 25°C overnight and pulsed for 2 hours with titration of peptide and put at 37°C for 2 hours to degrade unstable MHC molecules. Cells were stained with anti-Kb clone M1/42 and analyzed by flow for MHC expression.

2C Functional Analysis: 2C effector T cells, stimulated from splenocytes with peptide for 5 days, were harvested and re-stimulated with RMA-S cells peptide pulsed overnight. T cells and RMA-S cells were incubated at a 1:1 ratio along with Golgi-stop and Golgi-block and CD107a (FITC,1D4B). After 6 hours, cells were stained with viability stain (ThermoFisher, L23101) and anti-$CD8^{+}$a (PerCp, 53 6.7). Cells were fixed and permeabilized (BD, 554714) and stained for INFg (PE, XMG1.2), TNFa (PECy7, MP6 XT22), and IL-2 (APC, JES6 5H4).

Competitive binding assay: 2C effectors T cells were stimulated with SIY peptide for five days and then stained with fluorescent dimer for one hour. Afterwards, saturating amounts of an unconjugated competitor 1B2 antibody was added and TCR-dimer binding was measured by flow cytometry over time.

Bifidobacteria quantification: Fecal samples were collected from mice from Jackson Laboratories and Taconic Biosciences. DNA was isolated using the ZymoBIOMICS DNA/RNA miniprep kit (Zymo Research). Bifidobacteria colonization relative to total eubacteria was quantified by multiplexed quantitative real-time PCR analysis of microbial rRNA genes. The following primers and Taqman probe were used for detection of Bifidobacteria rRNA: 5'-cgggtgagtaatgcgtgacc-3', 5'-tgataggacgcgacccca-3', and 5'-6FAM-ctcctggaaacgggtg-QSY-3'[106]. The following primers and Taqman probe were used for detection of total eubacteria rRNA: 5'-tcctacgggaggcagcagt-3', 5'-ggactaccagggtatctaatcctgtt-3', and 5'-JUN-cgtattaccgcggctgctggcac-QSY-3'[107].

Bifidobacteria stimulation of murine T cells: Splenocytes and mesenteric lymph node cells were isolated from C57Bl/6 mice obtained from Jackson Laboratories. Cells were suspended in media (RPMI containing 10% heat-inactivated FBS, 50 uM beta mercaptoethanol, 1 unit/mL penicillin, 1ug/mL streptomycin, and 20 IU/mL recombinant murine IL-2 [R&D Systems]) at $2x10^6$ viable cells per mL. $4x10^6$ cells were seeded per well in a 24-well plate. *Bifidobacterium* and *Lactobacillus* probiotic capsules were obtained from SeekingHealth®. One capsule was resuspended in 10 mL of PBS and heated at 57 ˚C for one hour. Splenocytes were stimulated with 160 uL of the heat killed resuspended bacteria (approximately 50-u100 bacterial cfu per splenocyte) or left unstimulated. Cultures were maintained at 37 ˚C at 5% CO_2 for eleven days. Fresh media and IL-2 were added every other day. Cultures were then stained with APC-Cy7-anti-CD8a Clone 53-6.7 (Biolegend), DAPI, and either PE-Kb-SIY dimer or a control PE-Kb dimer. Cell were analyzed on an LSRII flow cytometer (BD). Cells were gated on live cells and $CD8^+$ T cells. Antigen specific frequency was calculated by subtracting the non-cognate background staining. DNA was extracted from $4x10^5$ remaining cells using the DNAeasy Blood and Tissue kit (Qiagen). Extracted DNA was submitted to Adaptive Biotechnologies for survey-level TCR beta chain sequencing.

Preparation of MHC-Ig Dimers and Nanoparticles: Soluble MHC-Ig dimers K^b-Ig was prepared in house and loaded with SIY or SVY peptides as described[108]. αCD28 antibody was purchased from Biolegend (37.51; Biolegend San Diego, CA, USA). KbSIY particles were manufactured in house and by Miltentyi. Soluble MHC-Ig dimer and Nano-aAPC αCD28 antibody were conjugated to 100nm paramagnetic iron oxide particles by Milenyi. In house particles were manufactured by directly conjugating KbSIY-Ig or KbSVY-Ig and αCD28 to amine coated labeled 80-100 nm super paramagnetic iron-oxide particles (SPIONS) purchased from Micromod

(Rostock, Germany) and functionalized according to manufacturer's recommendations. Briefly, amines on particles reacted with Sulfo SMCC (Proteochem, Hurricane, UT) and then magnetically washed. Soluble peptide-MHC-Ig and αCD28 were modified with 2 iminothiolane (Traut's reagent) purchased from Sigma Aldrich (St. Louis, MO). Excess 2 iminothiolane was washed away from protein solution by using a Vivaspin 20 50kDa MWCO concentrator (GE Healthcare, Little Chalfont, United Kingdom). Peptide-MHC-Ig and αCD28 are mixed to 1:1 ratio and added to washed particles and mixed overnight at 25°C. Particles are then washed and stored at 4°C. Nano-aAPC were stored at a concentration of 5×10^{12} particles/mL.

T cell E&E stimulations and Cross-reactivity: C57BL/6 mice spleens and lymph nodes were harvested, and isolated with no touch CD8 kits (Miltenyi) as manufacturer's instructions. $CD8^+$ T cells were incubated with nanoparticles at 10ul of particles per 10^7 $CD8^+$ T cells at 4° C for 1 hr and cells are washed over MS Miltenyi column. Then, the positive fraction was eluted and plated at $2.5x10^5$ cells/mL for a 7 day stimulation. Isolated fractions were mixed and cultured in 96-well round-bottom plates for 7 days in complete RPMI-1640 medium supplemented with 10% human autologous serum and 3% T cell growth factor, a cytokine cocktail derived from stimulated PBMC as described in the literature[4], in a humidified 5% CO_2, 37 °C incubator for 1 week. Specificity of CTL was monitored on day 7, by FACS analysis following dimeric MHC-Ig staining and rat anti mouse CD8a, clone 53-6.7 (Biolegend). The number of antigen-specific cells was calculated by multiplying the number of total live cells by the fractions of $CD8^+$ and antigen-specific cells; the fraction of antigen-specific cells was calculated after subtracting the noncognate MHC staining from cognate MHC staining. Splenic E&E stimulations modified with particles added to RBS lyzed splenic cells at 1ul particles/10^7 cell and after particle elution plated in 96 well u bottom plate at $5x10^5$ cells/mL and stimulated for 7 days.

T cell cytokine response: After 7 days of culture, T cells were counted using a hemocytometer. 200,000 T cells were taken per condition and separated into restimulation or no stimulation groups. A solution of 1:350 BD GolgiStop Protein Transport Inhibitor (BD Biosciences) and 1:350 BD GolgiPlug Protein Transport Inhibitor (BD Biosciences) and αCD107a FITC was added to the cells in RPMI 1640 medium supplemented with 10% fetal bovine S23 serum. RMA-S pulsed overnight at 25°C with peptide (cognate/crossreactive/irrelevant) were washed and added to cells to be restimulated at a 1:2 ratio. Cells were then allowed to incubate in a cell incubator for 6 hours at 37°C. Following the incubation, cells were washed and then stained with 50 µL of a 1:100 solution of PerCP conjugated rat anti mouse CD8a, clone 53 6.7 (Biolegend) and 1:1000 LIVE/DEAD® Fixable Green Dead Cell Stain (ThermoFisher) for 15 minutes at 4°C. Cells were then washed with PBS and 100 µL of BD Cytofix/Cytoperm Fixation and Permeabilization Solution was added to the cells and allowed to sit overnight at 4°C. Following the fixation step, 100 µL of 1x BD Perm/Wash Buffer (10x solution diluted to 1x in a solution of 2% bovine serum albumin in dH_2O) was added to the cells and washed. Cells were again washed with 200 µL 1x BD Perm/Wash Buffer. Cells were then stained with a solution of 1:100 solution of PE conjugated rat anti mouse IFNγ, clone XMG1.2 (BD Pharmingen), APC conjugated rat anti mouse IL2, clone JES6 5H4 (BD Pharmingen), and PE Cy7 conjugated rat anti mouse TNFα, clone MP6 XT22 (Biolegend) for 1 hour at 4°C. Cells were washed with FACS wash buffer and then read on a BD LSR II flow cytometer. Background cytokine staining was accounted for by subtracting cytokine positive cells in non-stimulated conditions from the re-stimulated cells.

MD simulation setup: Each system consists of a protein complex in one of the following three states: 1) the epitope only, 2) the epitope bound to H2-Kb MHC (Kb/epitope binary complex),

and 3) 2C TCR bound to the H2-Kb/epitope complex (Kb/epitope/2C TCR ternary complex). The epitope sequence of each system was chosen to be either SIYRYYGL (SIY) or SVYRYYGL (SVY). The initial coordinates of H2-Kb and 2C TCR were taken from the X-ray crystal structure of each (PDB 3P9L[99]: H2-Kb; PDB 2OI9[100]: 2C TCR). The initial configuration of the epitope was built based on the $OVA_{257-264}$ epitope (SIINFEKL), which is complexed with H2-Kb in the crystal structure. The OVA epitope was mutated to either SIY or SVY epitopes using VMD mutator plugin[109]. The H2-Kb/epitope/2C TCR complex was constructed in the following steps: the coordinates of 2C TCR in the crystal structure were adjusted by aligning the alpha carbons of H2-Kb and MHC protein between the two crystal structures, then the structures of H2-Kb, epitope, and 2C TCR were combined into one system. The protein complex was placed in the center of a rectangular box with a periodic boundary condition. The rest of the empty space of the box was filled with water molecules using the Gromacs tool *solvate*[110]. The size of the simulation box for the protein complex in the states 1, 2, and 3 were 60 Å × 60 Å × 60 Å, 83 Å × 90 Å × 114 Å, and 86 Å × 90 Å × 145 Å, respectively. The length of each side of the box was set to be sufficiently large that proteins at the center of the box are separated at least 30 Å away from their periodic images. The protonation states of His residues of the proteins were determined based on an optimal hydrogen bonding conformation, determined by the Gromacs tool *pdb2gmx*. His93 of the α-chain of H2-Kb MHC, and His29 of the β-chain of 2C TCR were singly protonated at the $N^{\delta 1}$ atom. His84 of the β-chain of H2-Kb was doubly protonated at the $N^{\delta 1}$ and the $N^{\varepsilon 2}$ atoms. All other His residues were singly protonated at the $N^{\varepsilon 2}$ atom. Standard protonation states were chosen for all other residues. Na^+ and Cl^- ions were added in the solvent using the Gromacs tool *genion*, to neutralize the protein systems, as well as mimicking the physiological ionic concentration, 150 mM. The CHARMM36 force field[111] was employed for

the protein and ions, and TIP3P model[112] for waters. The MD simulations were performed with Gromacs package version 5.14[110]. Long-ranged electrostatic interactions were treated with the Particle Mesh Ewald (PME) method[113]. The cut-off distance for both the Lennard-Jones and the real space Coulomb interaction was set to be 12 Å. All covalent bonds involving the hydrogen atoms of the protein and water molecules are constrained by the LINC algorithm[114]. Each system was minimized at zero temperature for 1000 steps, then equilibrated in NPT ensemble with a temperature of 300 K and a pressure of 1 atm for 1 ns. The timestep was set to be 2.0 fs. After the total volume of the system was stabilized in NPT ensemble, the system was equilibrated again in NVT ensemble at 300 K for 100 ns. Then, the NVT simulation was extended for another 500 ns for the production run. The temperature and the pressure were controlled by Nose-Hoover[115] and Berendsen[116] schemes,. The system coordinates were written every 100 ps during the production run, then all MD frames were clustered by the RMSD of the protein complex using gromos method[117]. The RMSD cutoff value of each cluster was set to be 2.5 Å.

Free energy perturbation (FEP): The FEP calculation was performed to calculate the relative free energy changes of the systems in three states, while Val2 of the SIY epitope is mutated to Ile2. The hybrid structure and topology of each system were generated by the PMX software[118]. The alchemical transformation from Val2 to Ile2 was governed by the hybrid Hamiltonian $\mathbf{H}(\lambda)$, as a function of the coupling parameter λ[99].

$$\mathbf{H}(\lambda) = (1-\lambda)\cdot\mathbf{H}_{\mathrm{V}} + \lambda\cdot\mathbf{H}_{\mathrm{I}} + \mathbf{H}_{0} \quad (1)$$

$\mathbf{H}_{\mathrm{V}}$ and $\mathbf{H}_{\mathrm{I}}$ are the Hamiltonians for the atoms of Val2 and Ile2, respectively, which undergo the alchemical transformation during the simulation, and $\mathbf{H}_{0}$ is the Hamiltonian for the rest of the

system, with a fixed topology. 34 λ-windows were generated between λ = 0 and λ = 1, where the λ-interval between neighboring windows was fixed to 0.04 between λ = 0.02 and λ = 0.98, and gradually decreased from 10^{-2} to 10^{-5}, as λ approaches to both ends, λ = 0 and λ = 1. To circumvent numerical instability caused by insertion or deletion of atoms in the simulation, the soft-core potential[119] was applied to both the Van der Waals and the electrostatic interactions for the atoms in the alchemical domain. The λ value for the electrostatic interaction was fixed to zero at the windows between λ = 0 and λ = 0.1, then rescaled linearly to [0, 1] at the windows between λ = 0.1 and λ = 1, while the λ value for the Van der Waals and the bonded interactions was set to be equal to that of the window. At each λ-window, the system was equilibrated for 100 ps, followed by the production run for 500 ps. The simulation was carried out sequentially from λ = 0 to λ = 1, so that the initial coordinates and velocities of each window were taken from the last MD frame of the previous window. The setup for the MD simulation part was the same used in the NPT simulation in the earlier section. All other FEP setups were the same used in our previous studies[120–123] on other MHC-epitope-TCR systems.

The free energy change (ΔG) was calculated using the thermodynamic integration (TI) method[108,124,125], in the equation as follows[100],

$$\Delta \mathbf{G} = \int_{\mathbf{0}}^{\mathbf{1}} \langle \left(\frac{\boldsymbol{\partial H}(\lambda, \mathbf{x})}{\boldsymbol{\partial \lambda}} \right) \rangle_{\lambda} \, \boldsymbol{d\lambda} \tag{2}$$

where $\langle (\boldsymbol{\partial H}(\lambda, \mathbf{x}) / \boldsymbol{\partial \lambda}) \rangle_{\lambda}$ is the ensemble average of the derivative of the hybrid potential with respect to λ. $\boldsymbol{\partial H}(\lambda, \mathbf{x}) / \boldsymbol{\partial \lambda}$ was written every 0.1 ps. ΔG was calculated for each of three systems with different protein complexes as listed above (ΔG_{epi}, $\Delta G_{Kb/epi}$, and $\Delta G_{Kb/epi/TCR}$). Statistical error of ΔG was estimated using the block average method by dividing the trajectory of each window into four consecutive blocks. To better sample the conformational change of the protein complex, $\Delta G_{Kb/epi}$ and $\Delta G_{Kb/epi/TCR}$ were averaged over five independent runs, started from

different initial configurations. Each initial configuration was taken from the frame at the center of each of the top five most populated clusters from the MD simulations, as shown in Figure S3. ΔG of each individual run was weighted by the population of each cluster. Due to its small system size, ΔG_{epi} was calculated from a single run. The calculation details are shown in Table S2. The relative free energy changes for the two reaction steps during the formation of the protein complex, $\Delta\Delta G_{Kb+epi}$ and $\Delta\Delta G_{Kb/epi+TCR}$, defined in the main text, were calculated in the equations as follows[109,110].

$$\Delta\Delta G_{Kb+epi} = \Delta G_{Kb/epi} - \Delta G_{epi} \quad (3)$$

(Humphrey et al., 1996)(Humphrey et al., 1996)

$$\Delta\Delta G_{Kb/epi+TCR} = \Delta G_{kb/epi/TCR} - \Delta G_{Kb/epi} \quad (4)$$

Immunization Assay: Protocol taken from Schutz et. al. Briefly, recipient C57BL/6 mice were injected intraperitoneal with 10 µg/mouse of anti-CD40 mAb (clone 3/23; BioLegend, San Diego, CA) and a day later immunized subcutaneously with 250ug indicated of either $^{OVA-}K^b$-Ig or $^{SVY-}K^b$-Ig dimer.

In Vivo Killing Assay: Target cells for the *in vivo* cytotoxic assay were obtained from splenocytes of naïve C57BL/6 mice, cleaned from erythrocytes by osmotic lysis, washed and split into two populations. The control population was pulsed with 1 µM SIY peptide, incubated at 37°C for 20 min, and labeled with a high concentration of CFSE (2.5 µM) ($^{unlabelled-}CFSE^{high}$ cells). The second control target population was pulsed with 1 µM SVY,SIY or OVA peptide and was labeled with a low concentration of CFSE (0.25 µM) ($^{target-}CFSE^{low}$ cells) (Invitrogen, Eugene, OR). The two populations were mixed together at 1:1 ratio and intravenously injected in $^{pep-}$MHC dimer immunized C57BL/6 mice (10×10^6/population/mouse) 7 days after immunization with KbSVY-Ig dimer, KbOVA-Ig dimer, or no immunization control

mice. After 18 h the mice were sacrificed and spleen. The cell suspensions obtained from the spleen were analyzed by FACS for presence of two differentially CFSE labeled target populations. The recovery and percent killing of the various CFSE-labeled, peptide-pulsed target cells were calculated as follows: % of *in vivo* killing = 100 − ([(% specific peptide pulsed cells in immunized C57BL/6/% unspecific peptide pulsed cells in immunized C57BL/6)/(% specific peptide pulsed in naïve C57BL/6/% unspecific peptide pulsed cells in naïve C57BL/6)] × 100).

In Vivo Tumor Experiments: 8 week old C57BL/6 mice were injected with B16.SIY ($2x10^6$ cells) or B16.F10 ($1x10^5$ cells) in the flank and measure for tumor growth with calipers over timer and monitored for survival.

Co-housing experiment: 8 week old C57BL/6 mice from Taconic and Jackson facilities were co-housed in fresh cages for 7 days. On day 7, age matched Taconic mice, co-house Taconic mice, and co-housed Jackson mice were sacrificed and spleens isolated for $CD8^+$ T cell E&E for KbSVY and KbOVA T cell stimulations.

TCR repertoire analysis: In order to compare repertoires between Jackson and Taconic mice with SIY vs. SVY stimulations and their cognate versus non-cognate stains, a custom R script was developed to analyze CDR3 data obtained from Adaptive Biotech based on both exact and homology overlaps between groups. Only sequences with a productive frequency >0.01% were included in the analysis. For exact overlap analysis, CDR3 reads were normalized within samples and then compared across all samples. First, the number of unique CDR3s and the overall contribution from shared sequences were compared. Next, principal component analysis (PCA) was performed and samples were plotted in terms of their top two principal components to examine sample clustering behavior in the lower dimensional space. Additionally, a heatmap

representation was drawn using row-wise Z scores. Finally, the Jensen Shannon Divergence was computed in terms of the Shannon's entropy of each CDR3 distribution as[126]:

$$D_{JS}(P||Q) = H\left(\frac{1}{2}P + \frac{1}{2}Q\right) - \frac{1}{2}(H(P) + H(Q))\#(5)$$

where the Shannon's entropy in terms of the frequency of all N unique CDR3s, $p(i)$ is[100]:

$$H(P) = -\sum_{i=1}^{N} p(i)\log_2 p(i)\ \#(6)$$

For homology overlap analysis, the Immunomap algorithm was used.[2] Briefly, pairwise distance scores between all unique CDR3s were calculated using a PAM10 substitution matrix, a gap opening penalty of 30, and a gap extension penalty of 0, and the Immunomap distance metric was calculated. Then average hierarchical clustering was performed and a homology threshold of 0.35 was used. Finally, dominant motifs were defined as homology clusters with a frequency greater than 3%. Homology overlaps were represented in a similar manner as above.

Tumor ACT: To test the anti-tumor benefits of effector T cell populations B16.SIY bearing mice were treated with adoptive cellular therapy (ACT) and monitored for tumor growth and survival. Jackson mice were stimulated with KbSVY nanoparticles and transferred into partially ablated tumor bearing mice. Jackson C57BL/6 were injected with B16.SIY tumor cell line at $2x10^6$ cells subcutaneously per mouse. 7 days after tumor injection mice were partially ablated with 5 cGy to create room for adoptively transferred cells. On day 8, day 7 stimulated KbSIY or KbSVY specific $CD8^+$ T cells were transferred into tumor bearing animals by retro-orbital injection with $1.3x10^5$ antigen specific cells/mouse. On day 8 and day 9 mice receive IL-2 30,000 units by intraperitoneal injection. Mice were measured 3 times/week for tumor growth and survival and tumor volume was reported in mm^2.

TILs Isolation: Tumor infiltrating lymphocytes were obtained from tumors by manual digestion and washing, a density gradient centrifugation (Lympholyte Cell Separation Media, Mouse, Cedar Lane), and then tumor cells were counted and used flow cytometry analysis. All cell lines underwent testing for mycoplasma contamination.

Statistics: Information on statistical tests is present in all figure legends. One and two-way ANOVA were used when making multiple comparisons. Bonferroni post-tests were performed when comparing all groups, and Dunnett's post-tests were performed when the hypotheses being tested involved comparison against a single group. One-tailed and two-tailed *t* tests were used when comparing two groups, as indicated in figure legends. All data sets were assumed to fit a normal distribution, and all graphs show mean and error bars represent SEM. All *n* values are present within figure legends. Mice with outlier tumor size before the beginning of treatment were removed from the studies. Randomization was performed by cage in all animal studies. All statistical analysis was performed using GraphPad Prism software.

11 Additional Work

11.1 Contribution to other Schneck Laboratory Projects

11.1.1 Introduction of Incomplete Projects

Sprouty2 Project: Sprouty2 (Spry2) was initially identified in the Schneck lab from a microarray analysis of proteins upregulated after increasing anti-CD3/anti-CD28 T cell stimulation of healthy $CD8^+$ T cells (data not shown). Spry2 is a negative regulator of the Erk signaling pathway during TCR T cell signaling. Sprouty-1 had previously been identified as a regulator of effector function in $CD4^+$ and $CD8^+$ T cells[127]. From the work in the Schneck lab, Spry2 was identified to be key in regulating polyfunctionality of $CD8^+$ T cells, polyfuctionality is the ability for an effector $CD8^+$ T cell to produce multiple cytokines in a single T cell upon antigen stimulation[128]. The loss of polyfunctionality in $CD8^+$ T cells is associated with T cell exhaustion, the process of effector T cells to lose expansion, lyses and cytokine function toward their antigen of interest which is common in chronic T cell stimulation with poor clearance of antigen[129]. Spry2 was specifically enriched along with PD-1 expression in HIV specific $CD8^+$ T cells in HIV+ patients, while the viral influenza response was not impacted in function or exhaustion markers[128]. Below is data collected in both murine and human cancer systems to determine if Spry2 is upregulated in exhausted T cells in the setting of tumor immunology. The work has not been published but suggests to potentially explain how chronic T cell stimulation in the tumor microenvironment could inhibit T cell function through Spry2, but further work would be beneficial to understand the induction of Spry2 in tumor infiltrating T cells.

Neo-antigen Characterization Project: The neo-antigen T cell compartment has been suggested as the potential dominate T cell response responsible for positive outcomes for cancer immunotherapy patients[17,21]. Neo-antigen T cell responses have the potential to be less inhibited and maintain higher affinity T cell clones in the repertoire compared to self-tumor antigens[8] . We wanted to compared the exhaustion phenotype between neo-antigen and self-tumor antigen responses in tumors, and determine the exhaustion phenotype profile for both types of antigens. Below is data collected using neo-antigens epitopes in B16-F10 murine melanoma[12] identified by an aAPC T cell stimulation screen, conducted by the Schneck group. These neo-antigen T cell responses were compared to KbTRP2, a self-tumor melanoma response. The work has not been published but with future experiments may show the beneficial neo-antigen responses compared to self-tumor antigen responses, and/or a difference in T cell exhaustion markers after tumor infiltration.

11.2 Spry2 in Tumor Expression

Spry2 has been identified as a negative feedback regulator of the Erk signaling pathway during T cell activation[127]. From *in vitro* studies in the lab, Spry2 is upregulated with increasing the concentration of plate bound α-CD3 during α-CD3/α-CD28 $CD8^+$ T cell activation in both human[128] and murine systems (data not shown). With increasing α-CD3 signal, murine $CD8^+$ T cells increase proliferation activity, decrease cytokine production ability, and increasing Spry2 expression (data not shown). Separate from TCR activation strength, a cytokine screening revealed TGF-β can increase Spry2 expression during T cell activation (data not shown). To test if the inhibitory microenvironment of the tumor will increase Spry2 expression in $CD8^+$ T cells,

PMEL CD8+ T cells were adoptively transferred into B16.F10 tumor bearing mice and after 2 weeks were harvested from spleens and tumors of mice. The PMEL CD8+ T cells recognize the Dbgp100 tumor antigen expressed by the melanoma cells, and are marked with Thy1.1 congenic marker for identification of transferred cells. Compared to splenic PMEL T cells, PMEL tumor infiltrating lymphocytes (TIL) had a higher MFI in Spry2 (Figure 11.1). Within the TILs compartment, the PMEL cells had a PD-1 hi and a PD-1 low expression population (data not shown) and Spry2 expression was increased in the PD-1 hi population (Figure 11.2). Taken together, the data suggests Spry2 is induced in the tumor microenvironment and is co-expressed with Pd-1+ TILs but more work Spry2 induction and co-exhaustion markers must be completed.

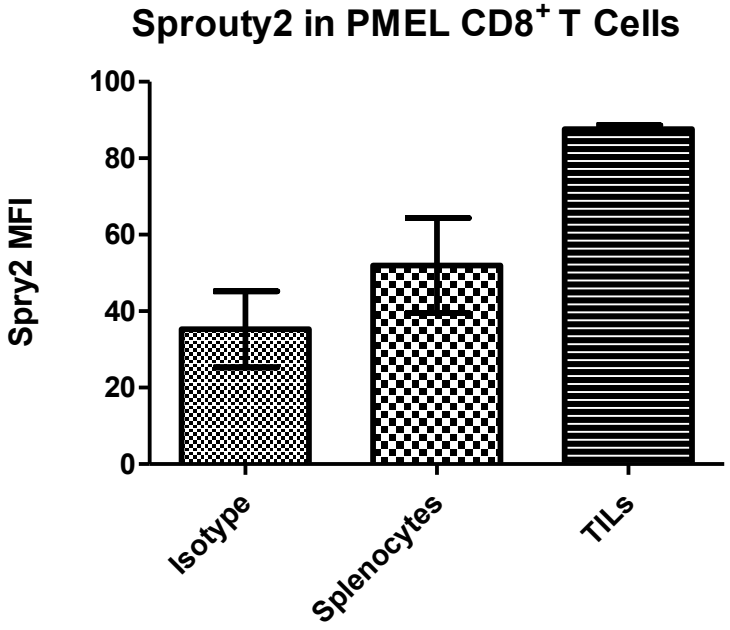

Figure 11.1 Spry2 Expression in TILs.

PMEL T Cells in Tumor have higher Spry2 expression compared to splenocytes and isotype control. B6 mice with B16-F10 subQ tumors were irradiated and transferred with PMEL Thy1.1 T cells, APCs, and IL-2 (IP) and collected after 14 days. Second IL-2 treatement D1 after transfer. (n=3)

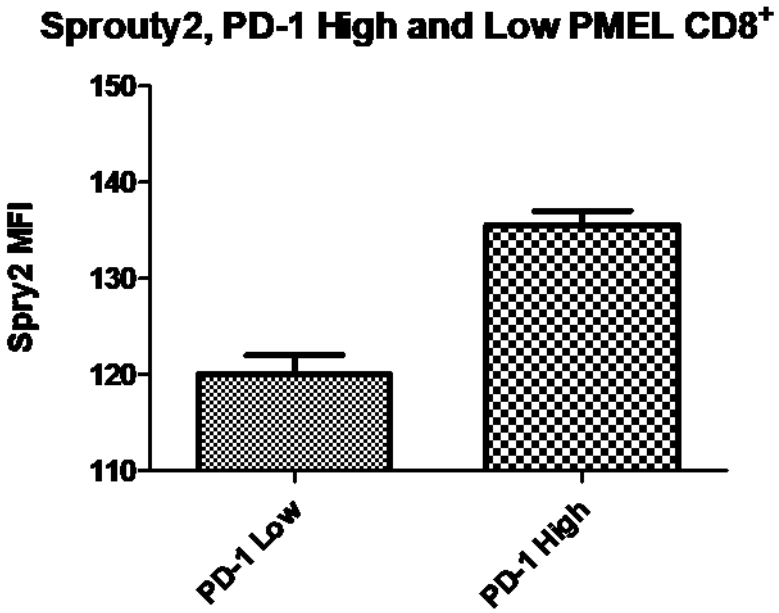

Figure 11.2 Spry2 is Co-expressed with PD-1 Hi TILs

Spry2 MFI levels compared between PMEL PD-1 Low (PD-1 Low MFI 113) and PD-1 High (PD-1 High MFI 11793) TILs. B6 mice with B16F10 tumors were irradiated and PMEL and aAPCs were transferred into recipient mice for 2 weeks. TILs isolated and analyzed by flow cytometry. Cells gated on Live/CD8/Thy1.1 (n=3)

In an alternative approach, pancreatic ductal adenocarcinoma tissue slides were stained by IHC with Spry2 and DAPI to compare Spry2 expression in lymphocytes. Compared to healthy adjacent tissue, more lymphocytes surrounding the abnormal ductal tissue had Spry2 expression. Below is a representative picture of healthy control tissue and abnormal ductal tissue, both stained with DAPI and Spry2 (Figure 11.3). Both tissues had lymphocyte infiltration, although the abnormal tissue has an increase of lymphocytes, but Spy2 expression is detected robustly in the abnormal tissue slide. Lymphocytes were identified by the size of the cell relative

to the nuclear size and shape. With multiple pancreatic patient samples and adjacent healthy tissue controls, Spry2+ in the lymphocytes increases 3 fold in abnormal tissue compared to healthy tissue (Figure 11.4). Future work to identify the phenotype of the infiltrating lymphocytes will confirm if Spy2 is an additional marker of exhaustion in TILs.

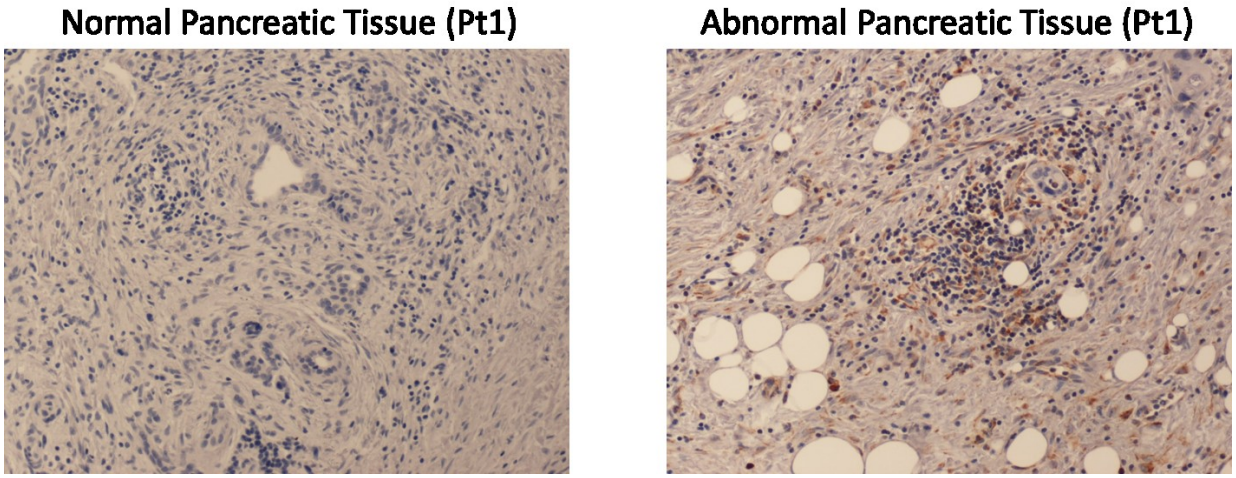

Figure 11.3 Spry2 IHC in pancreatic cancer tissue.

Abnormal pancreatic tissue and adjacent normal ductal tissue stained for DAPI and Spry2 by IHC. Size of cell relative to nuclear stain, identifies a lymphocyte cell.

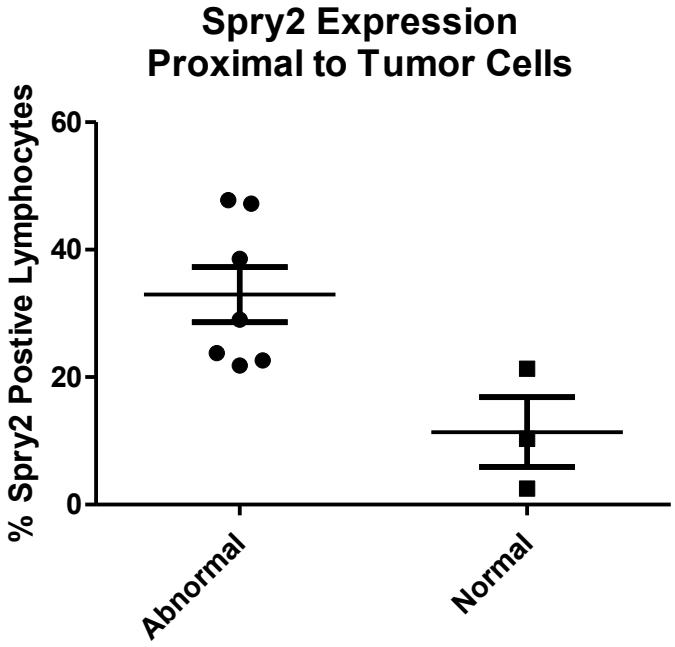

Figure 11.4 Higher Spry2 infiltration in pancreatic cancer.

Lymphoctye cells in healthy and abnormal compared by Spry2 staining. Compared to lymphocyte infiltration in healthy adjacent tissue, abnormal ducts in pancreatic cancer have higher Spry2+ lymphocytes. (7 abnormal samples, 3 normal controls). P-value < 0.05 by unpaired T-test.

11.3 Characterization of Neo-antigens

Neo-epitope T cell responses have been detected in immunotherapy patients years after initial treatment and response[17]. The Schneck lab has been interested in comparing neo-antigen specific T cells to self-tumor specific T cell phenotype after tumor infiltration, to understand the therapeutic potential of both T cell subsets. Neo-antigens were identified in B16-F10 murine melanoma model[12] but the short 9-10 amino acid sequences were not confirmed. The Scheck lab

identified potential neo-antigens epitopes using the NetMHC prediction algorithm and created aAPCs to screen B6 CD8+ T cells for stimulation ability in naïve animals (Figure 11.5). The Schneck lab screened 18 potential neo-antigens and confirmed 11 neo-antigen responses in naïve B6 animals (data not shown). B6 mice were then injected subcutaneously with B16.F10 melanoma cells and after 14 days CD8+ T cells from the spleen were harvested and stimulated for 2 neo-antigens KbVDW and KbVTF, and compared to KbTRP2 and KbSIY T cell stimulations; and naïve animals were harvested and stimulated for naïve expansion ability. KbVDW and KbVTF neo-antigen T cells had 4 fold higher expansion ability in tumor-bearing compared to naïve animals, while the KbTRP2 response was not changed (Figure 11.6). KbSIY was expected to be unchanged between tumor-bearing and naïve animals, since B16-F10 does not express the SIY antigen. Future work to characterize neo-antigen and self-tumor antigen response will include testing additional neo-antigens and other self-tumor responses to compare the expansion ability of the T cells. Furthermore, by looking directly at TILs, neo-antigens and self-tumor antigens can be phenotyped for activation and exhaustion markers with and without check point blockade treatments.

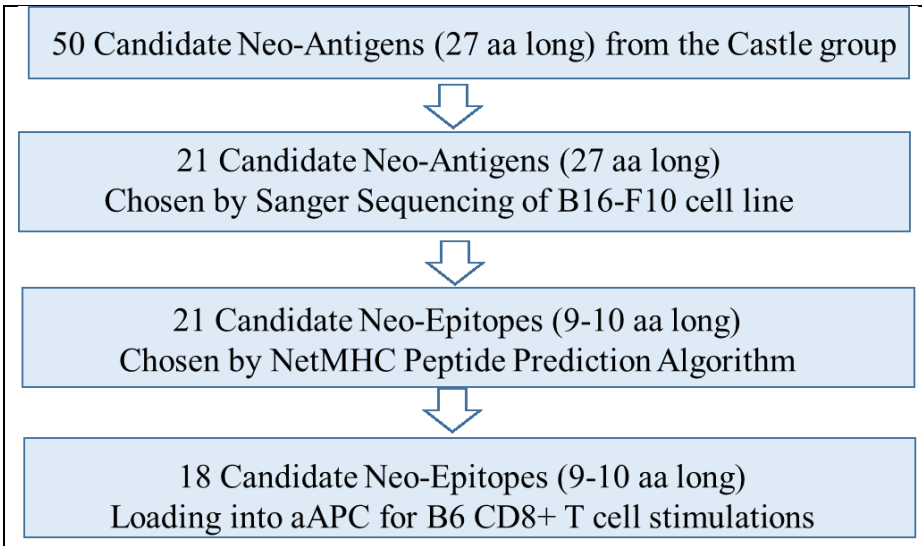

Figure 11.5 Pipeline for Identifying Neo-antigens Epitopes in B16-F10 Model

A schematic to show the pipeline to screen potential neo-antigen epitope sequences from Castle et al. (ref) to identify 9-10 amino acid (aa) long sequences from 27 aa long sequence. After potential neo-antigen epitopes are loaded into MHC-Ig molecules, T cell stimulations screens were used to identify neo-antitgen T cell respones in naïve B6 animals.

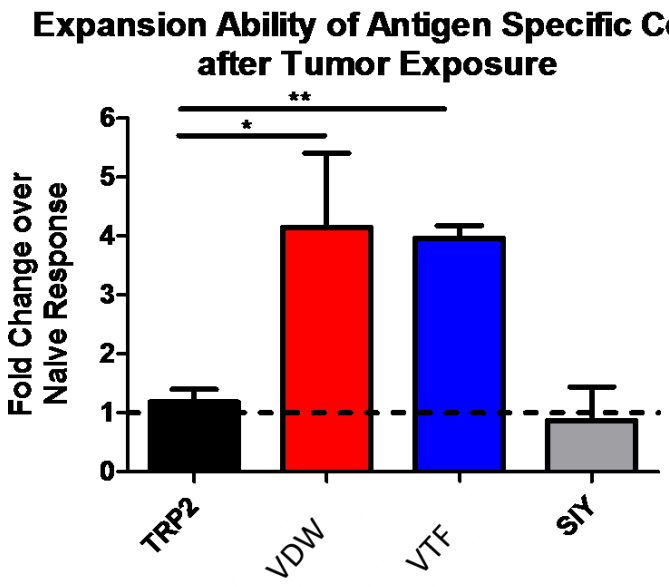

Figure 11.6 Tumor selectively stimulates Neo-antigen Specific Response

B6 mice were injected subquetaneously with B16-F10 tumors and after 14 days, splenic T cells were harvested and tumor antigens specificities were compared to naïve T cell frequencies. Compared to KbTRP2, the self-tumor antigen, both neo-antigens KbVDW and KbVTF increase expansion ability. KbSIY antigen is not expressed by this tumor and is expected not to change in with tumor presence.

11.4Conclusion

Spry2 project: Although the spry2 needs additional experiments, the work we have done so far is encouraging toward identifying spry2 as an upregulated marker in lymphocytes that have infiltrated and become exhausted in the tumor. Spry2 upregulation in TILs would be a novel marker of exhaustion in the tumor, and identify the subset of TILs with limited function based

not only on PD-1 signaling, but a separate negative regulator of the Erk signaling pathway. Another biomarker of T cell exhaustion could serve has a method to distinguish different levels of T cell inhibition and be correlated with response to check-point blockade treatment.

Characterization of neo-antigens: Although many groups have shown benefit in patients by targeting the neo-antigen T cell response. Yet only a subset of patients have long term survival with checkpoint blockade therapy[18]. Understanding how self-tumor responses and neo-antigen T cell responses react in the tumor and with different immunotherapies may increase the predictable patient outcome given the mutational landscape and the lymphocyte infiltration rate in tumors. The work we have conducted so far, as shown a selective benefit of neo-antigens, with increased expansion ability and less T cell exhaustion in peripheral lymphoid organs. Also, if selecting tumor specific T cells in the periphery, understanding the functional state of the tumor specific cells will be helpful for adoptive transfer therapies. Overall, this is exciting research but will require additional experiments to understand completely.

12 Bibliography

1. Klein L, Hinterberger M, Wirnsberger G, Kyewski B. Antigen presentation in the thymus for positive selection and central tolerance induction. *Nat Rev Immunol*. 2009;9(12):833-844. doi:10.1038/nri2669
2. Peng M, Mo Y, Wang Y, et al. Neoantigen vaccine: An emerging tumor immunotherapy. *Mol Cancer*. 2019;18(1):1-14. doi:10.1186/s12943-019-1055-6
3. Kalekar LA, Mueller DL. Relationship between CD4 Regulatory T Cells and Anergy In Vivo. *J Immunol*. 2017;198(7):2527-2533. doi:10.4049/jimmunol.1602031
4. Perica K, Bieler JG, Schütz C, et al. Enrichment and expansion with nanoscale artificial antigen presenting cells for adoptive immunotherapy. *ACS Nano*. 2015;9(7):6861-6871.
5. Perica K, Bieler JG, Schütz C, et al. Enrichment and Expansion with Nanoscale Artificial Antigen Presenting Cells for Adoptive Immunotherapy. *ACS Nano*. 2015;9(7):6861-6871. doi:10.1021/acsnano.5b02829
6. O'Donnell JS, Teng MWL, Smyth MJ. Cancer immunoediting and resistance to T cell-based immunotherapy. *Nat Rev Clin Oncol*. 2019;16(3):151-167. doi:10.1038/s41571-018-0142-8
7. Mittal D, Gubin MM, Schreiber RD, Smyth MJ. New insights into cancer immunoediting and its three component phases-elimination, equilibrium and escape. *Curr Opin Immunol*. 2014;27:16-25. doi:10.1016/j.coi.2014.01.004
8. Yarchoan M, Johnson III BA, Lutz ER, Laheru DA, Jaffee EM. Targeting neoantigens to augment. *Nat Rev Cancer*. 2017;17(4):209-222. doi:10.1038/nrc.2016.154
9. Rosenberg SA, Restifo NP, Yang JC, Morgan RA, Dudley ME. Adoptive cell transfer: A clinical path to effective cancer immunotherapy. *Nat Rev Cancer*. 2008;8(4):299-308. doi:10.1038/nrc2355
10. Efremova M, Finotello F, Rieder D, Trajanoski Z. Neoantigens generated by individual mutations and their role in cancer immunity and immunotherapy. *Front Immunol*. 2017;8(November):1-8. doi:10.3389/fimmu.2017.01679
11. Rosenberg SA, Restifo NP. Adoptive cell transfer as personalized immunotherapy for human cancer. *Science (80-)*. 2015;348(6230):62-68. doi:10.1126/science.aaa4967
12. Castle JC, Kreiter S, Diekmann J, et al. Exploiting the mutanome for tumor vaccination. *Cancer Res*. 2012;72(5):1081-1091. doi:10.1158/0008-5472.CAN-11-3722
13. Kreiter S, Vormehr M, van de Roemer N, et al. Mutant MHC class II epitopes drive therapeutic immune responses to cancer. *Nature*. 2015;520(7549):692-696. doi:10.1038/nature14426
14. Gubin MM, Zhang X, Schuster H, et al. Checkpoint blockade cancer immunotherapy targets tumour-specific mutant antigens. *Nature*. 2014;515(7528):577-581. doi:10.1038/nature13988
15. Carreno BM, Magrini V, Becker-Hapak M, et al. A dendritic cell vaccine increases the breadth and diversity of melanoma neoantigen-specific T cells. *Science (80-)*. 2015;348(6236):803-808. doi:10.1126/science.aaa3828
16. Ott PA, Hu Z, Keskin DB, et al. An immunogenic personal neoantigen vaccine for patients with melanoma. *Nature*. 2017;547:217.
17. Rizvi NA, Hellmann MD, Snyder A, et al. Mutational landscape determines sensitivity to PD-1 blockade in non-small cell lung cancer. *Science (80-)*. 2015;348(6230):124-128. doi:10.1126/science.aaa1348

18. Topalian SL, Hodi FS, Brahmer JR, et al. Safety, activity, and immune correlates of anti-PD-1 antibody in cancer. *N Engl J Med*. 2012;366(26):2443-2454. doi:10.1056/NEJMoa1200690
19. Havel JJ, Chowell D, Chan TA. The evolving landscape of biomarkers for checkpoint inhibitor immunotherapy. *Nat Rev Cancer*. 2019;19(3):133-150. doi:10.1038/s41568-019-0116-x
20. Gros A, Parkhurst MR, Tran E, et al. Prospective identification of neoantigen-specific lymphocytes in the peripheral blood of melanoma patients. *Nat Med*. 2016;22(4):433-438. doi:10.1038/nm.4051
21. Schumacher TN, Schreiber RD. Neoantigens in cancer immunotherapy. *Science (80-)*. 2015;348(6230):69-74. doi:10.1126/science.aaa4971
22. Wang DY, Johnson DB, Davis EJ. Toxicities Associated with PD-1/PD-L1 Blockade. *Cancer J (United States)*. 2018;24(1):36-40. doi:10.1097/PPO.0000000000000296
23. Rosenberg SA. Raising the bar: The curative potential of human cancer immunotherapy. *Sci Transl Med*. 2012;4(127):1-6. doi:10.1126/scitranslmed.3003634
24. Lu YC, Yao X, Crystal JS, et al. Efficient identification of mutated cancer antigens recognized by T cells associated with durable tumor regressions. *Clin Cancer Res*. 2014;20(13):3401-3410. doi:10.1158/1078-0432.CCR-14-0433
25. Zacharakis N, Chinnasamy H, Black M, et al. Immune recognition of somatic mutations leading to complete durable regression in metastatic breast cancer. *Nat Med*. 2018;24(6):724-730. doi:10.1038/s41591-018-0040-8
26. Shi N, Li N, Duan X, Niu H. Interaction between the gut microbiome and mucosal immune system. 2017:1-7. doi:10.1186/s40779-017-0122-9
27. Rromano-Keeler J, Moore DJ, Wang C, et al. Early life establishment of site-specific microbial communities in the gut. *Gut Microbes*. 2014;5(2). doi:10.4161/gmic.28442
28. Bandeira A, Mota-Santos T, Itohara S, et al. Localization of γ/δ T cells to the intestinal epithelium is independent of normal microbial colonization. *J Exp Med*. 1990;172(1):239-244. doi:10.1084/jem.172.1.239
29. Östman S, Rask C, Wold AE, Hultkrantz S, Telemo E. Impaired regulatory T cell function in germ-free mice. *Eur J Immunol*. 2006;36(9):2336-2346. doi:10.1002/eji.200535244
30. Zenewicz LA, Yancopoulos GD, Valenzuela DM, Murphy AJ, Stevens S, Flavell RA. Innate and Adaptive Interleukin-22 Protects Mice from Inflammatory Bowel Disease. *Immunity*. 2008;29(6):947-957. doi:10.1016/j.immuni.2008.11.003
31. Mcdermott AJ, Huffnagle GB. The microbiome and regulation of mucosal immunity. *Immunology*. 2014;142(1):24-31. doi:10.1111/imm.12231
32. Mazmanian SK, Round JL, Kasper DL. A microbial symbiosis factor prevents intestinal inflammatory disease. *Nature*. 2008;453(7195):620-625. doi:10.1038/nature07008
33. Round JL, Mazmanian SK. Inducible Foxp3+ regulatory T-cell development by a commensal bacterium of the intestinal microbiota. *Proc Natl Acad Sci U S A*. 2010;107(27):12204-12209. doi:10.1073/pnas.0909122107
34. Sonnenberg GF, Monticelli LA, Elloso MM, Fouser LA, Artis D. CD4+ Lymphoid Tissue-Inducer Cells Promote Innate Immunity in the Gut. *Immunity*. 2011;34(1):122-134. doi:10.1016/j.immuni.2010.12.009
35. Wang H-C, Zhou Q, Dragoo J, Klein JR. Most Murine CD8 + Intestinal Intraepithelial Lymphocytes Are Partially But Not Fully Activated T Cells . *J Immunol*. 2002;169(9):4717-4722. doi:10.4049/jimmunol.169.9.4717

36. Moretto M, Weiss LM, Khan IA. Induction of a Rapid and Strong Antigen-Specific Intraepithelial Lymphocyte Response during Oral Encephalitozoon cuniculi Infection . *J Immunol*. 2004;172(7):4402-4409. doi:10.4049/jimmunol.172.7.4402
37. Boismenu R, Havran WL, Boismenu R, Havran WL. Modulation of Epithelial Cell Growth by Intraepithelial $ \ gamma \ delta $ T Cells Published by : American Association for the Advancement of Science Stable URL : https://www.jstor.org/stable/2885395 digitize , preserve and extend access to Science Modul. 2020;266(5188):1253-1255.
38. M R, M U, B V, et al. Dendritic cells express tight junction proteins and penetrate gut epithelial monolayers to sample bacteria. *Nat Immunol*. 2001;2(4):361-367.
39. Colombo BM, Scalvenzi T, Benlamara S, Pollet N. Microbiota and mucosal immunity in amphibians. *Front Immunol*. 2015;6(MAR):1-15. doi:10.3389/fimmu.2015.00111
40. Sierro F, Dubois B, Coste A, Kaiserlian D, Kraehenbuhl JP, Sirard JC. Flagellin stimulation of intestinal epithelial cells triggers CCL20-mediated migration of dendritic cells. *Proc Natl Acad Sci U S A*. 2001;98(24):13722-13727. doi:10.1073/pnas.241308598
41. Muñoz M, Heimesaat MM, Danker K, et al. Interleukin (IL)-23 mediates Toxoplasma gondii-induced immunopathology in the gut via matrixmetalloproteinase-2 and IL-22 but independent of IL-17. *J Exp Med*. 2009;206(13):3047-3059. doi:10.1084/jem.20090900
42. Narushima S, Vlamakis H, Motoo I, et al. A defined commensal consortium elicits. *Nature*. 2019. doi:10.1038/s41586-019-0878-z
43. Reboldi A, Cyster JG. Peyer's patches: Organizing B-cell responses at the intestinal frontier. *Immunol Rev*. 2016;271(1):230-245. doi:10.1111/imr.12400
44. Peterson SN, Bradley LM, Ronai ZA. The gut microbiome: an unexpected player in cancer immunity. *Curr Opin Neurobiol*. 2020;62:48-52. doi:10.1016/j.conb.2019.09.016
45. Matson V, Fessler J, Bao R, et al. The commensal microbiome is associated with anti-PD-1 efficacy in metastatic melanoma patients. *Science (80-)*. 2018;359(6371):104-108. doi:10.1126/science.aao3290
46. Routy B, Chatelier E Le, Derosa L, et al. Gut microbiome influences efficacy of PD-1 – based immunotherapy against epithelial tumors. 2018;97(January):91-97.
47. Sivan A, Corrales L, Hubert N, et al. Commensal Bifidobacterium promotes antitumor immunity and facilitates anti-PD-L1 efficacy. *Science (80-)*. 2015;350(6264):1084-1089. doi:10.1126/science.aac4255
48. Vétizou M, Pitt JM, Daillère R, et al. Anticancer immunotherapy by CTLA-4 blockade relies on the gut microbiota. 2015;350(6264).
49. Gopalakrishnan V, Spencer CN, Nezi L, et al. Gut microbiome modulates response to anti–PD-1 immunotherapy in melanoma patients. *Science (80-)*. 2018;359(6371):97-103. doi:10.1126/science.aan4236
50. Routy B, Gopalakrishnan V, Daillère R, Zitvogel L, Wargo JA, Kroemer G. The gut microbiota influences anticancer immunosurveillance and general health. *Nat Rev Clin Oncol*. 2018;15(6):382-396. doi:10.1038/s41571-018-0006-2
51. Le Chatelier E, Nielsen T, Qin J, et al. Richness of human gut microbiome correlates with metabolic markers. *Nature*. 2013;500(7464):541-546. doi:10.1038/nature12506
52. Li Y, Tinoco R, Elmén L, et al. Gut microbiota dependent anti-tumor immunity restricts melanoma growth in Rnf5 −/− mice. *Nat Commun*. 2019;10(1). doi:10.1038/s41467-019-09525-y
53. Cubillos-Ruiz JR, Silberman PC, Rutkowski MR, et al. ER Stress Sensor XBP1 Controls

Anti-tumor Immunity by Disrupting Dendritic Cell Homeostasis. *Cell*. 2015;161(7):1527-1538. doi:10.1016/j.cell.2015.05.025
54. Rojas M, Restrepo-Jiménez P, Monsalve DM, et al. Molecular mimicry and autoimmunity. *J Autoimmun*. 2018;95(October):100-123. doi:10.1016/j.jaut.2018.10.012
55. Balachandran VP, Luksza M, Zhao JN, et al. Identification of unique neoantigen qualities in long-term survivors of pancreatic cancer. *Nature*. 2017;551(7681):S12-S16. doi:10.1038/nature24462
56. Luksza M, Riaz N, Makarov V, et al. A neoantigen fitness model predicts tumour response to checkpoint blockade immunotherapy. *Nature*. 2017;551(7681):517-520. doi:10.1038/nature24473
57. Gil-Cruz C, Perez-Shibayama C, de Martin A, et al. Microbiota-derived peptide mimics drive lethal inflammatory cardiomyopathy. *Science (80-)*. 2019;366(6467):881-886. doi:10.1126/science.aav3487
58. Ruff WE, Dehner C, Kim WJ, et al. Pathogenic Autoreactive T and B Cells Cross-React with Mimotopes Expressed by a Common Human Gut Commensal to Trigger Autoimmunity. *Cell Host Microbe*. 2019;26(1):100-113.e8. doi:10.1016/j.chom.2019.05.003
59. Boyd SD, Marshall EL, Merker JD, et al. Measurement and clinical monitoring of human lymphocyte clonality by massively parallel V-D-J pyrosequencing. *Sci Transl Med*. 2009;1(12). doi:10.1126/scitranslmed.3000540
60. Vollmers C, Sit R V., Weinstein JA, Dekker CL, Quake SR. Genetic measurement of memory B-cell recall using antibody repertoire sequencing. *Proc Natl Acad Sci U S A*. 2013;110(33):13463-13468. doi:10.1073/pnas.1312146110
61. Robins HS, Campregher P V., Srivastava SK, et al. Comprehensive assessment of T-cell receptor β-chain diversity in αβ T cells. *Blood*. 2009;114(19):4099-4107. doi:10.1182/blood-2009-04-217604
62. Wang C, Sanders CM, Yang Q, et al. High throughput sequencing reveals a complex pattern of dynamic interrelationships among human T cell subsets. *Proc Natl Acad Sci U S A*. 2010;107(4):1518-1523. doi:10.1073/pnas.0913939107
63. Jackson KJL, Liu Y, Roskin KM, et al. Human responses to influenza vaccination show seroconversion signatures and convergent antibody rearrangements. *Cell Host Microbe*. 2014;16(1):105-114. doi:10.1016/j.chom.2014.05.013
64. Logan AC, Gao H, Wang C, et al. High-throughput VDJ sequencing for quantification of minimal residual disease in chronic lymphocytic leukemia and immune reconstitution assessment. *Proc Natl Acad Sci U S A*. 2011;108(52):21194-21199. doi:10.1073/pnas.1118357109
65. Grupp SA, Kalos M, Barrett D, et al. Chimeric antigen receptor-modified T cells for acute lymphoid leukemia. *N Engl J Med*. 2013;368(16):1509-1518. doi:10.1056/NEJMoa1215134
66. Sherwood AM, Emerson RO, Scherer D, et al. Tumor-infiltrating lymphocytes in colorectal tumors display a diversity of T cell receptor sequences that differ from the T cells in adjacent mucosal tissue. *Cancer Immunol Immunother*. 2013;62(9):1453-1461. doi:10.1007/s00262-013-1446-2
67. Gros A, Robbins PF, Yao X, et al. PD-1 identi fi es the patient-speci fi c in fi ltrating human tumors. *J Clin Invest*. 2014;124(5):2246-2259. doi:10.1172/JCI73639.2246
68. Stewart JJ, Lee CY, Ibrahim S, et al. A Shannon entropy analysis of immunoglobulin and

T cell receptor. *Mol Immunol*. 1997;34(15):1067-1082. doi:10.1016/S0161-5890(97)00130-2
69. Venturi V, Kedzierska K, Tanaka MM, Turner SJ, Doherty PC, Davenport MP. Method for assessing the similarity between subsets of the T cell receptor repertoire. *J Immunol Methods*. 2008;329(1-2):67-80. doi:10.1016/j.jim.2007.09.016
70. Victor CT-S, Rech AJ, Maity A, et al. Radiation and dual checkpoint blockade activate non-redundant immune mechanisms in cancer. *Nature*. 2015;520(7547):373-377. doi:10.1038/nature14292
71. Glanville J, Huang H, Nau A, et al. Identifying specificity groups in the T cell receptor repertoire. *Nature*. 2017;547(7661):94-98. doi:10.1038/nature22976
72. Dash P, Fiore-Gartland AJ, Hertz T, et al. Quantifiable predictive features define epitope-specific T cell receptor repertoires. *Nature*. 2017;547(7661):89-93. doi:10.1038/nature22383
73. Madi A, Poran A, Shifrut E, et al. T cell receptor repertoires of mice and humans are clustered in similarity networks around conserved public CDR3 sequences. *Elife*. 2017;6:1-17. doi:10.7554/eLife.22057
74. Needleman SB, Wunsch CD. A general method applicable to the search for similarities in the amino acid sequence of two proteins. *J Mol Biol*. 1970;48(3):443-453. doi:10.1016/0022-2836(70)90057-4
75. Altschul SF. Amino acid substitution matrices from an information theoretic perspective. *J Mol Biol*. 1991;219(3):555-565. doi:10.1016/0022-2836(91)90193-A
76. Carey AJ, Gracias DT, Thayer JL, et al. Rapid Evolution of the CD8 + TCR Repertoire in Neonatal Mice . *J Immunol*. 2016;196(6):2602-2613. doi:10.4049/jimmunol.1502126
77. Kyewski B, Klein L. a Central Role for Central Tolerance. *Annu Rev Immunol*. 2006;24(1):571-606. doi:10.1146/annurev.immunol.23.021704.115601
78. Piccirillo CA, Thornton AM. Cornerstone of peripheral tolerance: Naturally occurring CD4 +CD25+ regulatory T cells. *Trends Immunol*. 2004;25(7):374-380. doi:10.1016/j.it.2004.04.009
79. Chodon T, Comin-Anduix B, Chmielowski B, et al. Adoptive transfer of MART-1 T-cell receptor transgenic lymphocytes and dendritic cell vaccination in patients with metastatic melanoma. *Clin Cancer Res*. 2014;20(9):2457-2465. doi:10.1158/1078-0432.CCR-13-3017
80. Wang F, Bade E, Kuniyoshi C, et al. Phase I trial of a MART-1 peptide vaccine with incomplete Freund's adjuvant for resected high-risk melanoma. *Clin Cancer Res*. 1999;5(10):2756-2765.
81. Rosenberg SA, Zhai Y, Yang JC, et al. Immunizing Patients With Metastatic Melanoma Using Recombinant Adenoviruses Encoding MART-1 or gp100 Melanoma Antigens. *JNCI J Natl Cancer Inst*. 1998;90(24):1870-1872. doi:10.1093/jnci/90.24.1894
82. Hanson HL, Donermeyer DL, Ikeda H, et al. Eradication of established tumors by CD8+ T cell adoptive immunotherapy. *Immunity*. 2000;13(2):265-276. doi:10.1016/S1074-7613(00)00026-1
83. Morgan RA, Dudley ME, Wunderlich JR, et al. Cancer regression in patients after transfer of genetically engineered lymphocytes. *Science (80-)*. 2006;314(5796):126-129. doi:10.1126/science.1129003
84. Vatakis DN, Koya RC, Nixon CC, et al. Antitumor activity from antigen-specific CD8 T cells generated in vivo from genetically engineered human hematopoietic stem cells. *Proc*

Natl Acad Sci U S A. 2011;108(51). doi:10.1073/pnas.1115050108
85. Dudley ME, Rosenberg SA. Adoptive-cell-transfer therapy for the treatment of patients with cancer. *Nat Rev Cancer*. 2003;3(9):666-675. doi:10.1038/nrc1167
86. Speiser DE, Miranda R, Zakarian A, et al. Self antigens expressed by solid tumors do not efficiently stimulate naive or activated T cells: Implications for immunotherapy. *J Exp Med*. 1997;186(5):645-653. doi:10.1084/jem.186.5.645
87. Lennerz V, Fatho M, Gentilini C, et al. The response of autologous T cells to a human melanoma is dominated by mutated neoantigens. *Proc Natl Acad Sci U S A*. 2005;102(44):16013-16018. doi:10.1073/pnas.0500090102
88. Gros A, Parkhurst MR, Tran E, et al. Prospective identification of neoantigen-specific lymphocytes in the peripheral blood of melanoma patients. *Nat Med*. 2016;22(4):433-438. doi:10.1038/nm.4051
89. Rudqvist NP, Pilones KA, Lhuillier C, et al. Radiotherapy and CTLA-4 blockade shape the tcr repertoire of tumor-infiltrating t cells. *Cancer Immunol Res*. 2018;6(2):139-150. doi:10.1158/2326-6066.CIR-17-0134
90. Oelke M, Maus M V., Didiano D, June CH, Mackensen A, Schneck JP. Ex vivo induction and expansion of antigen-specific cytotoxic T cells by HLA-Ig-coated artificial antigen-presenting cells. *Nat Med*. 2003;9(5):619-624. doi:10.1038/nm869
91. Perica K, De León Medero A, Durai M, et al. Nanoscale artificial antigen presenting cells for T cell immunotherapy. *Nanomedicine Nanotechnology, Biol Med*. 2014;10(1):119-129. doi:10.1016/j.nano.2013.06.015
92. Oelke M, Vogl S, Cerundolo V, Andreesen R, Mackensen A. Generation and enrichment of antigen-specific cytotoxic t lymphocytes for adoptive transfer in tumor immunotherapy. *Blood*. 2000;96(11 PART I):1997-2005.
93. Carlson CS, Emerson RO, Sherwood AM, et al. Using synthetic templates to design an unbiased multiplex PCR assay. *Nat Commun*. 2013;4:1-9. doi:10.1038/ncomms3680
94. Suessmuth Y, Mukherjee R, Watkins B, et al. CMV reactivation drives posttransplant T-cell reconstitution and results in defects in the underlying TCRβ repertoire. *Blood*. 2015;125(25):3835-3850. doi:10.1182/blood-2015-03-631853
95. Gros A, Parkhurst MR, Tran E, et al. Prospective identification of neoantigen-specific lymphocytes in the peripheral blood of melanoma patients. *Nat Med*. 2016;(February). doi:10.1038/nm.4051
96. Routy B, Le Chatelier E, Derosa L, et al. Gut microbiome influences efficacy of PD-1–based immunotherapy against epithelial tumors. *Science (80-)*. 2018;359(6371):91-97. doi:10.1126/science.aan3706
97. Iida N, Dzutsev A, Stewart CA, et al. Commensal Bacteria Control Cancer the Tumor Microenvironment. 2013;342(November):967-971.
98. Viaud S, Viaud S, Saccheri F, et al. The Intestinal Microbiota Modulates Cyclophosphamide. 2013;971(November):971-977. doi:10.1126/science.1240537
99. Denton AE, Wesselingh R, Gras S, et al. Affinity thresholds for naive CD8+ CTL activation by peptides and engineered influenza A viruses. *J Immunol*. 2011;187(11):5733-5744.
100. Colf LA, Bankovich AJ, Hanick NA, et al. How a single T cell receptor recognizes both self and foreign MHC. *Cell*. 2007;129(1):135-146.
101. Schütz C, Zoso A, Peng S, Bennett JD, Schneck JP, Oelke M. MHC-Ig induces memory T cell formation in vivo and inhibits tumour growth. *Immunity, Inflamm Dis*. 2014;2(3):181-

192. http://www.pubmedcentral.nih.gov/articlerender.fcgi?artid=4257763&tool=pmcentrez&rendertype=abstract. Accessed December 12, 2014.
102. Sidhom J-W, Bessell CA, Havel JJ, Kosmides A, Chan TA, Schneck JP. ImmunoMap: A Bioinformatics Tool for T-cell Repertoire Analysis. *Cancer Immunol Res*. 2017:151-163. doi:10.1158/2326-6066.CIR-17-0114
103. Blank C, Brown I, Kacha AK, Markiewicz MA, Gajewski TF. ICAM-1 Contributes to but Is Not Essential for Tumor Antigen Cross-Priming and CD8+ T Cell-Mediated Tumor Rejection In Vivo. *J Immunol*. 2005;174(6):3416-3420. doi:10.4049/jimmunol.174.6.3416
104. Zitvogel L, Raoult D, Kroemer G, Gajewski TF. The microbiome in cancer immunotherapy: Diagnostic tools and therapeutic strategies. 2018;1370(March):1366-1370.
105. Zitvogel L, Ayyoub M, Routy B, Kroemer G. Microbiome and Anticancer Immunosurveillance. *Cell*. 2016;165(2):276-287. doi:10.1016/j.cell.2016.03.001
106. Sivan A, Corrales L, Hubert N, et al. Commensal Bifidobacterium promotes antitumor immunity and facilitates anti–PD-L1 efficacy. *Science (80-)*. 2015;350(6264):1084 LP - 1089. http://science.sciencemag.org/content/350/6264/1084.abstract.
107. Haarman M, Knol J. Quantitative Real-Time PCR Assays To Identify and Quantify Fecal Bifidobacterium Species in Infants Receiving a Prebiotic Infant Formula Quantitative Real-Time PCR Assays To Identify and Quantify Fecal Bifidobacterium Species in Infants Receiving a Prebio. *Appl Environ Microbiol*. 2005;71(5):2318-2324. doi:10.1128/AEM.71.5.2318
108. Frenkel D, Smit B. *Understanding Molecular Simulation: From Algorithms to Applications*. Vol 1. Elsevier; 2001.
109. Humphrey W, Dalke A, Schulten K. VMD: visual molecular dynamics. *J Mol Graph*. 1996;14(1):33-38.
110. Abraham MJ, Murtola T, Schulz R, et al. GROMACS: High performance molecular simulations through multi-level parallelism from laptops to supercomputers. *SoftwareX*. 2015;1:19-25.
111. Best RB, Zhu X, Shim J, et al. Optimization of the additive CHARMM all-atom protein force field targeting improved sampling of the backbone ϕ, ψ and side-chain $\chi 1$ and $\chi 2$ dihedral angles. *J Chem Theory Comput*. 2012;8(9):3257-3273.
112. Jorgensen WL, Chandrasekhar J, Madura JD, Impey RW, Klein ML. Comparison of simple potential functions for simulating liquid water. *J Chem Phys*. 1983;79(2):926-935.
113. Darden T, York D, Pedersen L. Particle mesh Ewald: An N· log (N) method for Ewald sums in large systems. *J Chem Phys*. 1993;98(12):10089-10092.
114. Hess B, Bekker H, Berendsen HJC, Fraaije JGEM. LINCS: a linear constraint solver for molecular simulations. *J Comput Chem*. 1997;18(12):1463-1472.
115. Nosé S. A unified formulation of the constant temperature molecular dynamics methods. *J Chem Phys*. 1984;81(1):511-519.
116. Berendsen HJC, Postma JPM van, van Gunsteren WF, DiNola A, Haak JR. Molecular dynamics with coupling to an external bath. *J Chem Phys*. 1984;81(8):3684-3690.
117. Daura X, Gademann K, Jaun B, Seebach D, Van Gunsteren WF, Mark AE. Peptide folding: when simulation meets experiment. *Angew Chemie Int Ed*. 1999;38(1-2):236-240.
118. Gapsys V, Michielssens S, Seeliger D, de Groot BL. pmx: Automated protein structure

and topology generation for alchemical perturbations. *J Comput Chem*. 2015;36(5):348-354.
119. Beutler TC, Mark AE, van Schaik RC, Gerber PR, van Gunsteren WF. Avoiding singularities and numerical instabilities in free energy calculations based on molecular simulations. *Chem Phys Lett*. 1994;222(6):529-539.
120. Xia Z, Chen H, Kang S, et al. The complex and specific pMHC interactions with diverse HIV-1 TCR clonotypes reveal a structural basis for alterations in CTL function. *Sci Rep*. 2014;4:4087.
121. Hölzemer A, Thobakgale CF, Cruz CAJ, et al. Selection of an HLA-C* 03: 04-restricted HIV-1 p24 gag sequence variant is associated with viral escape from KIR2DL3+ natural killer cells: data from an observational cohort in South Africa. *PLoS Med*. 2015;12(11):e1001900.
122. Chowell D, Morris LGT, Grigg CM, et al. Patient HLA class I genotype influences cancer response to checkpoint blockade immunotherapy. *Science (80-)*. 2018;359(6375):582-587.
123. Joglekar A V, Liu Z, Weber JK, et al. T cell receptors for the HIV KK10 epitope from patients with differential immunologic control are functionally indistinguishable. *Proc Natl Acad Sci*. 2018:201718659.
124. Kirkwood JG. Statistical mechanics of fluid mixtures. *J Chem Phys*. 1935;3(5):300-313.
125. Straatsma TP, McCammon JA. Multiconfiguration thermodynamic integration. *J Chem Phys*. 1991;95(2):1175-1188.
126. Russ BE, Denton AE, Hatton L, Croom H, Olson MR, Turner SJ. Defining the molecular blueprint that drives CD8(+) T cell differentiation in response to infection. *Front Immunol*. 2012;3(December):371. doi:10.3389/fimmu.2012.00371
127. Collins S, Waickman A, Basson A, et al. Regulation of $CD4^+$ and $CD8^+$ effector responses by Sprouty-1. *PLoS One*. 2012;7(11):e49801. doi:10.1371/journal.pone.0049801
128. Chiu Y, Shan L, Huang H, et al. Sprouty-2 regulates HIV-specific T cell polyfunctionality. 2014;124(1). doi:10.1172/JCI70510.198
129. Wherry EJ. T cell exhaustion. *Nat Immunol*. 2011;131(6):492-499. doi:10.1038/ni.2035

13 Curriculum Vitae

CURRICULUM VITAE FOR Ph.D. CANDIDATES
The Johns Hopkins University School of Medicine

Catherine Ami Bessell 7/17/2020

Educational History:

Ph.D. expected 2020 Program in Immunology Johns Hopkins School of Medicine

Mentors: Jonathan P Schneck M.D., Ph.D

B.S. 2012 Cellular Biology and Molecular Genetics University of Maryland, College Park

Professional Experience

Industry Internship Oct-Nov 2020 miRecule, Inc., CEO: Anthony D. Saleh, Ph.D

Publications

Bessell, C.A.*, Isser, A.*, Havel, J.J.*, Lee, S., Bell, D.R., Hickey, J.W., Chaisawangwong, W., Bieler, J.G., Srivastava, R., Kuo, F., Purohit, T., Zhou, R., Chan, T.A., Schneck, J.P, (2020) Commensal bacteria *Bifidobacterium* stimulates anti-tumor response via cross-reactivity. *JCI-Insight*

Hickey, J.W., Dong, Y., Chung, J.W., Salathe, S.F., Pruitt, H.C., Li, X., Chang, C., Fraser, A.K., **Bessell, C.A**., Ewald, A.J., Gerecht, S., Mao, H.Q., Schneck, J.P. (2019). Engineering an Artificial T-Cell Stimulating Matrix for Immunotherapy. *Adv Mater*., (23):e1807359

Sidhom, J.W., **Bessell, C.A.**, Havel, J.J., Kosmides, A., Chan, T.A., Schneck, J.P. (2018). ImmunoMap: A Bioinformatics Tool for T-cell Repertoire Analysis. *Cancer Immunol Res*., 6(2) 151-162

Kosmides, A.K., Sidhom, J.W., Fraser, A., **Bessell, C.A.**, Schneck, J.P. (2017). Dual Targeting Nanoparticle Stimulates the Immune System To Inhibit Tumor Growth. *ACS Nano, Article ASAP*

Bruns H., **Bessell, C.,** Varela, J.C., Haupt, C., Fang, J., Pasemann, S., Mackensen, A., Oelke, M., Schneck, J.P., Schütz, C. (2015). CD47 Enhances *In Vivo* Functionality of Artificial Antigen-Presenting Cells. *Clinical Cancer Research, 21*(9), 2075-83.

Chiu, Y.-L., Shan, L., Huang, H., Haupt, C., **Bessell, C.,** Canaday, D. H., Zhang H., Ho, Y., Powell, J.D., Oelke, M., Margolick, J.B., Blankson, J.N., Griffin, D.E., Schneck, J. P. (2014). Sprouty-2 regulates HIV-specific T cell polyfunctionality. *The Journal of Clinical Investigation*, *124*(1), 198–208.

Poster Presentations

Bessell, CA, Isser, A, Havel, J, Lee, S, Bell, DR, Hickey, JW, Sidhom, JW, Zhou, R, Chan, TA, Schneck, (2018) Commensal bacteria Bifidobacterium stimulates an anti-tumor response via cross-reactivity, American Association for Cancer Research, Cancer Immunotherapy Conference, New York, NY, September 30, 2018

Bessell, CA, Isser, A, Havel, J, Lee, S, Zhou, R, Chan, TA, Schneck, JP (2018) Commensal bacteria stimulate a cross-reactive antigen-specific CTL response, American Associations of Immunologists (AAI) Conference, Houston, TX, May 4, 2018

Bessell, CA, Bieler, JG, Sidhom, M, Schneck, JP (2017) Nanoparticle Based Enrichment and Expansion of Self and Neo-epitope Specific $CD8^+$ T cells in Murine Melanoma, Society of Immunotherapy of Cancer Meeting, Washington, DC, November 10, 2017

Bessell, CA, Bieler, JG, Sidhom, JW, Oelke, M, Schneck, JP (2017) Nanoparticle Based Enrichment and Expansion of Self and Neo-epitope Specific $CD8^+$ T cells in Murine Melanoma, American Associations of Immunologists (AAI) Washington, DC, May 14, 2017

Bessell, CA, Aje, K, Oelke, M, Schneck, JP (2015) Sprouty2 Induction in $CD8^+$ Tumor Infiltrating Lymphocytes, Keystone Symposia Tumor Immunology: Multidisciplinary Science Drive Combination Therapy, Banff, Canada, Febuary 8, 2015.

Service

2017 STEM Day Speaker at Maryland Elementary and High School

2015 Tutoring Graduate Students